USAAEFA PROJECT NO. 78-21-2

MICROPHYSICAL PROPERTIES OF ARTIFICIAL AND NATURAL CLOUDS AND THEIR EFFECTS ON UH-1H HELICOPTER ICING

FINAL REPORT

GRADY W. WILSON
MAJ, TC
US ARMY
PROJECT OFFICER/PILOT

RALPH WORATSCHEK
PROJECT ENGINEER

AUGUST 1979

Approved for public release; distribution unlimited

UNITED STATES ARMY AVIATION ENGINEERING FLIGHT ACTIVITY
EDWARDS AIR FORCE BASE, CALIFORNIA 93523

DISCLAIMER NOTICE

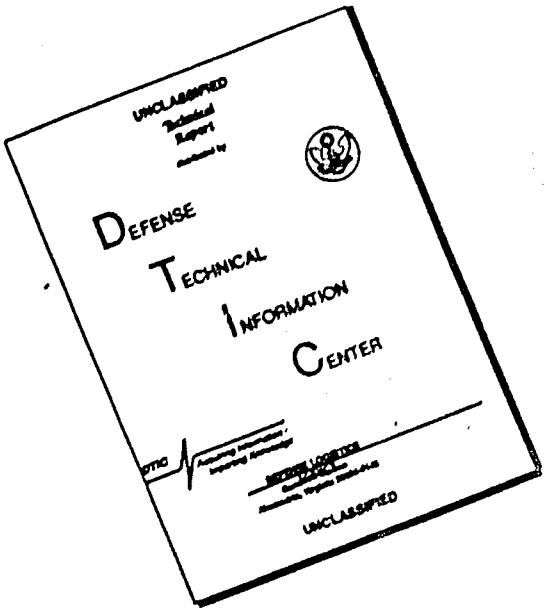

THIS DOCUMENT IS BEST QUALITY AVAILABLE. THE COPY FURNISHED TO DTIC CONTAINED A SIGNIFICANT NUMBER OF PAGES WHICH DO NOT REPRODUCE LEGIBLY.

DISCLAIMER NOTICE

The findings of this report are not to be construed as an official Department of the Army position unless so designated by other authorized documents.

DISPOSITION INSTRUCTIONS

Destroy this report when it is no longer needed. Do not return it to the originator.

TRADE NAMES

The use of trade names in this report does not constitute an official endorsement or approval of the use of the commercial hardware and software.

UNCLASSIFIED
SECURITY CLASSIFICATION OF THIS PAGE (When Data Entered)

REPORT DOCUMENTATION PAGE

READ INSTRUCTIONS BEFORE COMPLETING FORM

1. REPORT NUMBER: USAAEFA [redacted]-78-21-2	2. GOVT ACCESSION NO.: AD-A084 633
3. RECIPIENT'S CATALOG NUMBER:	
4. TITLE (and Subtitle): MICROPHYSICAL PROPERTIES OF ARTIFICIAL AND NATURAL CLOUDS AND THEIR EFFECTS ON UH-1H HELICOPTER ICING.	5. TYPE OF REPORT & PERIOD COVERED: FINAL REPORT. Jan [redacted]–Mar [redacted]79
	6. PERFORMING ORG. REPORT NUMBER: 78-21-2
7. AUTHOR(s): [redacted] GRADY W. WILSON RALPH WORATSCHEK	8. CONTRACT OR GRANT NUMBER(s):
9. PERFORMING ORGANIZATION NAME AND ADDRESS: US ARMY AVIATION ENGINEERING FLIGHT ACTIVITY EDWARDS AIR FORCE BASE, CALIFORNIA 93523	10. PROGRAM ELEMENT, PROJECT, TASK AREA & WORK UNIT NUMBERS: 1K-9-EQ006-02-1K-EC
11. CONTROLLING OFFICE NAME AND ADDRESS: US ARMY AVIATION ENGINEERING FLIGHT ACTIVITY EDWARDS AIR FORCE BASE, CALIFORNIA 93523	12. REPORT DATE: AUG [redacted]79 13. NUMBER OF PAGES: 101
14. MONITORING AGENCY NAME & ADDRESS(if different from Controlling Office)	15. SECURITY CLASS. (of this report): UNCLASSIFIED 15a. DECLASSIFICATION/DOWNGRADING SCHEDULE

16. DISTRIBUTION STATEMENT (of this Report):

Approved for public release; distribution unlimited.

17. DISTRIBUTION STATEMENT (of the abstract entered in Block 20, if different from Report)

18. SUPPLEMENTARY NOTES

19. KEY WORDS (Continue on reverse side if necessary and identify by block number)

Artificial Icing
Cloud Microphysical Properties
Helicopter Deicing Systems
Helicopter Icing Characteristics
Helicopter Icing Spray System (HISS)
Ice Detection Systems
Laser Nephelometers
Natural Icing
Partial Ice Protection System, "Kit A"

20. ABSTRACT (Continue on reverse side if necessary and identify by block number)

Natural and artificial icing tests were conducted from 22 January to 22 February 1979 in the vicinity of St. Paul, MN with follow-on natural tests conducted from 26 February to 21 March 1979 in the vicinity of Syracuse, NY. A total of 6.7 hours were flown in the artificial environment and 7.8 hours in the natural environment. Artificial conditions were tested at liquid water content (LWC) range of 0.25 to 0.90 gm/m^3 with a temperature range of -10 to -20°C. Natural conditions were encountered at LWC range of 0.06 to 0.23 gm/m^3 and a temperature range of -2.5 to -22°C. Tests were conducted to determine the feasibility of operational deployment of a partial ice protection system consisting of electrothermally heated windshields, a sensitive outside air temperature (OAT) system, a LWC indicator and associated electrical changes. The test aircraft was a JUH-1H helicopter equipped with

DD FORM 1 JAN 73 1473 EDITION OF 1 NOV 65 IS OBSOLETE

UNCLASSIFIED 409025
SECURITY CLASSIFICATION OF THIS PAGE (When Data Entered)

electrothermally deiced blades as a safety device and laser nephelometers which were used to quantify the microphysical properties of the test environment. It was determined that the artificial environment (Helicopter Icing Spray System (HISS)) was not an adequate simulation in its present configuration. This was due in part to the large droplet size, heterogeneous characteristic of the plume and concentration of large droplets in the lower portion of the plume. It was also determined that the partial ice protection system did not increase the operational capability of the UH-1H helicopter and that LWC is not an adequate indication of icing severity. The low level stratus clouds encountered during testing were found to conform to the particle distributions and concentrations reported for high altitude stratus by other investigators. It is recommended that a modification program be implemented on the HISS to produce a more realistic simulation of the natural environment. It is also recommended that future artificial testing be conducted at conditions of high relative humidity to better simulate natural icing. Future testing should be limited to maximum LWC of 1 gm/m^3 to better approximate the natural stratus environment that is of interest to the rotary wing community.

DEPARTMENT OF THE ARMY
HQ, US ARMY AVIATION RESEARCH AND DEVELOPMENT COMMAND
P O BOX 209, ST. LOUIS, MO 63166

DRDAV-DI

23 JAN 1980

SUBJECT: Directorate for Development and Qualification Position on the Final Report, Microphysical Properties of Artificial and Natural Clouds and Their Effects on UH-1H Helicopter Icing, USAAEFA Project Number 78-21-2

SEE DISTRIBUTION

1. The purpose of this letter is to establish the Directorate for Development and Qualification position on the subject report. The U. S. Army Aviation Engineering Flight Activity (AEFA) conducted an artificial and natural icing evaluation of the UH-1H at Minneapolis, MN during the 1978/1979 icing season. This evaluation also included an assessment of the JCH-47C Helicopter Icing Spray System (HISS) characteristics for simulating natural icing conditions. The intent of this report is to satisfy Federal Aviation Administration requirements relative to establishing icing certification and operations requirements for civil helicopters operating with minimum ice protection systems capability. Specifically, this report was written as required by Interagency Agreement DOT-FA78WAI-930 between U. S. Department of Transportation Federal Aviation Administration and U. S. Army Aviation Research and Development Command (AVRADCOM).

2. The report does not include all data generated during the icing tests since, historically, AEFA reports are structured in terms of typical engineering data which is sufficient to produce a comprehensive report. This approach is taken for purposes of cost control. Complete data, to include all time histories, are available in the form of unofficial documentation provided to Government agencies by Meteorological Research Institute (MRI) as a subcontractor to Bell Helicopter Textron (BHT) and BHT as a contractor for AVRADCOM in support of the icing tests. Documentation was provided in the form of graphs, tables and time histories. All available data was provided to the FAA and is available to other agencies from this Headquarters under the Freedom of Information Act.

3. The following comments are made to the Abstract and the Results and Discussion sections of the report to provide additional clarification. Comments are directed to the report paragraph as indicated:

DRDAV-DI 23 JAN 1980

SUBJECT: Directorate for Development and Qualification Position on the Final Report, Microphysical Properties of Artificial and Natural Clouds and Their Effects on UH-1H Helicopter Icing, USAAEFA Project Number 78-21-2

a. Abstract and Paragraph 6: It is important to note that while tests were conducted at Liquid Water Content (LWC) ranges of 0.06 to 0.23 gm/m^3 and temperature ranges of -10 to -20°C these conditions were not all encompassing due to the limited availability of environmental conditions. Consequently, a thorough evaluation of all conditions was not possible.

b. Paragraph 10: All prior year artificial icing tests had been conducted at a low relative humidity (RH). The impact of RH on artificial ice accumulation became apparent during this evaluation and future testing will require RH as a factor in attempting to duplicate natural icing conditions with the HISS.

c. Paragraph 37, second sentence: This sentence states that under most conditions tested the main rotor exhibited a symmetric shed tendency which did not adversely affect the aircraft characteristics. This sentence could be misleading since most conditions tested relates to 54% of the test conditions. Because of the limited testing conducted, it cannot be assumed that the main rotor would not be the limiting component during natural icing flight in the LWC and temperature ranges encountered during these tests.

4. This Directorate concurs with the conclusions and recommendations in the report except for paragraphs 63a and 64c. The conclusion and recommendation in these sub-paragraphs would summarily dismiss a LWC indicator for determining the icing severity level. While the shortcomings of the system used for the subject test are understood, the same concept with design improvements will be evaluated during future tests of the US Army UH-60A. Improvement of the LWC indicator consists of additional damping of the system to reduce erratic operation and to more closely indicate average liquid water content under icing conditions. We therefore do not agree with the dismissal of the LWC indicator concept at this time.

5. Action has been taken to incorporate short and long range improvements to the HISS with the objective of producing an artificial icing environment which duplicates as close as possible the natural icing environment. Short range improvements have been incorporated and tested under limited conditions, results of which have been encouraging. The most significant improvement has been the incorporation of Sonic nozzles, which have reduced the Mean Volumetric Diameter (MVD) of the water droplet size in the HISS

DRDAV-DI 23 JAN 1980

SUBJECT: Directorate for Development and Qualification Position on the Final Report, Microphysical Properties of Artificial and Natural Clouds and Their Effects on UH-1H Helicopter Icing, USAAEFA Project Number 78-21-2

plume from a relatively constant concentration of 200 microns to 40 microns. Results of the short range improvement will be evaluated extensively during the 1979/1980 icing tests.

FOR THE COMMANDER:

CHARLES C. CRAWFORD, JR.
Director of Development
and Qualification

TABLE OF CONTENTS

INTRODUCTION

BACKGROUND

1. The Army's requirement for an all-weather operational capability in its helicopter fleet has resulted in an extended test program designed to provide a data base and establish equipment requirements to meet this need. This icing test program was a two-phase effort designed to satisfy the research and development (R&D) objectives of the Federal Aviation Administration (FAA) and the US Army Aviation Research and Development Command's Applied Technology Laboratories (ATL), and to provide qualification data for the UH-1H equipped with the Bell Helicopter Textron (BHT) partial ice protection system ("Kit A").

2. It was anticipated that while the UH-1H equipped with "Kit A" would be severely limited due to the lack of a rotor blade deicing system, an envelope could be developed which would provide a limited capability to operate in light icing conditions. An icing severity level indicator system would be provided to allow the crew to assess the icing environment and its effects on helicopter operations.

3. Under prior contracts, the ATL had developed an icing research aircraft (JUH-1H) equipped with an ice protection system for the investigation of the icing environment and its effects on helicopter operations. This aircraft was utilized during this test program to continue those investigations and provide an extended data base for both ATL and FAA.

TEST OBJECTIVES

4. The objectives of this test were three fold:

a. Qualify the "Kit A" equipped aircraft for intentional flight into icing conditions. Define the limits of the "Kit A" aircraft's ability to operate in icing conditions quantitatively in terms of liquid water content (LWC), outside air temperature (OAT) and time of exposure.

b. Collect data in simulated and natural icing conditions to form a valid data base upon which to establish icing certification and operations requirements for helicopters operating with ice protection systems.

c. Acquire R&D related icing test data for better understanding of the icing environment, its effects upon helicopter performance, handling qualities, and ice protection system requirements.

DESCRIPTION

5. The test JUH-1H helicopter, serial number 70-16318, was manufactured by Bell Helicopter Textron (BHT). A detailed description of the standard UH-1H helicopter is contained in the Operator's Manual (ref 1, app A). The test aircraft was modified by the installation of an electrothermal deice system and a partial ice protection system ("Kit A"). These systems are described in detail in appendix B and references 2 and 3 of appendix A. The Helicopter Icing Spray System (HISS)

used to provide the artificial icing environment is also described in appendix B and reference 4 of appendix A. A detailed listing of test instrumentation installed in the aircraft is contained in appendix C with a description of unique equipment contained in appendix B.

TEST SCOPE

6. Artificial icing tests, utilizing the HISS, were conducted in the vicinity of St. Paul, MN, from 22 January through 22 February 1979. A total of 12 artificial icing flights were conducted consisting of 6.7 hours in the HISS plume. In addition, 8 natural icing flights were conducted during this time for a total of 6.3 hours in natural ice. Further natural icing tests were conducted in the vicinity of Syracuse, NY from 26 February to 21 March 1979. These tests consisted of 7 flights for a total of 1.5 hours in natural ice. The artificial icing tests were conducted at a liquid water content (LWC) range of 0.25 to 0.90 grams per cubic meter ($^{gm}/m^3$) and an ambient temperature range of -10 to -20°C. Natural tests were conducted at a LWC range of 0.06 to 0.23 $^{gm}/m^3$ and an ambient temperature range of -2.5 to -22°C. A summary of the test conditions is contained in tables 1 and 2. The target airspeed during the icing tests was 90 knots true airspeed (KTAS) with a constant rotor speed of 324 rpm. Takeoff gross weight was approximately 8550 pounds with a mid longitudinal cg station of 138 inches. Flight limitations contained in the operator's manual and the safety-of-flight release (ref 5, app A) were observed throughout the testing.

TEST METHODOLOGY

7. The initial flights under artificial icing conditions were used to verify proper operation of the blade deice system which was to be used as a safety device during the remaining flights. After operation was confirmed by the hub-mounted camera and the chase aircraft, flights were utilized to accumulate the maximum amount of ice on the airframe and rotor system. This was accomplished by maintaining position in the HISS plume or the natural icing environment until one of the following conditions was experienced: excessive torque rise (5 psi), asymmetric main rotor shed as evidenced by an increase in lateral vibrations, or visibility totally obscured by ice accumulation on both windshields. Data were recorded by hand, oscillographs, and on magnetic tape.

Table 1. Artificial Icing Summary

Flight Number	Programmed LWC[1] (gm/m^3)	Outside Air Temperature (°C)	Relative Humidity (%)	Immersion Time (Minutes)	Maximum IRU[2] Counts	Time To Ice Pilot's Windshield (Minutes)	Time To Ice Copilot's Windshield (Minutes)
2	0.25	-10	79	5-1/2 15 17	294 760 186	N/A[3]	N/A
3	0.25	-15	79	56	1064	47	39
4	0.50	-15	79	22-1/2 1-1/2	1134 83	16	22-1/2
5	0.25	-20	39	4-1/2	406	N/A	N/A
6	0.25	-10	53	51-1/2 19	392 68	N/A	N/A
8	0.25	-20	45	44	1024	N/A	N/A
9	0.50 ≈0.90	-20	45	30 5-1/2	759 9	21	28
10	0.25 0.50	-15	60	49 9	429 79	43	53-1/2
13	0.50	-10	20	10	339	N/A	N/A
18	0.50	-17	78	19-1/2	1343	16	19-1/2
21	0.25	-10	36	53	1516	N/A	N/A

[1] LWC = Liquid water content
[2] IRU = Integrating rate unit
[3] N/A = Not applicable

Table 2. Natural Icing Summary

Flight Number	Outside Air Temperature (°C)	Rosemount LWC[1] (gm/m^3)	Leigh LWC (gm/m^3)	ASP[2] LWC (gm/m^3)	Immersion Time (Minutes)	Maximum IRU[3] Counts	Torque Rise (PSI)
7	-12	0.07	0.10	0.14	21-1/2	265	5.4
		0.05	0.08	0.11	28-1/2	215	3
14	-7.5	0.10	0.14	0.06	26-1/2	502	
		0.12	0.13	0.11	14	334	None
		0.15	0.15	0.14	3	82	
15	-7	0.12	0.14	0.15	31-1/2	644	None
		0.06	0.08	0.10	35	391	
17	-8	0.07	0.10	0.10	34	398	2
	-9	0.06	0.08	0.10	18	212	1.5
19	-3.5	0.22	0.34	0.13	17-1/2	1015	4.1
	-3	0.22	0.29	0.13	23	1015	1
	-2.5	0.18	0.25	0.11	48	1387	1
20	-3	0.24	0.31	0.21	16-1/2	708	3.5
	-3	0.23	0.35	0.23	15-1/2	830	3.5
	-2.5	0.12	0.26	0.17	43	1545	None
23	-6	0.21	0.26	0.23	29-1/2	1134	4.4
	-5.5	0.13	0.21	0.21	14-1/2	368	1.3
24	-0.5	0.09	0.15	0.16	12	186	None
26	-3.5	0.10	0.14	0.12	43	789	None
27	-3.5	0.07	0.17	0.11	12	311	None
28	-22	0.03	0.15	0.06	10	194	None

[1] LWC = Liquid water content
[2] ASP = Axially scattering probe
[3] IRU = Integrating rate unit

RESULTS AND DISCUSSION

ARTIFICIAL ICING ENVIRONMENT

General

8. The United States Army has utilized the HISS since 1974 to provide an artificial icing environment in which to evaluate helicopter icing characteristics and operation of ice protection systems. It is apparent from visual observation of the HISS plume and the associated ice accretion on the test aircraft that this type of testing is susceptible to a number of variables. The plume is a heterogeneous medium which appears to vary with cross sectional position, horizontal distance from the source, humidity of the ambient air, and HISS flow rate. These anomalies have led to considerable discussion concerning the adequacy of the artificial cloud as a representation of natural conditions.

9. Using the laser nephelometers installed on the test aircraft, much of the test effort was directed at evaluating the microphysical characteristics of the natural and artificial icing environment. These characteristics, which included concentration of cloud droplets, droplet size distribution, and liquid water content, were then related to the physical characteristics which were observed in the environment and ice accretion on the test aircraft. Complete data obtained during testing is contained in references 6 and 7 of appendix A with representative figures contained in appendix E.

Relative Humidity Effect

10. The effects of relative humidity (R_H) were readily apparent during this testing where humidity extremes ranged from 20 to 80%. The variations were evidenced by plume density, formation of a visible wake from the HISS (photo 1), and variations in ice accretion on the test aircraft. Under high humidity conditions the HISS plume visual density increased sufficiently to require instrument flight while immersed, and the HISS rotor and fuselage produced a clearly visible wake.

11. These characteristics may be explained by examination of the typical droplet size distributions shown in figure 1, appendix E. Due to a difference in probe compliment on these two occasions, a comparison of spray characteristics for droplet sizes larger than 45 micron (μm) is not possible. This distribution displays a marked increase in the number of small droplets ($<15\mu$m) at 78% R_H over a comparable distribution obtained at 36% R_H. This increase is attributed to two phenomena associated with the high humidity. First, high humidity reduces the evaporation of the small droplets due to the relatively small difference between partial pressure of the water vapor at the surface of the droplet and the ambient air. Second, the high moisture content leads to a relatively unstable air mass with respect to cloud formation. When this air mass is disturbed by the addition of energy, introduction of a low pressure area (adiabatic cooling) from the CH-47 rotor or fuselage, or the addition of water vapor by the spray boom, very small cloud droplets ($<15\mu$m) form. Other variables such as ambient temperature and/or HISS flow rate settings may also be involved.

Photo 1. HISS Rotor Wake Under High Relative Humidity

12. This abundance of small droplets then forms the opaque cloud due to light scattering and extinction effects which are not present in larger droplet clouds of equal LWC. Hence the occurrence of visual obscurity (instrument meteorological conditions (IMC)) in the plume, which was experienced with high relative humidity. The small droplet has relatively low momentum compared to the aerodynamic forces and thus is free to follow the streamline avoiding impact with the obstruction, except at the stagnation point in the flow. Thus the cloud which has the greater proportion of its mass composed of small droplets will generally produce less hazardous icing conditions due to failure of most of the droplets to impact the aircraft structure.

13. The reduction in ice accretion witnessed during testing under high relative humidity cannot be directly attributed to the increase in small droplet density since there is little evidence to indicate that the concentration of large droplets changes during relative humidity variations. The probable cause was the location of the test aircraft in the HISS plume. Under the high humidity conditions the aircraft was flown under IMC conditions, indicating the aircraft was located in the upper half of the plume and the major portion of the droplets encountered were of small size (see paragraph 17). Thus the high humidity environment generally results in an increased concentration of smaller droplets which leads to a reduction in ice accretion.

Range Effect

14. The first of the variables that can be controlled is the range or stand-off (horizontal) distance behind the spray boom. The range of interest is from 150 to 250 feet since the test aircraft encounters the fully developed HISS rotor wake at greater distances, while safety aspects and station keeping tasks become unacceptable at distances closer than 150 feet. The longitudinal cloud appearance within this range was relatively constant and station keeping was normally accomplished at 200 ±25 feet. To evaluate the effects of location in the vertical plume, vertical sweeps were conducted at 150, 200, and 250 feet behind the HISS. Typical droplet concentrations from 150 and 250 feet sweeps are shown in figure 2. It is apparent that the stand-off distance does not materially affect the cloud composition. Increased distance would be expected to have two consequences. First, the concentration of small droplets, with large surface area to mass ratio, should be reduced due to evaporative effects. This is realized to a slight degree in that at 250 feet the concentration of 10 to 15μm droplets has been reduced. The second effect should be dilution or dispersion of the plume with increased distance from the source, however, this result was not realized.

Flow Rate Effect

15. The second variable over which the test team has control is the water flow rate of the HISS. The system has the capability of producing flow rates up to 110 $^{gal}/_{min}$ (approximately 0.9 $^{gm}/_{m^3}$). The effects of flow rate were evaluated by conducting a vertical plume sweep at 150 feet stand off distance with flow rates necessary to produce LWC of 0.25, 0.50 and 0.75 $^{gm}/_{m^3}$. Typical droplet concentration profiles for 0.25 and 0.75 $^{gm}/_{m^3}$ are contained in figure 3.

16. Two results are readily evident. First, the concentration of droplets less than 50μm is relatively unchanged and second, the concentration of larger droplets has been increased by approximately two orders of magnitude at the higher flow rate.

This indicates that the nozzles used in the current HISS configuration have a limited capacity to produce small droplets and that this capacity is saturated at all flow rates of interest. Hence increasing the flow rate produces an increased concentration of large droplets, resulting in a more unrealistic representation of the natural icing environment (see paragraph 21).

Plume Position Effect

17. The third controlled variable is the test aircraft position in the HISS plume. The plume appears to vary in density from top to bottom with extreme variations laterally. These variations were evaluated by sweeping the plume both vertically and laterally at 150 feet stand off distance. The variations were so large and erratic during the lateral sweep that no meaningful conclusions could be drawn. Typical data from a vertical sweep is shown in figures 4 and 5. The envelope of mean volumetric droplet diameters (see paragraph 18, appendix D) clearly displays the gravitational sorting effect, which results in the majority of the large droplets lying in the lower third or below the visible plume.

18. Since the LWC is proportional to the mass of the droplets, and the mass is a function of the third power of the diameter, we find the plume variations are greatly magnified with respect to LWC. From figure 5 it becomes apparent that the LWC calculated from the HISS flow rate may be exceeded by a factor of five at some points in the plume. These extreme variations in LWC may result in localized areas of either the fuselage or rotor system experiencing different icing environments, thus reducing the validity of the simulation.

Artificial Versus Natural Cloud

19. Prior to discussing this comparison of artificial and natural environments, it should be understood that the data presented in figure 6 was obtained at peak concentrations during artificial plume sweeps and natural icing encounters. The artificial cloud data represents a calculated 0.25 $^{gm}/m^3$ HISS plume and the natural conditions are a nonprecipitating stratus cloud with an average LWC of 0.16 $^{gm}/m^3$. There are several pertinent points to be observed from this comparison. First, this data is presented in terms of droplet mass to provide a more representative indication of conditions that influence ice accretion as explained in appendix D. The natural cloud produces a characteristic peak in droplet concentration at approximately 15μm and then trails off rapidly to a maximum droplet size of approximately 90μm. The HISS plume reaches an initial peak concentration an order of magnitude lower at a droplet size of approximately 60μm and the concentration remains relatively constant to 200μm before trailing off with a maximum droplet size of approximately 300μm. The HISS plume is not a valid representation of the nonprecipitating natural cloud and the physical aspects of these droplet size distributions suggest that the natural cloud with its small droplets presents less severe icing conditions. This is due to the small particles' inability to impact the airfoil and aircraft structure as discussed in paragraph 12. On the other extreme the entire HISS droplet distribution is of sufficient size to impinge on the aircraft resulting in most cases in a more severe icing environment.

NATURAL ICING ENVIRONMENT

General

20. Since the HISS plume was not an accurate simulation of the natural environment an attempt was made to maximize exposure to the natural environment. The laser nephelometers provided a tool to evaluate the low altitude cloud structure that is encountered by rotary wing aircraft. The cloud formations encountered in St. Paul area were of the stratus type with bases at 1000 to 2000 feet above ground level (AGL) and tops to above 12000 feet. The icing conditions usually existed in relatively thin layers of 500 to 1000 feet thick. In the Syracuse area the phenomena of "Lake Effect" was encountered and the resulting cloud formations, laden with moisture from the Great Lakes, usually produced snow. The icing conditions encountered in Syracuse were noticeably different from those of the St. Paul area, with the major differences in the LWC and structure of the layers.

21. The data obtained from the natural encounters produced "text book" distributions and leads to the conclusion that the stratus type formation has a fairly uniform composition throughout the altitude range of interest to the rotary wing community. In these tests the natural icing conditions in stratiform clouds were generally encountered in defined layers. This suggests the possibility, subject to further experimental confirmation and definition of the controlled environment, of reduction in the impact of icing conditions on operational capability. Since this layered structure allows the crew to vacate the icing conditions with a climb or descent.

Droplet Size

22. As with most natural processes, the natural cloud droplet size approximates a Gaussian distribution (ref 8 and 9, app A). The distributions are right skewed (tail extending towards the large radii). A typical distribution from a stratus nonprecipitating cloud encountered during this testing is shown in figure 7. The curve exhibits peak numerical concentration at approximately 10μm.The same data is presented in terms of mass concentration in figure 8. As can be seen the shape of the curve remains unchanged but the peak is moved toward the larger droplet size of 15μm. This results from the weighting of the numerical concentration by the radius cubed to present a distribution more compatible with the mass contained in the cloud (app D).

23. A typical time history of the mean volumetric diameter (MVD) for an icing flight is presented in figure 9. While variations are encountered throughout the cloud the fluctuations were relatively small ($\pm$3μm) with the MVD of all clouds encountered falling between 10 and 30μm. All clouds sampled were of the stratus type with the exception of one nimbostratus penetrated for approximately 15 minutes.

Liquid Water Content (LWC)

24. Figure 10 shows the LWC's for the cloud with MVD depicted in figure 9. The values of LWC associated with the sampled droplet spectra show much less correlation and can change radically within an individual cloud. This occurs partly because the density of a cloud varies greatly and partly because the LWC of the droplet is dependent upon the third power of the droplet diameter. Thus, a slight

shift in the droplet spectrum to larger particle sizes can cause a pronounced increase in the associated LWC. The most drastic peaks shown in the individual detectors are probably the result of a statistically insignificant, chance occurrence of a large droplet.

25. Two major points are evident from this data; first, the agreement between the individual sensors is quite good when consideration is given to the fact that all occupied different locations on the aircraft and thus experienced varying flow fields. Second, the drastic and rapid fluctuations inherent to the natural environment render the LWC (icing rate) detector of little use to the pilot in determining an operational icing envelope. This point is further emphasized by the fact that icing rate appears to have little correlation with the operational degradation in the helicopter. The degradation is a result of total ice accumulation.

26. The time history of LWC in figure 11 shows that the formerly well behaved indications of figure 10 have developed considerable scattering. The data for figure 10 was obtained at -6°C while that for figure 11 was at -3.0°C. This is a common characteristic of all ice detectors that depend on ice accretion and is the result of a phenomenon known as the Ludlam limit which will be further discussed in the section on ice detector operation (para 53). The MRI detectors were not accretion devices and thus were considered the standard.

Natural Cloud Comparison

27. An indication that the natural cloud data collected during this testing was typical, is shown in figure 12. The cloud was a nonprecipitating stratus type with an average LWC of 0.16 gm/m^3. The comparison cloud was obtained by University of Wyoming cloud physicists in 1977 (ref 10, app A) and was the very early stage of a convective type with LWC that reached 0.44 gm/m^3. The peak concentrations and particle sizes are almost identical and conform to the values contained in many cloud physics texts (ref 8 and 9, app A). The major difference in the two clouds is the higher concentration of large droplets contained in the test cloud which indicates a more mature formation. The maturity of the cloud increases the larger droplets through collisions and coalescence of the smaller droplets.

Cloud With Freezing Rain

28. A nimbostratus cloud formation encountered on 14 March 1979 near Syracuse produced the distribution in figure 13. The cloud was a typical stratus layer with a broken scud layer and occasional snow flurries underneath. The data showed two distinct droplet concentrations. The smaller droplets are the nonprecipitating cloud which produced IMC. The concentration of larger droplets begins at approximately 150μm and increases in number until the 2100μm (2.1 mm) capacity of the cloud particle spectrometer (CPS) is exceeded. This represents the rain that was encountered. These conditions were accompanied by moderate turbulence with vertical currents resulting in climb and descent rates up to 750 ft/min. The flight was terminated after 15 minutes due to the severity of the conditions; however, no adverse flight characteristics were experienced due to ice formation. It should be noted that the HISS plume as represented in figure 6, had a relatively constant droplet concentration between 50 and 200μm. Therefore it must be concluded that the HISS cloud is not an accurate representation of either the natural icing cloud or freezing rain. Rather it approximates a freezing drizzle.

29. A representation of the MVD (figure 14) indicates that this precipitating cloud contained a mean volumetric droplet size of 400 to 1000μm. The high LWC's of this cloud are shown in figure 15. The combination of these two factors produce the severe icing conditions usually associated with freezing rain.

Snow

30. One hovering flight of 45 minutes duration was conducted in heavy blowing snow (3/4 to 1 1/4 in/hr). The ambient temperature was -3°C with a visibility of 3/8 mile and a ceiling of 100 feet obscured. The primary purpose of this flight was to determine the possibility of the engine inlet screens becoming blocked by accumulated snow. The left inlet screen was packed with blowing snow prior to starting the aircraft; however, after 45 minutes of hover the snow had been removed by the air flow through the screen. It was concluded that flight in snow may be conducted safely at temperatures down to -3°C with the inlet screens installed. The secondary objective of this test was to evaluate the snow accumulation characteristics of the helicopter. No appreciable accummulation was found on any components and the windshields remained clear utilizing the bleed-air defog system. The overall conclusion was that flight in heavy snow, at temperatures down to -3°C, does not appear to present a significant icing problem. The hazards of flight in heavy snow are a result of the severely restricted visibility compounded by the white-out, and resultant loss of visual reference, usually experienced during landing and take-off.

AIRCRAFT ICE ACCRETION CHARACTERISTICS

General

31. Ice accretion characteristics were observed and documented during all artificial and natural testing. Ice accumulations were photographed and measured at the termination of each flight where ambient conditions allowed retention of ice during return to the airfield. It must be realized that due to sublimation, these residual ice formations may not be accurate indications of the size and shapes of the ice that was actually accreted in the cloud. The ice accumulation characteristics under both natural and artificial conditions were similar with the major differences occuring in ice texture and thickness. The HISS formations were larger and of a more granular texture than those produced by natural conditions. Significant variations will be discussed in the applicable sections.

Forward Areas

32. The forward fuselage and all protrusions that provided a stagnation point had increased accretion rates because of the impacting of all size droplets (photo 2). Maximum accumulations behind the HISS reached 4 inches on the Rosemount detector mounting stand and 3 inches on the pitot tube and shark fin antenna (photo 3). Accretion was first noticed on the windshield wiper arms (photo 4 and 5) and the OAT probe with both providing similar indications of ice accumulation. The battery vent located on the nose of the aircraft accumulated ice readily which resulted in partial blockage (photo 6). Under more severe icing conditions, the possibility exists for total blockage, and a resultant battery explosion.

Photo 2. Ice Accumulation on Cabin Roof (38 min in HISS Plume with LWC of 0.25 g/m^3 and -10°C).

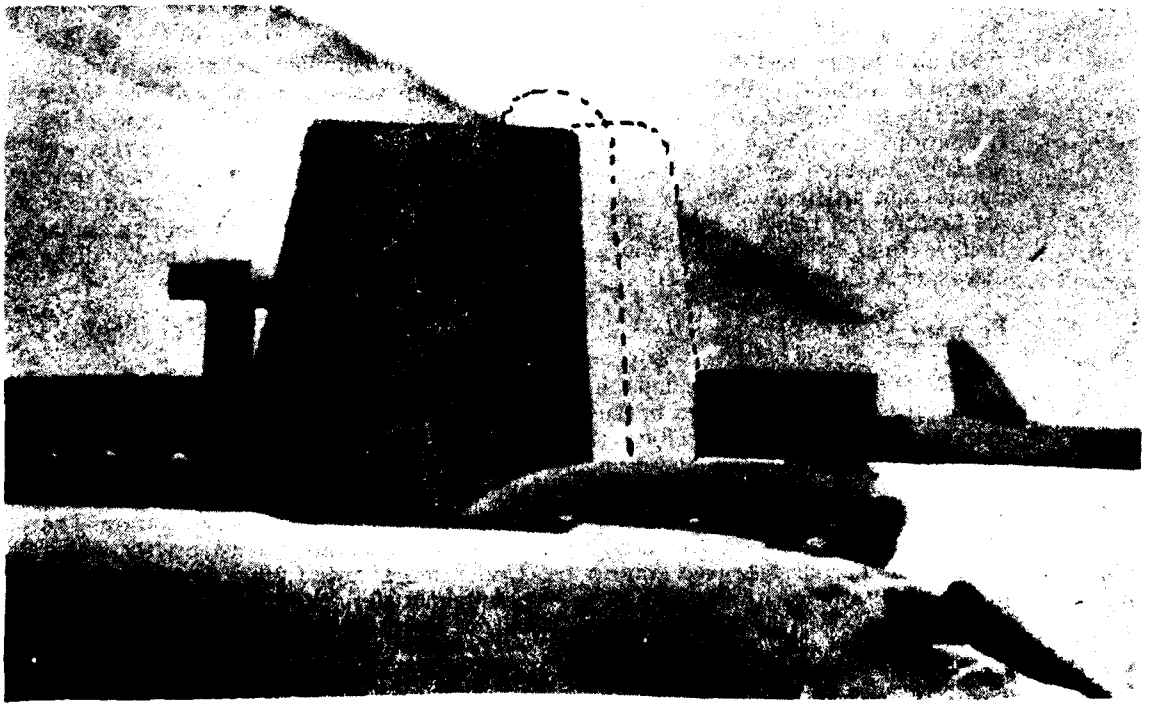

Photo 3. Ice Formation on Shark Fin Antenna (88 min in Natural Cloud with LWC of 0.025 to 0.32 g/m^3 and -3°C)

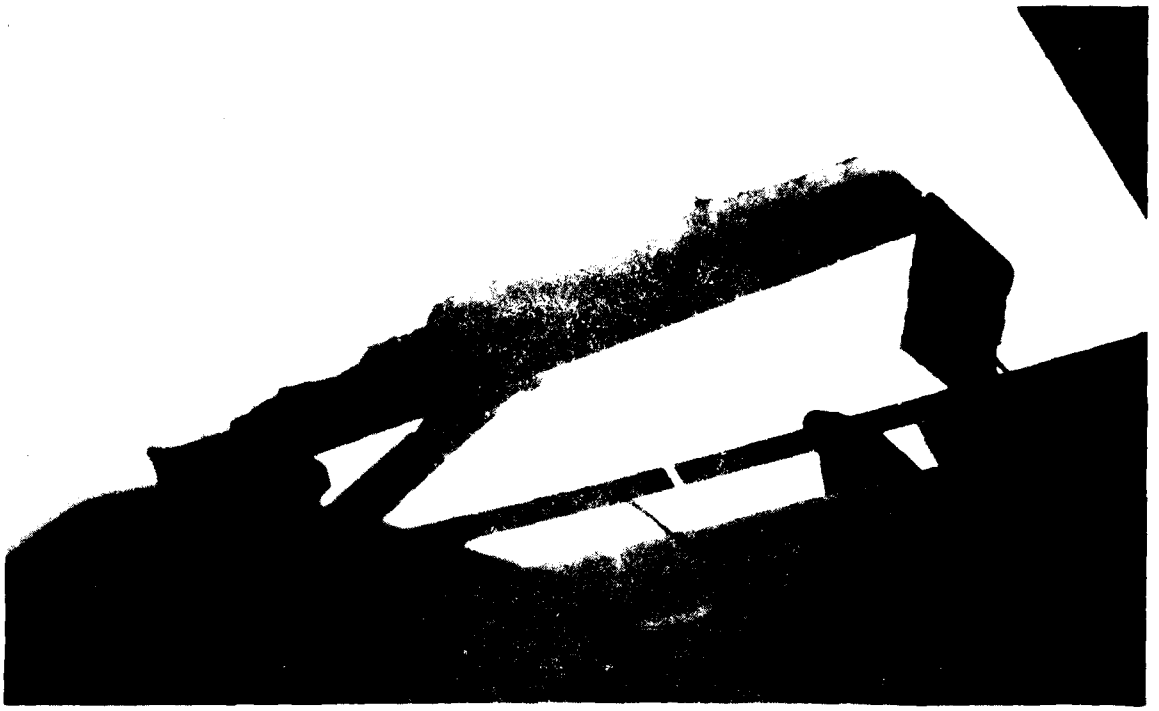

Photo 4. Ice Accumulation on Windshield Wiper Blade (44 min in Natural Cloud with LWC of 0.22 to 0.25 [illegible] m^3 and -6°C).

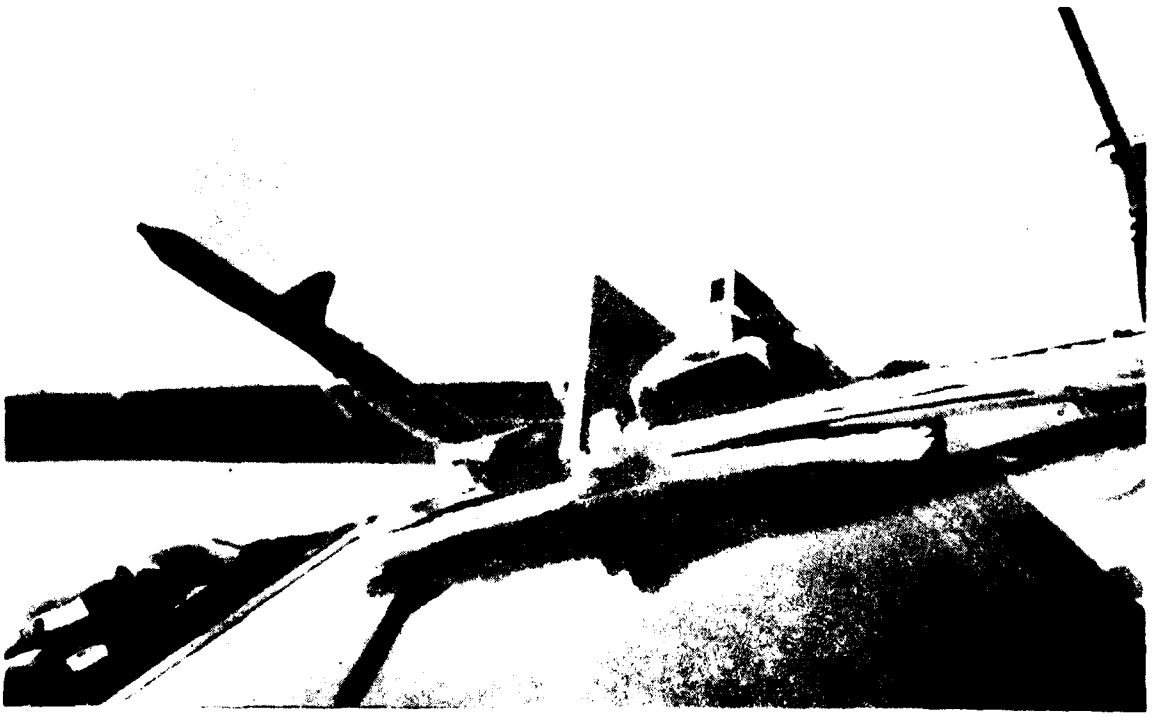

Photo 5. Ice Formation on Windshield Wiper Assembly (52 min in Natural Cloud of 0.08 to 0.[illegible] and -8°C).

Photo 6. Ice Accumulation on Battery Vent (38 min in HISS Plume with LWC $0.25^{gm}/m^3$ and -10C).

Side Areas

33. The sides of the fuselage showed little tendency to accummulate ice with maximum accretions less than 1/16 inch on the fuselage skin. The engine inlets displayed a tendency to collect ice in the natural environment (photo 7) but not under artificial conditions. This is to be expected since the large droplets high momentum prevents their following the streamline into the screens. The small droplets of the natural cloud readily follow the flow through the 90° turn and collect on the screen. The accummulation was minor under all conditions tested and presented no pressure drop across the screens. It appears that blockage of the inlet screens due to icing is only a remote possibility.

Rotating Components And Flight Controls

34. The maximum accumulation of ice on the flight controls occurred on the stationary swashplate and approached 1 1/2 inches (photo 8). The rotating components and rotor head accreted ice to a maximum thickness of approximately 3/8 inch which presented no problem (photos 9 and 10). The interaction between the rotating and fixed components and the movement caused by control inputs effectively dislodged ice from components that may have otherwise been restricted by its formation; however, full control travel was not attempted. Large ice accretions were also encountered on the unheated balance weights and stabilizer bar on several occasions (photo 11). This could be a problem due to increased centrifugal loads or the possibility of an asymmetric shed, leading to structural or rotor stability problems.

Aft Area And Tail Rotor

35. The aft fuselage, tail boom, and tail rotor exhibited negligible ice accretion (photo 12). High speed photography verifies that, at the airspeeds tested, the rotor downwash carries the exhaust plume along the tail boom and into the vertical fin and tail rotor. This effect together with kinetic heating on the tail rotor resulted in minimum surface temperatures of -8.5°C with ambient conditions as low as -20°C. These warmer temperatures coupled with the much higher centrifugal loads (approximately 4.5 times as great as those of the main rotor) appear to negate any serious icing effects on the tail rotor.

36. The only aft area that showed any tendency to accrete ice was the horizontal stabilizers. They accreted ice along the leading edge with maximum thickness to 3/4 inch (photo 13). The right stabilizer consistently accreted larger amounts of ice than the left due to the skewed flow of the downwash which caused greater impingement of the exhaust gases and warmer temperatues on the left stabilizer.

Blades

37. Due to the high rotational velocity, it was anticipated that the main rotor would be the limiting component during icing flight. However, under most conditions tested the main rotor exhibited a symmetric shed tendency which did not adversely affect the aircraft characteristics (photo 14). The point at which the natural symmetrical shed occured was a function of the ambient temperature. The ambient temperature at the blade surface was increased by kinetic heating and the latent heat of fusion from the impinging water droplets. The resultant freezing point

Photo 7. Ice Accumulation on Right Engine Inlet Screen (44 mm) in Natural Cloud with LWC [illegible] and -7 C.

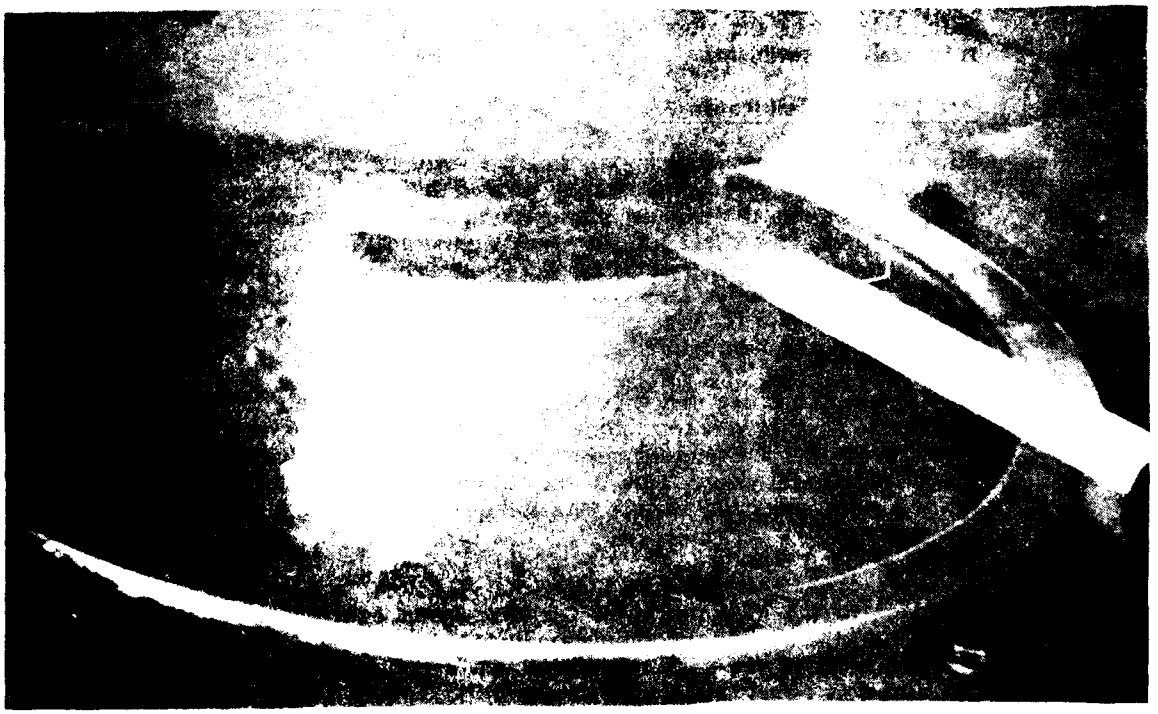

Photo 8. Ice Accumulation on Stationary Components (24 mm) in HSS Plume with LWC [illegible] and -15 C.

Photo 9. Ice Accumulation on [illegible] components (24 min in HISS Plume with LWC of 0.5 [illegible] and -15°C).

Photo 10. Ice Formation [illegible] Natural Cloud with LWC of [illegible] (-15°C).

Photo 11. Ice Accumulation on Stabilizer Bar and Weights (88 min in Natural Cloud with LWC of 0.25 to 0.32 $^{gm}/m^3$ and -3°C).

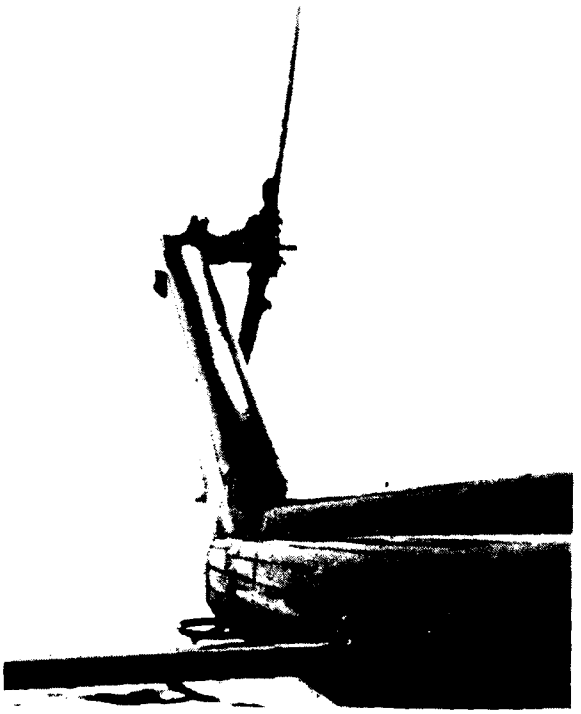

Photo 12. Ice Accumulation on Vertical Fin (52 min in Natural Cloud with LWC 0.08 to 0.09 $^{gm}/m^3$ and -8°C).

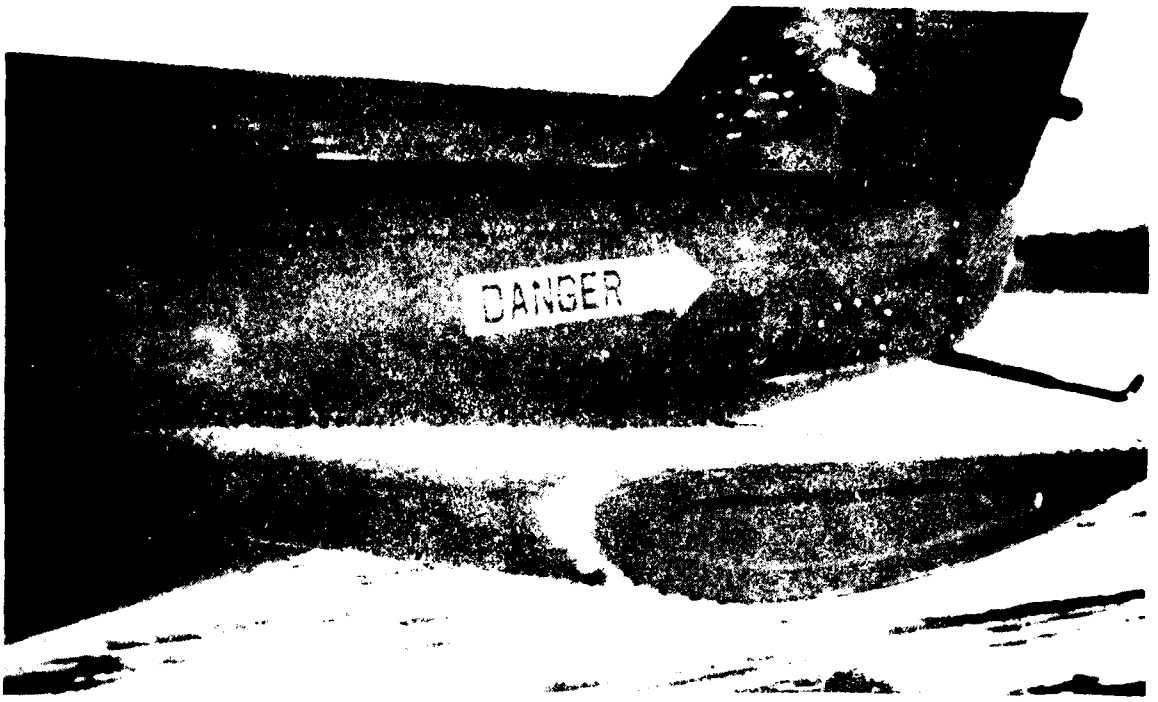

Photo [illegible] Hospital S[illegible] HESS Plane with [illegible]

Photo [illegible] HESS Plane with

on the blade span would be the anticipated limit of ice formation (figure 16). The actual shed point occurs inboard of this location due to the centrifugal forces of the rotor exceeding the surface adhesion forces of the ice formation.

38. A total of 13 test runs were conducted during 8 natural flights, resulting in a main rotor asymmetric shed on 6 occasions. These sheds increased the airframe vibration level from 1 to approximately 4 on the vibration rating scale (VRS) (App D, fig 1). The data from these flights produced poor repeatability and showed little correlation between the variables of LWC, OAT, Integrating Rate Unit (IRU) count and time to the shed point. The times required to reach the asymmetric shed point varied from 15 1/2 to 34 minutes and appeared to be related to OAT as shown in figure 17. These data produce little concrete evidence, when it is considered that less than 50% of the natural encounters produced an asymmetric shed. The fact that all but one of the asymmetric sheds occured at IRU counts greater than 700 would indicate the IRU's usefullness in determining an icing envelope for the unprotected blades. This type of device should be included in future testing.

39. In an effort to determine the cause of asymmetric shedding, several possible contributions are suggested. The first would be a discontinuity in the surface adhesion of the ice layer. This may be caused (among other things), by surface irregularities, impurities in the ice or contaminants on the surface of the blade. Once the discontinuity is initiated, it becomes a "stress riser" under the action of the centrifugal loads and leads to a shed from the discontinuity outboard. In an attempt to minimize this effect, the blades used were cleaned thoroughly with naptha or isopropyl alcohol prior to each flight.

AIRCRAFT PERFORMANCE AND HANDLING QUALITIES

General

40. Prior testing had indicated a number of problem areas to be expected during icing encounters. In addition to the asymmetric shed problems previously discussed, it was anticipated that problems would be encountered in the form of excessive torque rises, degradation of autorotational RPM, and stability and control. It is noteworthy that the major difficulties previously encountered in the areas of torque rise and autorotational degradation had been during artificial conditions. This appears to have been a more severe condition, which probably explains the absence of similar problems in this testing.

Torque Rise

41. A major concern was the torque increase experienced due to the effects of ice accretion on the main rotor blades with minor contributions from the increased parasite drag and additional weight of the fuselage. The major component of the increased power requirements by the main rotor is from added profile drag caused by ice accretion on the airfoil. Since profile power requirements are a function of radius cubed it would be expected that the greatest torque rise should occur at low ambient temperatures where surface adhesion of the ice is greatest and spanwise accretion is the largest.

42. This theory could not be verified during these tests due to extremely low LWC at the colder temperatures. In artificial conditions the torque rise was masked by the fuel burn-off and the power variations required to maintain positioning in the plume. Torque rises were encountered on some flights; the most severe occuring under natural conditions with an OAT of -12°C and LWC of 0.1 $^{gm}/m^3$ and OAT of -6°C and LWC of 0.21 $^{gm}/m^3$. Under artificial conditions a torque rise was encountered at an OAT of -10°C and LWC of 0.25 $^{gm}/m^3$. Figure 18 shows a torque requirement decrease after a deice cycle; however, the magnitude was not sufficient to be detected on the cockpit instrumentation. The torque rise noted in the time history is a result of the high power requirement placed on the 30 KVA alternator by the deice system.

Autorotational Capability

43. Another major hazard discovered during prior testing, was degradation of the ability to maintain autorotation RPM after exposure to icing. Extreme cases indicate that it may be impossible to maintain rotor speed within normal autorotational limits after icing encounters which result in torque rises greater than 10% of available power. This condition results from alteration of the airfoil section, with resultant loss of maximum lift and increased drag due to ice accretion. It was anticipated that this phenomenon would be prevalent at the warmer temperatures which result in maximum ice accretion near the root of the blade, since the inner radius of the blade provides the driving torque during autorotational descent.

44. This condition could not be duplicated during this testing. The maximum decrease in autorotational RPM during this testing was 20 RPM, leaving the autorotational RPM (294 to 324) well within the recommended operational range. It was also noted that entry into autorotation in many cases resulted in a partial or total shed of the accumulated ice. This was probably due to the change in stagnation point and resulting pressure distribution changes fracturing the ice which allowed the centrifugal force to overcome the adhesion force. This is aided by the change in coning angle and flap bending induced by the RPM and thrust change during autorotational entry.

Stability and Control

45. The stability and control characteristics of the helicopter were qualitatively evaluated throughout the test program with no apparent variations noted. It is to be expected that some changes could occur, especially at the extremes of the operational envelope. Since this program did not investigate the envelope extremes, these changes could not be confirmed.

EQUIPMENT OPERATION

General

46. The equipment that was evaluated during this testing consisted of the blade deice system, the ice detection systems and the "Kit A" components with particular emphasis on the heated windshield. Although the blade deice system's primary purpose was safety, its operation was closely monitored to provide data concerning this unique system (chordwise heater blankets). The ice detectors and LWC displays

were evaluated as a possible low-cost means of providing the pilot instrumentation to follow an operational envelope for the unprotected aircraft. The "Kit A" components were evaluated for possible installation of the Army UH-1 helicopter fleet. The major benefit to be gained from the "Kit A" installation was to be the heated windshield and ice detector. The following parapraphs discuss the results obtained in each of these areas.

Blade Deice System

47. The blade deice system was operated in the manual mode with temperature and LWC inputs selected through the cockpit controls. As discussed in appendix B, the heater ON times were fixed at the optimum values determined in prior testing. At temperatures warmer than -20°C, the system functioned properly under both natural and artificial conditions with ambient temperature and moderate icing level selected as inputs. On two occasions (one natural and one artificial), at -20°C and colder, the heater elements failed to remove accumulated ice from the blades with the above procedure and required a false temperature input signal of -30°C prior to successful operation. This indicates that the present heater ON schedule provides insufficient heat to overcome the increased surface adhesion of the ice at temperatures of -20°C and colder.

48. The normal test procedure utilized the blade deice system to remove residual ice from the blades after an asymmetric shed had been experienced (photo 15). The out-of-balance condition was usually relieved within 3 to 4 zones of the deice cycle indicating the point at which the ice accumulation was again balanced and hence the point at which the asymmetric shed had occurred. A typical time history of a deice cycle and the associated blade surface temperatures is shown in figure 19. The time lag between power application and peak temperature is a function of the thermal conductivity and thickness of the blade nose cap, and the differential between the ambient skin temperature and the heating element temperature. These factors are constants except for blade skin temperature which is a function of the relative velocity of the air with respect to the blade surface and other factors as discussed in paragraph 37. The time lag proved to be a minor factor when compared with the heating element ON times.

49. The reliability of the deice system was acceptable during this year's testing with two broken wires causing the only malfunction in more than 30 cycles (approximately 50 flight hours).

Ice Detection Systems

50. The operation and accuracy of all onboard ice detectors were evaluated by comparing time histories of natural and artificial encounters with LWC's calculated from the MRI laser nepholemeter droplet distribution data. The MRI calculations are discussed in appendix D. Under artificial conditions data from both the Leigh and Rosemount detectors (to include the IRU) were not useable in that the indications were erratic and provided poor correlation. These anomalies were to be expected considering the HISS droplet size.

51. This phenomona may be partially explained by close examination of the equation governing the mass of ice accreted on a given area

$$M = \eta LVt\ F\ A$$

η = collection efficiency (nondimensional)

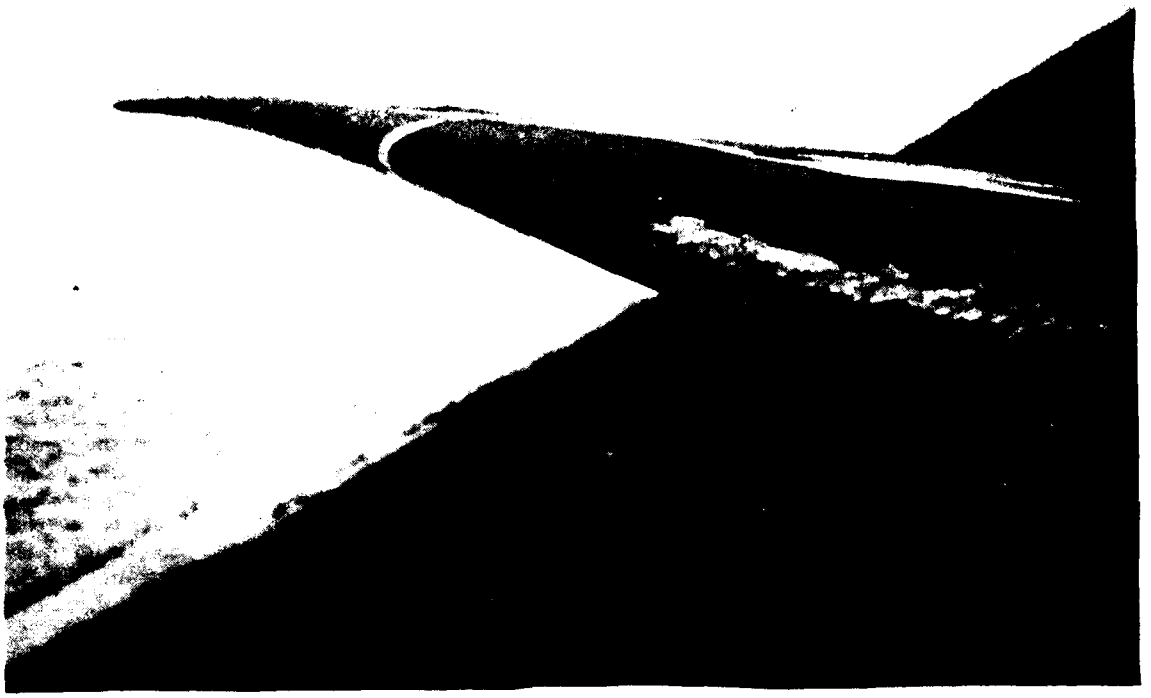

Photo 15. Blade Ice Remaining after 3 Deice Cycles (88 min in Natural Cloud with LWC of 0.25 to 0.32 $^{gm}/m^3$ and -3°C).

L = liquid water content (gm/m^3)
V = true airspeed (m/sec)
t = time (sec)
F = freezing fraction (nondimensional)
A = area perpendicular to flow (m^2)

Comparing probes of equivalent area at identical airspeeds and LWC, we eliminate all variables except collection efficiency (η), and freezing fraction (F). Closer examination shows that freezing fraction is a ratio of the water caught and frozen to the amount of water that has impinged over a given time interval, and as such is dependent on ambient temperature, airspeed, and LWC. Hence for purposes of comparison, it becomes an independent variable leaving only collection efficiency (η) as a dependent variable. Collection (catch) efficiency is defined as the ratio of the mass of water contained in the oncoming flow to the mass of water trapped by the surface over a given time, and is a function of velocity, geometry of the probe and droplet size. Again for comparison purposes geometry of the probe and velocity are fixed leaving droplet size as the governing parameter in the determination of the mass of ice accreted. The catch efficiency for the low airspeed ice detector is normally assumed to be 90%, which relates to a droplet size of approximately 20 to 40 μm. Therefore, the detector cannot be expected to provide accurate indications with the large droplets (>40μm). From the equation for ice accretion, we see that as the catch efficiency surpasses 90% (assumed), the indicated LWC is lower than actual.

52. Under natural conditions, at temperatures colder than -5°C, good correlation was obtained between all four detectors when allowance was made for the different physical locations on the airframe and the dissimilarities of flow between these locations.

53. Under natural conditions with ambient temperatures warmer than -5°C, the ice detectors (LWC indications) exhibited a random shift (fig 11). This characteristic is inherent to all ice detectors that rely on ice deposition as a detection source, and is called the Ludlam limit. It is a result of the inability to dissipate the latent heat of fusion from the impinging water droplets and is further complicated by the kinetic heating of the probe by the freestream. The latter effect is easily compensated for by the detector circuitry since the design is usually for a small airspeed range and thus results in a relatively constant temperature rise. The latent heat of fusion is not so easily handled and is realized at both warm temperatures and high LWC where the probe is heated above freezing and the impinging droplets either blow-back or run-off the probe without being detected. This severely limits the usefulness of the accretion type detector at temperatures near freezing.

"Kit A" (Windshields)

54. All artificial testing was conducted with both windshields electrothermally heated. The system was activated prior to plume entry and remained on throughout the immersion. The windshields functioned properly at ambient temperatures of -10°C and warmer with LWC to 0.9 gm/m^3. At colder temperatures, the windshields became totally opaque due to ice formation after immersion times of 18 to 54 minutes (photo 16). The time required for the windshields to become opaque was a function of LWC as shown in figure 20.

Photo 16. Windshield Obscured by Ice Formation (22.5 min in HISS Plume with LWC of 0.25 $^{gm}/m^3$ and -15°C).

55. Modifications to the windshields and controllers were made during the test in an attempt to rectify the icing problems. The first attempt was to increase the windshield power density from 2.6 to 2.9 watts/in^2 and then to 3.3 watts/in^2. Only a slight improvement was noted with the higher power densities. The second modification consisted of changing the controllers from an ON-OFF type, which cycled at 112°F with overtemp protection at 130°F, to a proportional type that maintained the windshield at 130°F through variable voltage inputs. Little apparent improvement was noted with this modification except for the long term reduction in thermal stresses resulting from the "soft start" and smaller thermal transients inherent to the proportional controller.

56. The windshield demonstrated satisfactory anti-icing characteristics until the controllers began to cycle, at which time the windshield lost heat rapidly and almost immediately formed ice. The signal which initiated the controller cycle was provided by a temperature sensor embedded in the upper center portion of each windshield. This area was susceptible to windshield wiper blow back which resulted in continuous water coverage and rapid ice accumulation. The formation of this ice layer effectively insulated the sensors from ambient conditions through the formation of a warm water layer next to the heated windshields (photo 17). Immediately upon formation of this ice "bridge" and the resulting warm layer on the windshield outer surface, the controller was supplied a false signal indicating warmer ambient temperatures which allowed the initiation of the controller cycle. This logic leads to the conclusion that the sensor location is partially responsible for the windshield icing problems experienced during these tests. The sensors should be relocated to a position not affected by the windshield wiper.

57. The problems encountered in the artificial environment may also be attributed to the large droplet size produced by the HISS (para 19). Subsequent design calculations have shown that the mass contained in the large droplet exceeds the windshield thermal capability. It appears that the HISS environment is capable of supplying sufficient water mass at high LWC and low temperatures (below -10°C) to exceed the capability of most heated windshields.

58. Natural icing tests were conducted with one windshield electrothermally heated and the other heated by the standard bleed air defog system which was activated prior to cloud entry. Both systems proved effective in both anti-ice and deice modes. The major difference noted was the increased time requirement for bleed air deice (approximately three times the time of the electrical system). The electrical system also evaporated the residual moisture from the melting ice while the bleed-air system required occasional use of the windshield wipers.

59. It was found that within the limited natural icing environment encountered during this testing, the electrothermally heated windshields do not increase the capability of the aircraft.

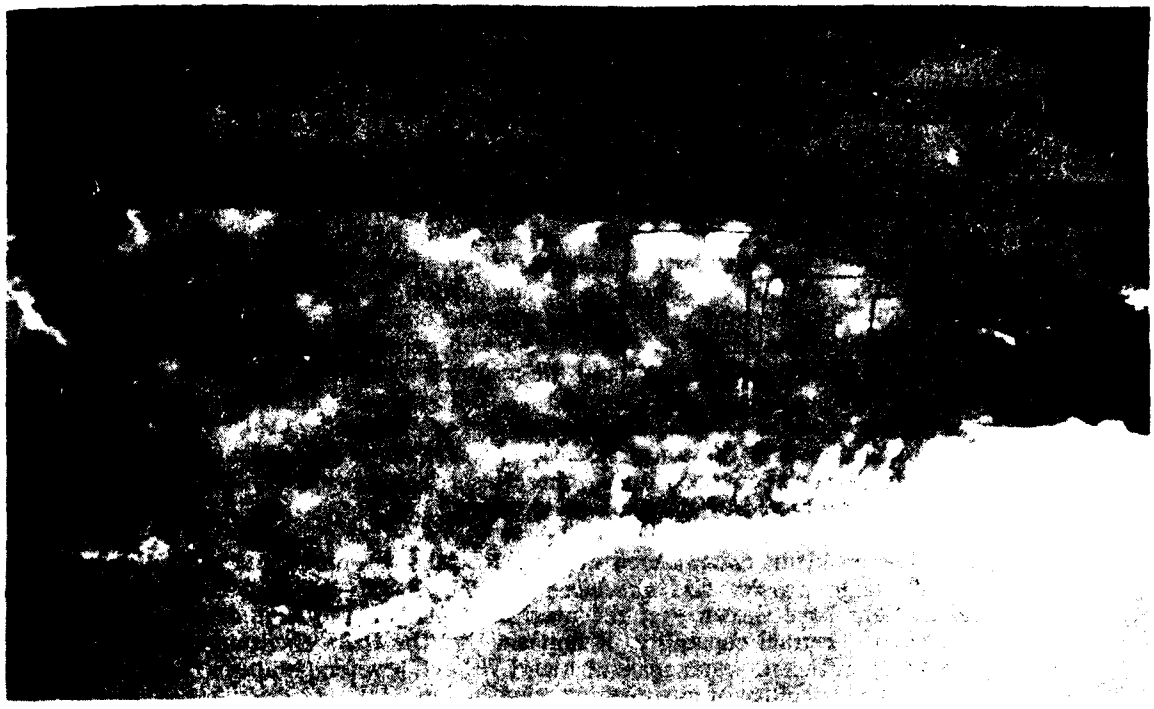

Photo 17. Ice Formation Insolating Windshield Temperature Sensors (19 min in HISS Plume with LWC of 0.5 g/m^3 and -17 C)

CONCLUSIONS

GENERAL

60. The conclusions drawn from these icing tests may be broken into the three areas of major concern. These areas dealt with the characteristics of the natural and artificial environments and the operation of the ice protection and test equipment. The conclusions applicable to each area are discussed below.

ARTIFICIAL ENVIRONMENT

61. The following conclusions were reached concerning the artificial environment as represented by the HISS plume:

a. The concentration of small droplets ($<15\mu m$) is greatly increased under conditions of high relative humidity (para 11).

b. The droplet distribution is relatively unchanged by variation in the horizontal distance (stand-off) of interest with the HISS, with the changes present attributed to gravitational sorting (para 14).

c. Increasing the flow rate on the HISS increases the concentration of large droplets while leaving the small droplet concentration relatively unchanged (para 16).

d. The peak numerical concentration of droplets in the HISS plume falls at approximately 10 μm; however, natural conditions produce a peak concentration at least an order of magnitude higher (para 19).

e. The mass concentration of the HISS plume indicates a fairly constant distribution between 50 and 200 μm; generally producing a more severe icing condition than that encountered in natural conditions (para 19).

f. The most severe artificial icing environment will be produced by the HISS under conditions of low relative humidity (para 19).

g. Artificial icing tests should be conducted during days with maximum cloud coverage to minimize sublimation (para 31).

NATURAL ENVIRONMENT

62. The following conclusions were reached concerning the natural environment encountered during this year's testing:

a. The small droplets ($<15\mu m$) produce IMC conditions and result in a reduced ice accretion (para 19).

b. Nonprecipitating stratus type cloud formations can be expected to contain droplet sizes from 10 to 30 μm MVD (para 23).

c. Rapid and drastic droplet variations encountered in the natural cloud are magnified in LWC indications (para 24).

d. Natural cloud formations of similar types tend to produce a characteristic droplet distribution with the concentration of larger droplets determined by the maturity of the cloud (para 27).

EQUIPMENT OPERATION

63. The following conclusions were reached concerning the ice protection and test equipment:

a. An LWC indicator is inadequate for determining icing severity level (para 25).

b. Icing of the engine inlet screens presented no problem in natural icing and snow (para 30 and 33).

c. The occurrence of tail rotor icing is minimal in the UH-1 helicopter (para 35).

d. The symmetrical shed on the main rotor blades occurs at a point determined by a combination of OAT, surface adhesion, centrifugal force and kinetic heating (para 37).

e. The asymmetric shed of the main rotor blades was the primary cause of icing flight termination (para 38).

f. An IRU type ice detector will provide more satisfactory icing information than an icing rate meter (para 38).

g. A thorough cleaning of the main rotor blades with naptha or alcohol may reduce the occurrence and severity of asymmetric sheds by removing impurities that initiate the shed (para 39).

h. An engine torque increase, at a fixed airspeed, is a positive indication of ice accumulation; however, the converse is not true (para 42).

i. The chordwise deicing concept provides a viable approach to the main rotor blade icing problem (para 47).

j. The Ludlum limit restricts the accuracy of accretion type ice detectors at temperatures near freezing (para 53).

k. In the natural environment electrothermally heated windshields are not necessary for the operation of a UH-1 not equipped with a main rotor deice system (para 59).

RECOMMENDATIONS

64. The following recommendations are made concerning future icing tests under natural and artificial conditions:

a. To produce a plume that most closely approximates the natural environment, testing should be conducted under conditions of high relative humidity (para 11).

b. The HISS should be modified to produce a more realistic icing environment (para 19).

c. Future icing tests should evaluate means of detecting ice accumulation in lieu of LWC (para 25).

d. Future testing should be restricted to LWC of 1 gm/m^3 or less to approximate the conditions that can be expected under natural conditions encountered by rotory wing aircraft (para 27).

e. A structural evaluation of the stabilizer bar should be conducted to determine the effects of increased centrifugal loads and/or an asymmetrical shed (para 34).

f. Further testing should be conducted at maximum allowable gross weights and airspeeds (para 45).

g. Additional tests should be conducted under natural conditions at higher LWC.

APPENDIX A. REFERENCES

1. Technical Manual, TM-55-1520-210-10, *Operator's Manual, Army Model UH-1D/H Helicopters,* 25 August 1971 with changes 1 through 22.

2. Technical Report, USAAMRDL-TR-75-34B, *The Development of an Advanced Anti-icing/Deicing Capability for US Army Helicopters,* November 1975.

3. Technical Report, USAAMRDL-TR-77-36, *Natural Icing Flight Tests and Additional Simulated Icing Tests of a UH-1H Helicopter Incorporating an Electrothermal Ice Protection System,* 1978.

4. Handbook, SM-280A, *Installation, Operation; and Maintenance Instructions with List of Parts, Icing Conditions. Simulation Equipment,* All American Engineering Co., with Supplement.

5. Letter, AVRADCOM, DRDAV-EQ, 18 January 1979, subject: Airworthiness Release for USAAEFA Project No. 78-21, Artificial and Natural Icing Tests, UH-1H Kit A Aircraft.

6. Report, Meteorology Research, Inc., No. MRI 79 FR-1700, *Drop Size Characteristics of the USAAEFA (CH-47) Helicopter Icing Spray System During Simulated Icing Tests of the UH-1H,* 27 July 1979.

7. Report Meteorology Research, Inc., No. MRI 79 DV-1679/1, *Bell Helicopter UH-1H Natural Icing Test Flights,* 27 July 1979.

8. Fletcher, N.H., *The Physics of Rainclouds,* Cambridge Unv. Press, 1969.

9. Mason, B.J., *The Physics of Clouds,* Clarendon Press, Oxford, 2nd Ed, 1971.

10. Paper, Cooper, W. A., *Precipitation Mechanisms in Summertime Storms in the Montana HIPLEX Area,* presented at the Conference on Cloud Physics and Atmospheric Electricity, July 31 - August 4, 1978, Issaquah, Washington.

11. Report, Environmental Research and Technology, Inc, *Characteristics of a Spray Plume,* April 1976.

12. System Specification, SS-951373, *Ice Detector Unit, IDU-3,* 22 February 1979.

13. Report, Meteorology Research Incorporated, MRI 78 IR-1538, Instrumented Cloud Base Aircrafts Support of HIPLEX, 1977, February 1978.

14. Final Report, USAASTA, Project No. 66-04, Engineering Flight Test, YUH-1H Helicopter, November 1970.

APPENDIX B. DESCRIPTION

HELICOPTER ICING SPRAY SYSTEM (HISS)

1. The HISS is carried on a modified CH-47C helicopter. The system consists of a spray boom, boom supports, boom hydraulic actuators, an 1800 gallon unpressurized water tank, operator control equipment, and associated bleed air and water plumbing (fig. 1). The spray boom consists of two 27 foot center sections and two 16.5 foot outrigger sections. The total empty weight of the system is approximately 4700 pounds. With the boom fully extended, the center sections are located 17 and 20 feet below the aircraft. The booms are jettisonable and the water supply (1500 gallons) can be dumped in approximately 10 seconds. A total of 172 nozzle locations are provided on the spray booms. During these tests, nozzles were installed at 57 of these locations, as shown in figure 2. Bleed air from the aircraft engines is used to prevent freezing of the booms and assist in atomization of the water as it exits the nozzles. For a more detailed description of the HISS, see reference 4, appendix A.

2. The LWC and water droplet size distribution of the spray cloud can be partially controlled by varying the water flow rate, the distance of the test aircraft behind the spray aircraft, and the bleed air pressure to the nozzles. The calculations required to determine LWC are contained in appendix D. Prior year testing conducted to evaluate the HISS spray cloud characteristics are covered in reference 11, appendix A.

PARTIAL ICE PROTECTION SYSTEM (KIT A)

AC Electrical System

3. The AC Electrical system of the Kit A equipped aircraft consists of a 30 KVA alternator, a 200 amp AC to DC converter, and associated control and distribution changes. The standard 28 VDC generator and quill assembly of the UH-1 has been replaced by a 30 KVA three-phase, 400 Hertz Bendix alternator (photo 1) which is driven at 12000 RPM by an offset quill and gear assembly. A 200 amp AC to DC converter (photo 2) powered by the alternator has been added as a standby DC power source. The distribution and control system has been modified to make the starter generator the main DC power source. The pilot's electrical control panels have been modified as shown in photo 3.

Heated Windshield and Controllers

4. Both windshields, manufactured by Pittsburgh Plate Glass (PPG), are electrothermally anti-iced at a power density of 3.3 watts/in^2. The 200 VAC three-phase power is obtained from the alternator with one third of the windshield heated by each phase. The windshield temperature is controlled through a proportional controller manufactured by Dynamic Control, Inc. The controller receives signals from temperature sensors embedded in the heated area, and varies power to the heating elements to maintain a temperature of 130°C. The controller provides over-temp protection by comparing amperage outputs to the three panels of each windshield. The pilot controls and fault indication system are depicted in photo 4.

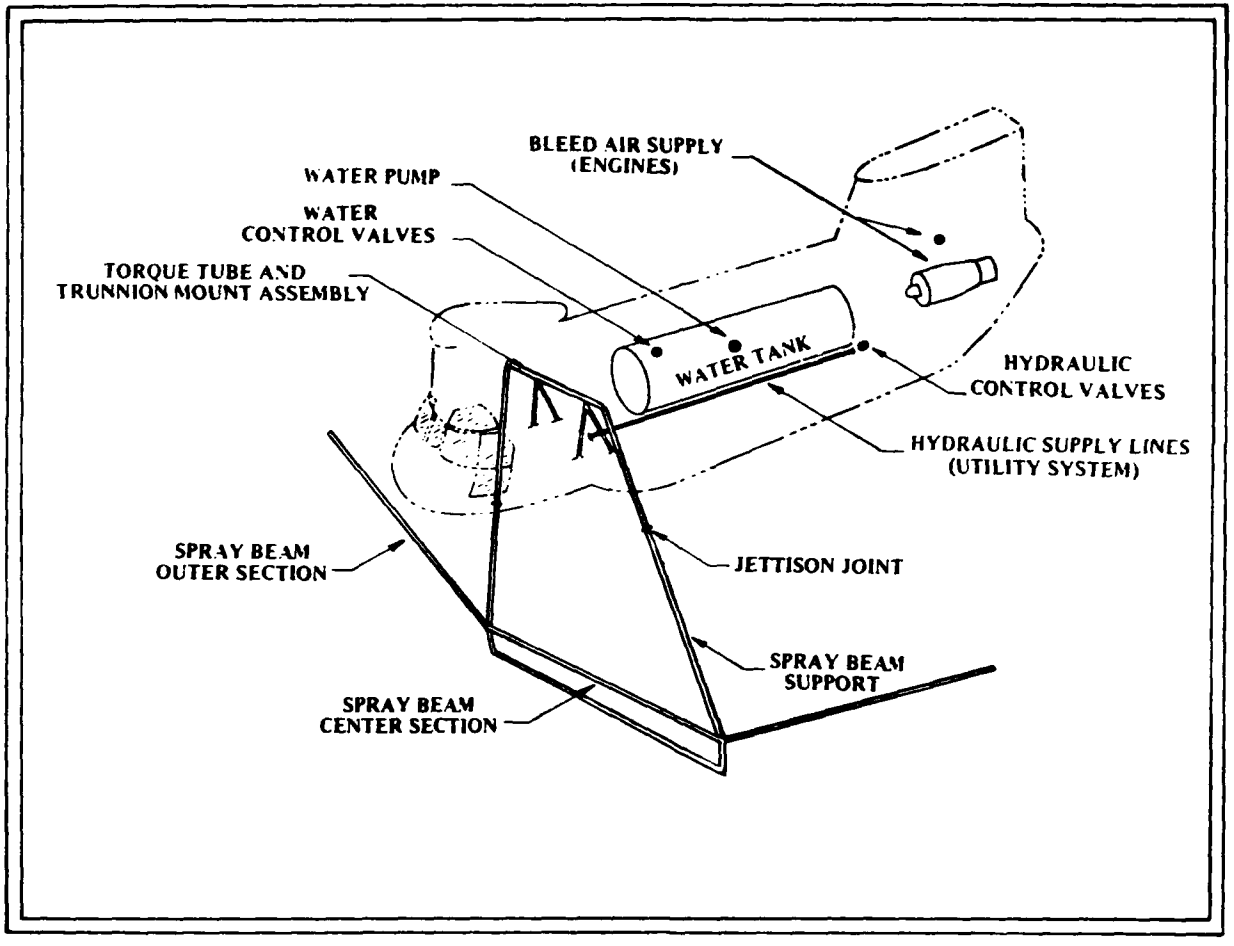

Figure 1. Helicopter Icing Spray System Schematic

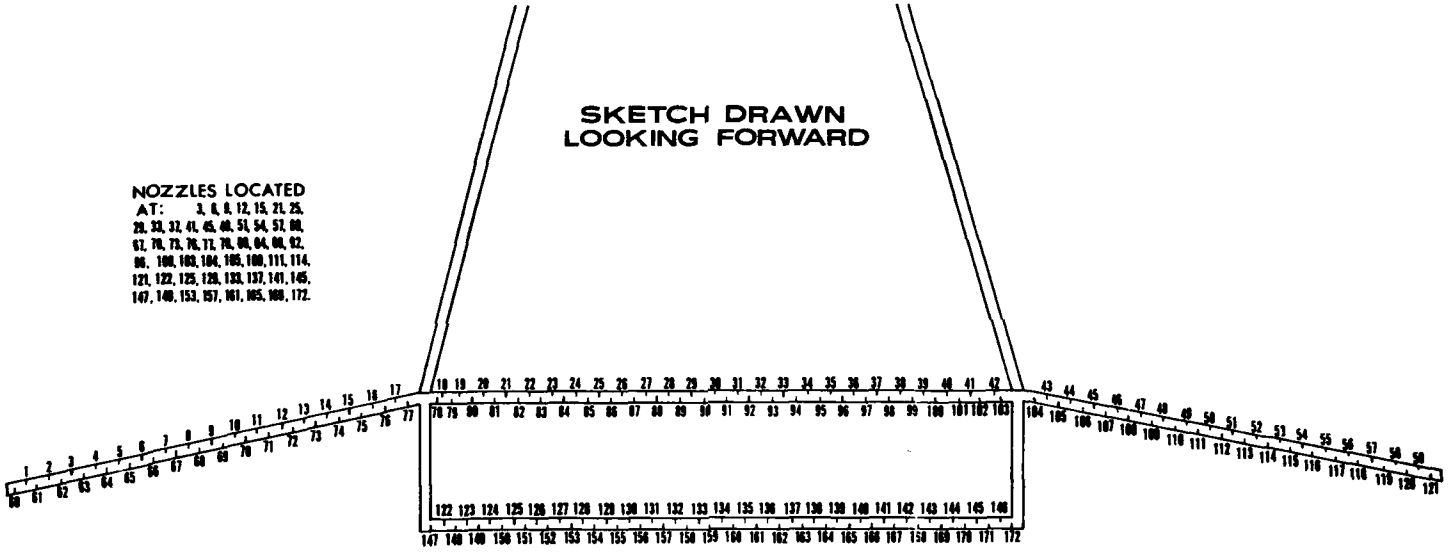

Figure 2. HISS Nozzle Locations.

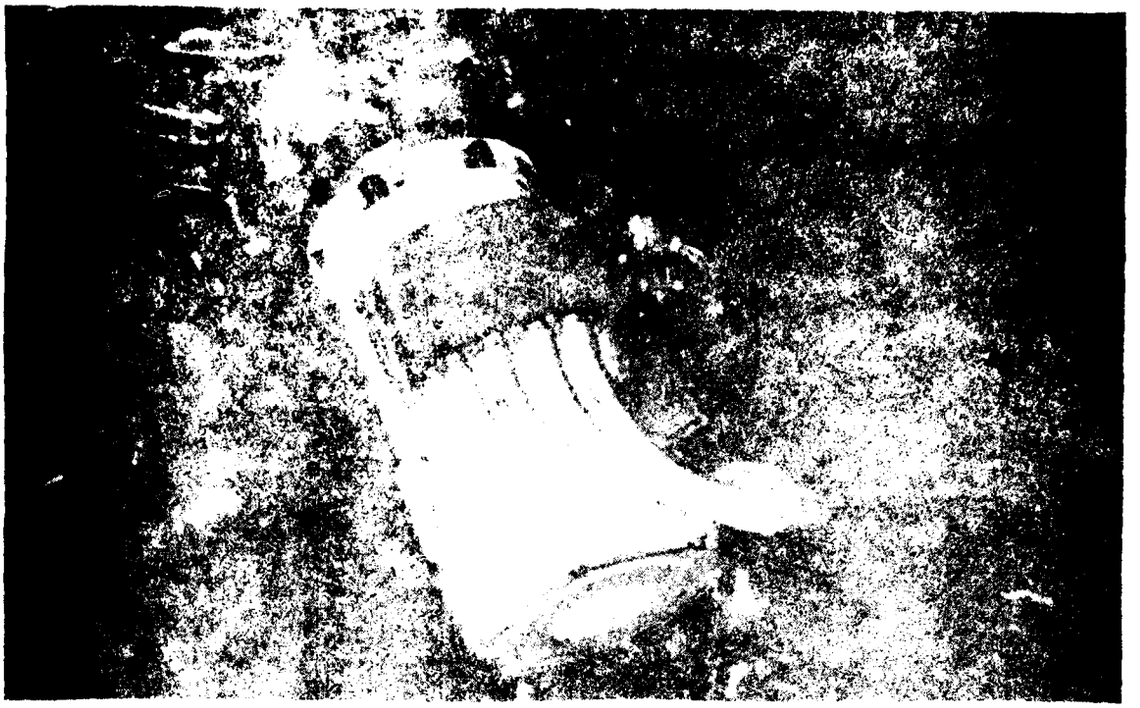

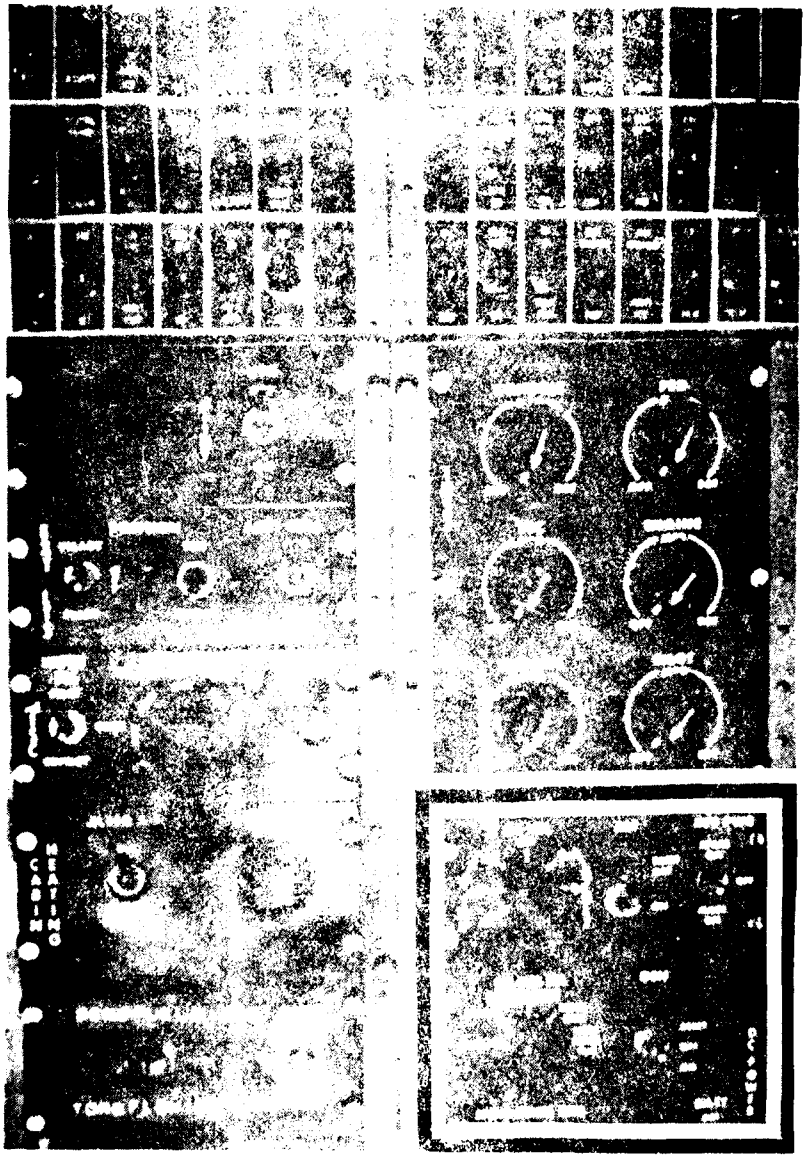

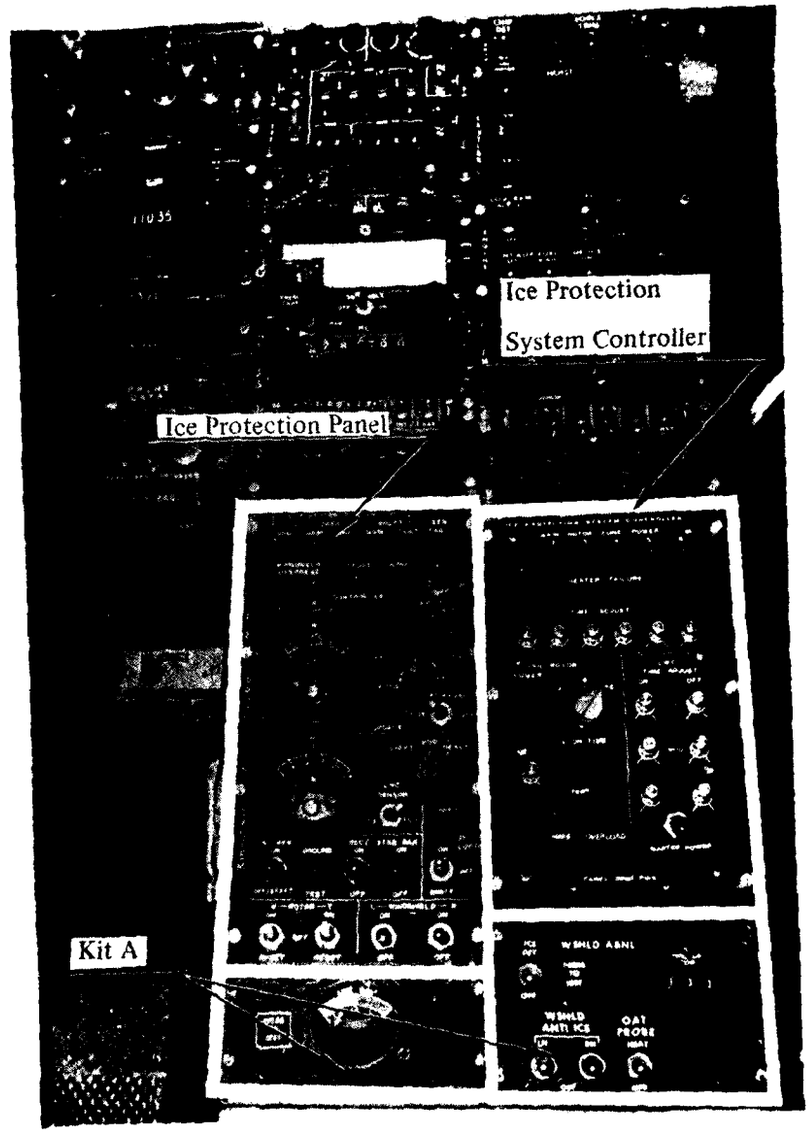

Photo 4. Lower Console "Kit A" and Ice Protection Panels

Ice Detector and Indicator

5. The ice detector is an ultrasonic-type manufactured by Rosemount Engineering Inc. (photo 5). The detector utilizes a vibrating probe which is excited at its natural frequency by a magnetostrictive oscillator mounted on the end of the probe. As the probe accretes ice, the natural frequency is reduced and the change is detected as an ice accretion rate. When the ice thickness reaches a pre-determined value the probe is deiced and the cycle repeated. The icing probe is housed in an electrically heated aspirator shroud which uses engine bleed air to induce flow over the probe during low airspeeds. The icing signal is displayed on an icing rate meter mounted on the center console. The shroud heat is controlled through an ice detector ON switch and the system operation is checked by a test button, both of which are located on the center console (photo 4).

OAT Sensor and Display

6. The OAT sensor is a non-heated resistance type detector manufactured by Rosemount Inc. The temperature signal is displayed on a digital display on the center console (photo 4).

Modified FM Antenna

7. The FM antenna has been canted outboard (42.5° from the vertical position) to prevent tail rotor contact should ice induced oscillations occur.

ICE PROTECTION SYSTEM

Main Rotor Blades

8. The main rotor blades are deiced by electrothermal, cyclic deicing heater elements as shown schematically in figure 3 . Each blade is divided spanwise into 6 zones; with corresponding zones on each blade heated simultaneously to provide symmetrical ice shedding. Heating progresses from the tip (zone I) to the root (zone VI). The upper surface is heated to approximately 12% chord (2.75 in) and the lower surface is heated to approximately 29% chord (6.45 in).

9. The power density varies from 12 watts/in^2 at the tip to 26 watts/in^2 at the root, while maintaining a constant total power of 6.7 kw/blade in each zone. This is accomplished by maintaining a constant heater element thickness (0.005 in) and varying the zone width spanwise. The power density variation compensates for the variation in kinetic heating and heat transfer coefficient which result from the blades rotational velocity.

10. The standard stainless steel and cobalt erosion shields have been removed from the blade and replaced with an 0.030 inch stainless steel shield from station 83 to the tip and 0.016 inch aluminum shield from station 83 to the root. The erosion shield covers an epoxy/fiberglass dielectric layer which is placed over the heater element (etched foil made from 0.005 inch stainless steel), and inner fiberglass epoxy layers (fig. 4).

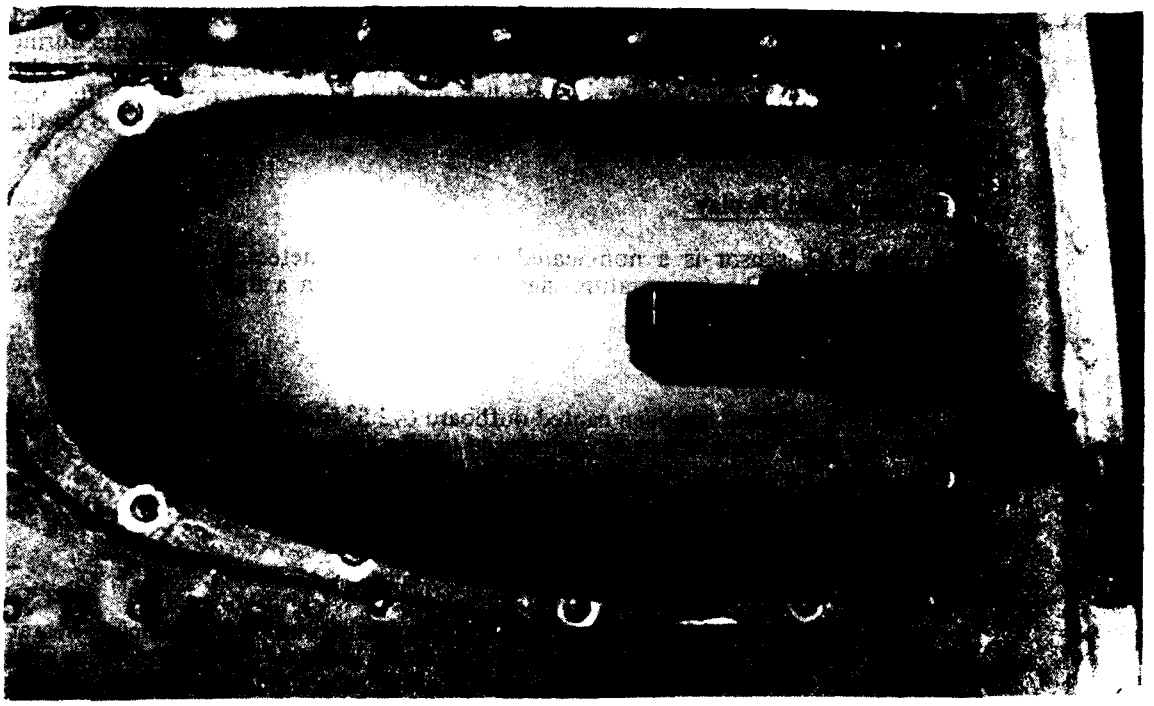

Photo 5. Rosemount Ice Detector Probe

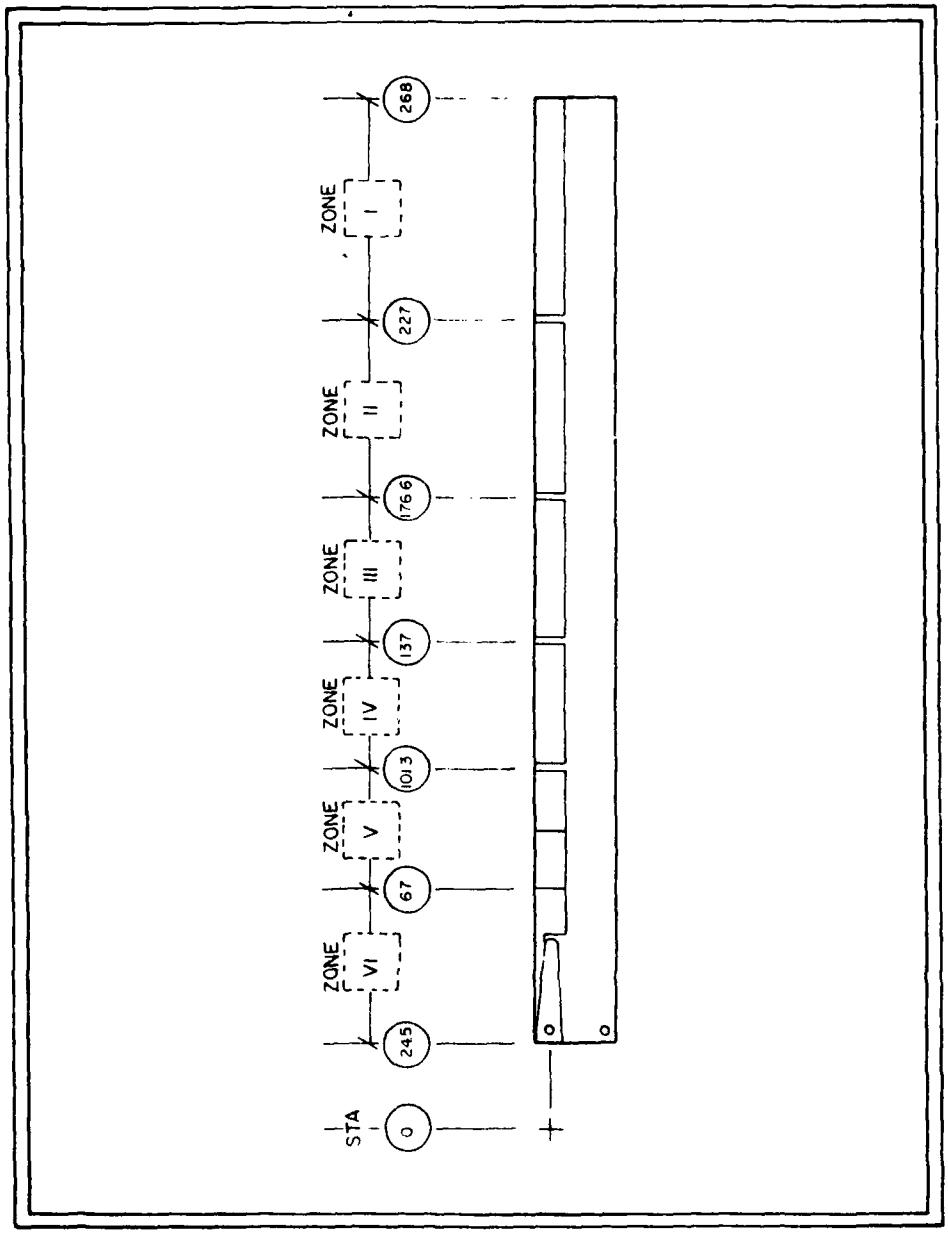

Figure 3. Main Rotor Blade Heater Zones.

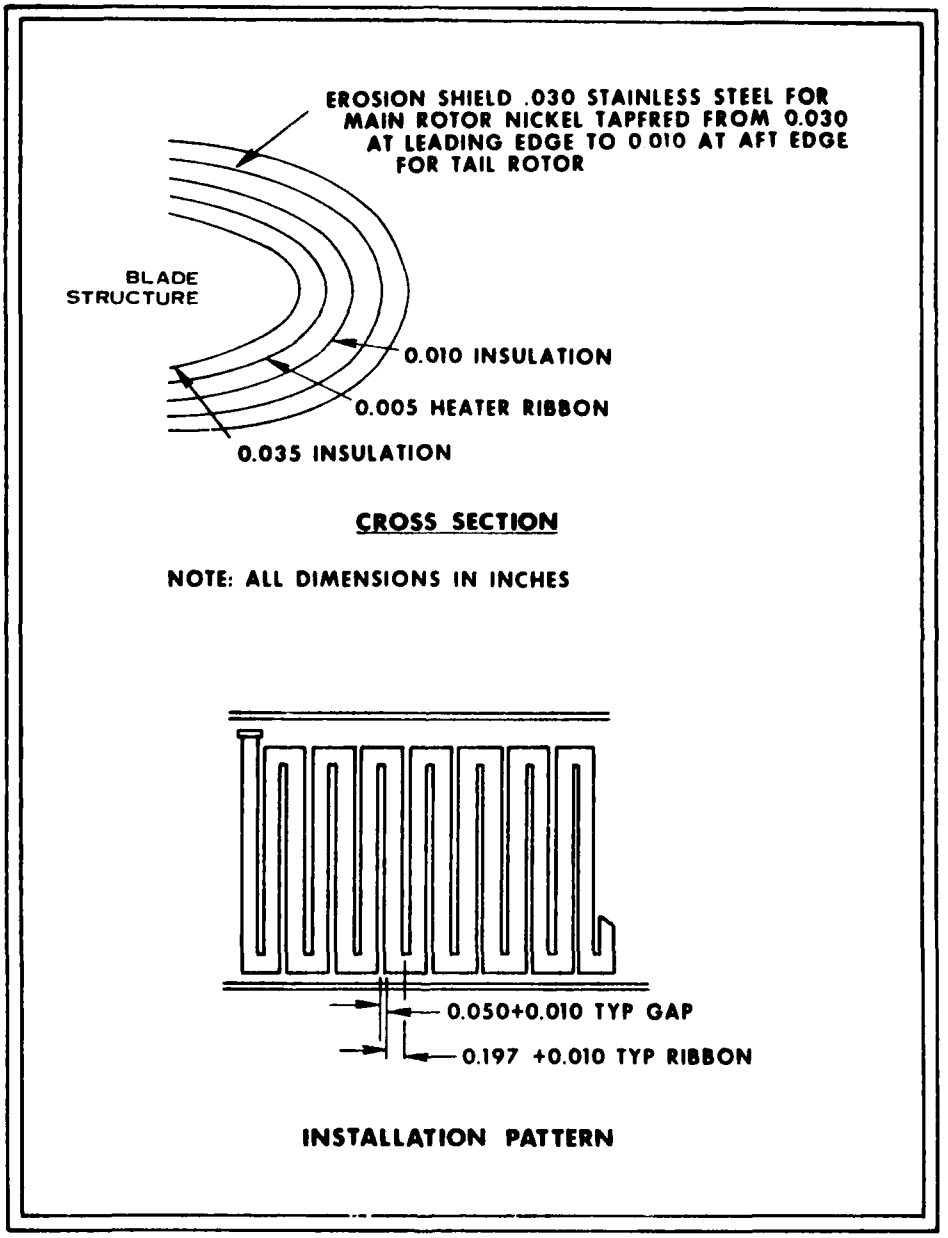

Figure 4. Main Rotor Blade Deicing Heater Elements

11. The blade heater uses three-phase power at 200 volts supplied by the 30 KVA alternator described as a component of "Kit A". Power leads extend out of the deicer boot in straps at the inboard end and then terminate in waterproof connectors for cable assemblies which lead into a power distribution stepper on top of the rotor mast.

Tail Rotor Blades

12. The tail rotor blades are deiced by cyclic electrothermal elements whose construction is similar to that of the main rotor blades. The erosion shield is electroformed nickel tapered from 0.030 inch at the leading edge to 0.010 inch at the trailing edge. Since the heated area of the tail rotor is small, the entire tail rotor is deiced by a single element on each blade. The tail rotor heated area extends from station 20.68 to station 50 (no deice coverage on the inboard doubler area). The elements extend aft to 10% chord (1 in.) on the upper (outboard) surface and to 25% chord (2.3 in.) on the lower (inboard) surface. A uniform power density of 20 watts/in^2 is maintained with the 200 VAC power source.

Stabilizer Bar

13. The stabilizer bar is deiced by continuous application of power (5 watts/in^2) to the heating elements imbedded in the heating blankets which cover the bar and counterweight assemblies. Control of the stabilizer bar is through a two-position switch on the pilot's deice control unit. The heater elements are provided power from a single phase of the 200 VAC alternator. The heated stabilizer bar was installed prior to the final two natural flights but was not activated.

Detectors

14. The deice system incorporates signals from two detectors to determine outside air temperature (OAT), liquid water content (LWC), and total ice accumulation. The LWC signal is provided by an infrared occlusion type detector (MK 10-3D) manufactured by Leigh Instruments Limited (photo 6). The ice thickness sensor consists of a light emitting diode/photo transistor assembly which provides an optical path that is partially occluded by the accretion of ice on the ice detector probe. The assembly is encased in an annular duct and ejector nozzle which is supplied with engine bleed air to induce high velocity air flow over the ice collecting probe and provide anti-icing. When the ice accumulation on the probe reaches a preset level, the probe is electrically deiced and the cycle is repeated. The icing signal is displayed by lights and an icing severity meter located on the icing control unit. The signal is also routed to the deice controller and the integrating rate unit (IRU).

15. The integrating rate unit (Model IRU-4) also manufactured by Leigh, accepts the icing signal and calculates this rate to indicate the amount of ice which has accreted up to the point where a new sample has been taken. It accumulates the integrated blocks of accretion data and compares the total to a quantity which is pre-selected via thumbwheel switches. When the accumulated total exceeds that selected, a signal is produced, which can be used to initiate a deice cycle, and illuminate a lamp on the IRU panel. A LWC display in gm/m^3 is also provided.

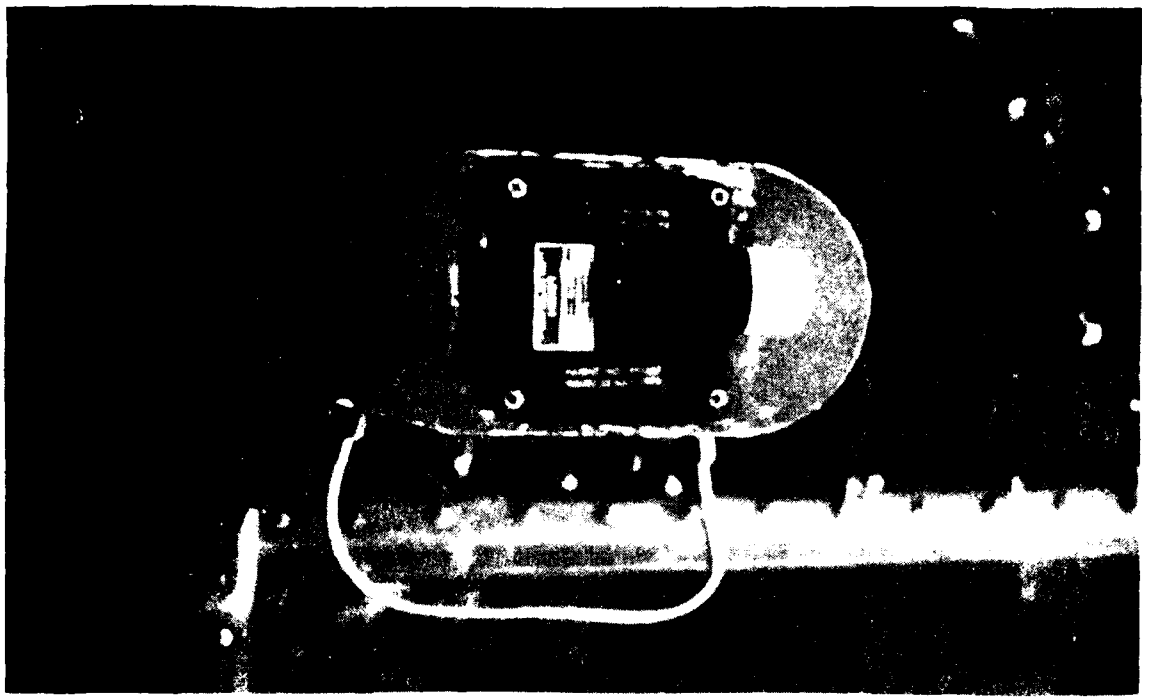

Photo 6. Leigh MK10 Ice Detector Probe

16. The OAT signal is obtained from a flush mounted Lewis detector. The signal is supplied to the deice controller and may be displayed on an OAT meter located on the deicing control unit.

Controller

17. The controller receives input signals from the detectors discussed above or from manual settings supplied by the pilot. These signals are converted to output signals which control the application of voltage to the slip ring assemblies for the main and tail rotor. The logic of the controller is programmed to vary main and tail rotor heater ON time as a function of OAT and main rotor OFF time as a function of LWC. The tail rotor OFF time is selected by the pilot as a multiple of tail rotor ON time. These heater schedules are adjustable to optimize heater operation but were maintained at the values shown in figure 5 throughout the test period.

System Operation and Control

18. The deicing control unit can be operated in either the automatic or semiautomatic mode. In the automatic mode the controller logic interprets the input signals of the LWC and OAT to program the blade deice cycle times. The cycle is initiated by the accumulation of a preselected IRU count or activation of the deice button located on the operator's console. In the semiautomatic mode, the signals for LWC and OAT are manually selected by the pilot. The deice cycle is then initiated by depressing the update button located on the deicing control unit.

19. The deicing controls consist of two units located on the lower center console between the pilot and copilot. These units provide controls for all phases of system operation and optimization, along with indications of system malfunctions. The control units are depicted in figures 6 and 7 with descriptions of the function of each switch or indicator.

Power Supply

20. The deice system uses the same three phase 200 VAC electrical system that is discussed as a component of the partial ice protection system ("Kit A").

FIGURE 5
MAIN AND TAIL ROTOR DEICING CYCLE TIMES

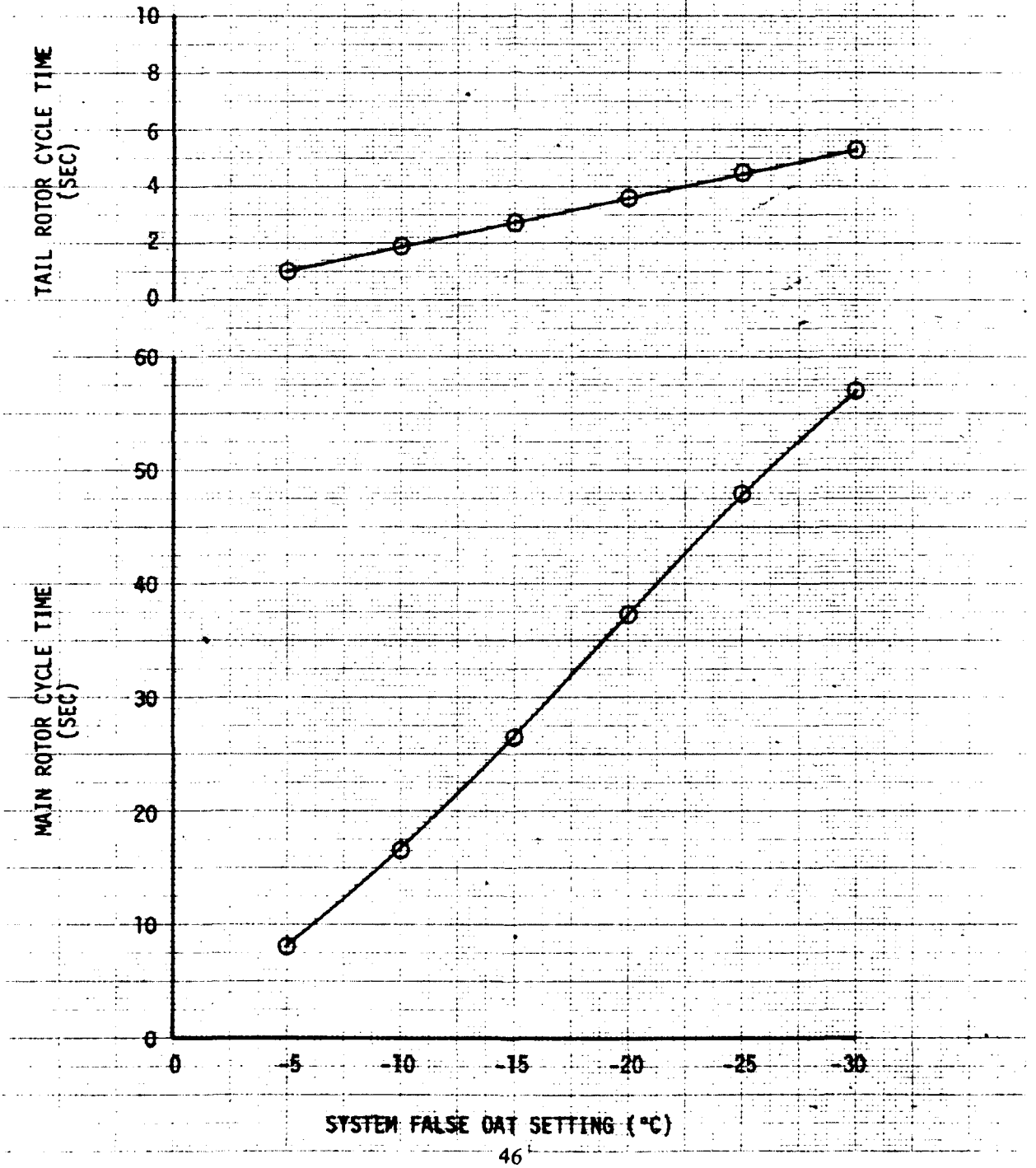

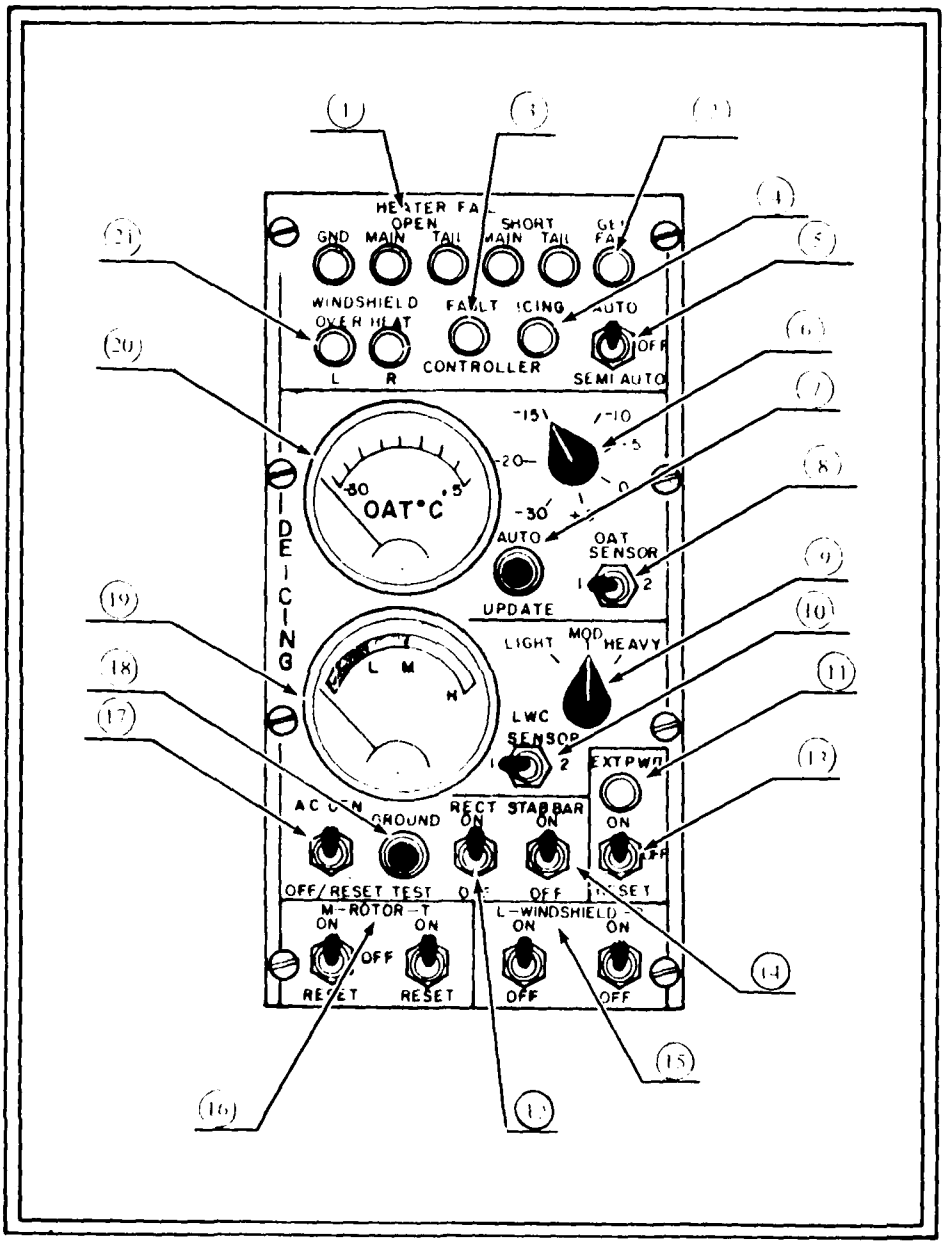

Figure 6. Deicing Control Unit.
(sheet 1 of 4)

Figure 6. Ice Protection System Control Unit (sheet 2 of 4).

INDEX	SWITCH OR INDICATOR	FUNCTION
1	HEATER FAIL AC GND	Provides warning of any line-to-ground leakage in the generator system or in the wiring of the main or tail rotor deicing system, such as a rotor blade element shorting to ground
	OPEN MAIN TAIL	Provides warning of an open element or open line for main or tail rotor deicing system NOTE The OPEN MAIN/TAIL lamp lights if the MASTER POWER switch on the deicing controller is ON and corresponding ROTOR switch on control unit is ON with AC GEN switch OFF.
	SHORT MAIN TAIL	Provides indication when current is excessive for main or tail rotor on any power phase
	SHORT MAIN	Provides indication that power switching stepper is out of synchronization
2	A.C. GEN FAIL	Deactivated
3	FAULT CONTROLLER	Provides indication when main rotor power doesn't follow time control but stays on
4	ICING	Provides indication that icing conditions are present outside helicopter when MASTER POWER switch is on, deicing controller is ON, and icing conditions are encountered or a false signal is introduced to simulate icing
5	MODE SWITCH	Allows selection of automatic or semiautomatic operation of ice protection system. Detented to prevent inadvertent operation
6	OAT SELECTOR	Allows setting outside air temperature into deicing system in semiautomatic mode

Figure 6. Ice Protection System Control Unit (sheet 3 of 4).

INDEX	SWITCH OR INDICATOR	FUNCTION
7	AUTO/UPDATE	Allows initiation of main rotor timer operation without waiting for normal 5-minute update period. Resets all timers for normal operation to begin again (with zone 1 of main rotor)
8	OAT SENSOR	Allows selection of FALSE or SYST OAT sensor for display on OAT meter and input to the deicing controller
9	ICING SEVERITY SELECTOR	Allows manual selection of icing severity level
10	LWC SELECTOR	Deactivated
11	EXT AC PWR AVAIL LAMP	Provides indication that AC external power is available
12	RECT ON/OFF	Deactivated
13	EXT AC PWR ON/OFF/RESET SWITCH	Allows external AC power to be applied to the helicopter
14	STAB BAR ON/OFF	Allows power to be applied to stabilizer bar heating blanket Detented to prevent inadvertent operation
15	L-WINSHIELD-R ON/OFF	Deactivated
16	M-ROTOR-T ON/OFF	Allows power to be applied to either or both main and tail rotor heater elements
	RESET	Allows resetting BITE circuits
17	AC GEN ON OFF/RESET	Deactivated
18	GROUND TEST	Allows overriding of normal timing circuits by a test oscillator to test rotor heating cycle. With normal loads, the main rotor blades will have one power ON period. The test oscillator is turned off at the end of the main rotor blade sequence

Figure 6. Ice Protection System Control Unit (sheet 4 of 4).

INDEX	SWITCH OR INDICATOR	FUNCTION
19	LWC meter	Provides indication of outside liquid water content (LWC) when MASTER POWER switch is ON
20	OAT Meter	Provides indication of outside air temperature (OAT) when MASTER POWER switch is ON
21	WINDSHIELD OVERHEAT L R	Deactivated -

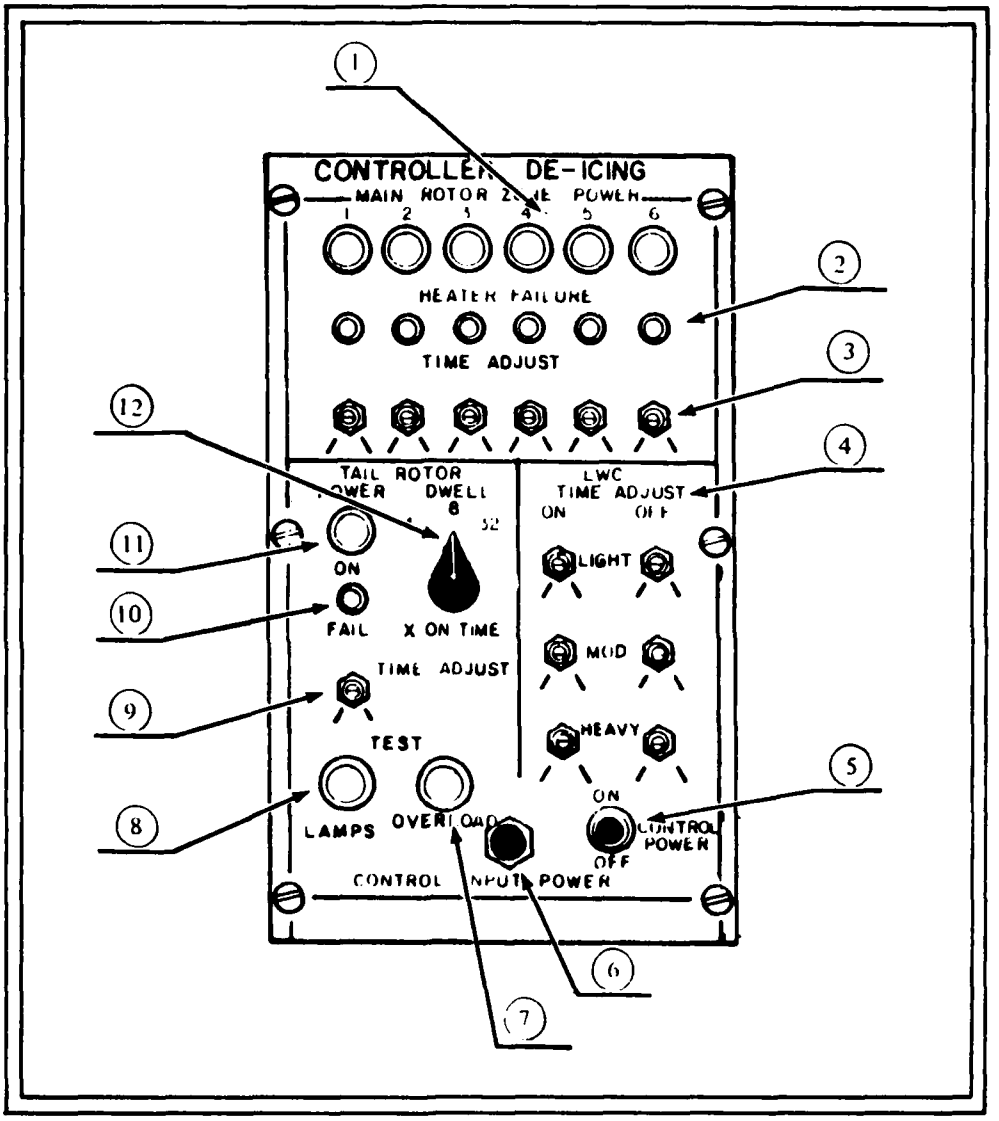

Figure 7. Deicing Control Unit (sheet 1 of 3).

Figure 7. Blade Deice Controller (sheet 2 of 3).

INDEX	SWITCH OR INDICATOR	FUNCTION
1	MAIN ROTOR ZONE POWER	Provides indications when power is applied to each of the six main rotor heated areas. As power is programmed to the main rotor heated areas, indicators come on and go off in sequence
2	HEATER FAILURE	Provides indication of failure of one of the six main rotor heater elements
3	TIME ADJUST	Provides adjustment for time period power is applied to each of the six main rotor heater elements. Locking nuts lock adjustments in place
4	LWC TIME ADJUST	Provides adjustments of the periods main and tail rotor heaters are ON and OFF for light, moderate, and heavy icing conditions
5	CONTROL POWER	Provides master power control for deicing system. With switch OFF, OAT and LWC sensors do not operate; ICING indicator does not light on deicing control unit. Detented to prevent inadvertent operation
6	CONTROL INPUT POWER	Controls 28 VDC power to deicing control system. Provides protection against excessive voltage
7	TEST OVERLOAD	Provides simulation of overload condition when pressed. When MAIN ROTOR ZONE POWER lamps are sequencing and the TEST OVERLOAD pushbutton is pressed, the OVERLOAD lamp lights
8	TEST LAMPS	Provides test of all lamps on deicing control unit when pressed
9	TAIL ROTOR TIME ADJUST	Provides a ±50 percent adjustment of time period power is applied to tail rotor heater elements
10	TAIL ROTOR FAIL	Provides indication of a failure in the tail rotor deicing system

Figure 7. Blade Deice Controller (sheet 3 of 3).

INDEX	SWITCH OR INDICATOR	FUNCTION
11	TAIL ROTOR POWER ON	Provides indication that power is applied to tail rotor heaters
12	TAIL ROTOR DWELL	Provides selection of tail rotor heater element off time as 4, 8, or 32 times the heater element ON time

APPENDIX C.
INSTRUMENTATION AND SPECIAL EQIPMENT

INSTRUMENTATION

1. The test instrumentation was installed, calibrated, and maintained by BHT. Digital and analog data were obtained from calibrated instrumentation and were recorded on oscillographs (photo 1) and/or displayed in the cockpit.

2. In addition to standard ship's instruments, the following parameters were displayed on calibrated test instruments in the cockpit or on the engineer's console:

Fuel flow
Fuel used
Engine inlet screen differential pressure
Engine torque
Pilot's windshield temperatures (8)
Outside air temperature at right windshield
Leigh ice detector bleed air pressure
Leigh ice detector bleed air temperature
Rosemount ice detector bleed air pressure
Rosemount ice detector bleed air temperature

3. The following parameters were recorded on oscillographs:

Control position:
- Longitudinal
- Lateral
- Directional
- Collective

Engine torque
Fuel flow
Engine inlet screen differential pressure
Aircraft attitude:
- Pitch
- Roll

Aircraft rate:
- Pitch
- Roll
- Yaw

Pilot seat vertical acceleration
Transmission lateral acceleration
Ninety degree gearbox vertical acceleration
Center-of-gravity vertical acceleration
Main and tail rotor azimuth
Main rotor beam bending loads
Main rotor pitch link axial loads
Tail rotor beam bending loads
Tail rotor chord bending loads
Tail rotor pitch link axial loads
Main rotor temperatures at the following stations:
- Station 257.11 (zone 1)
- Station 201. 76 (zone 2)
- Station 110 (zone 4) (6 chordwise points)

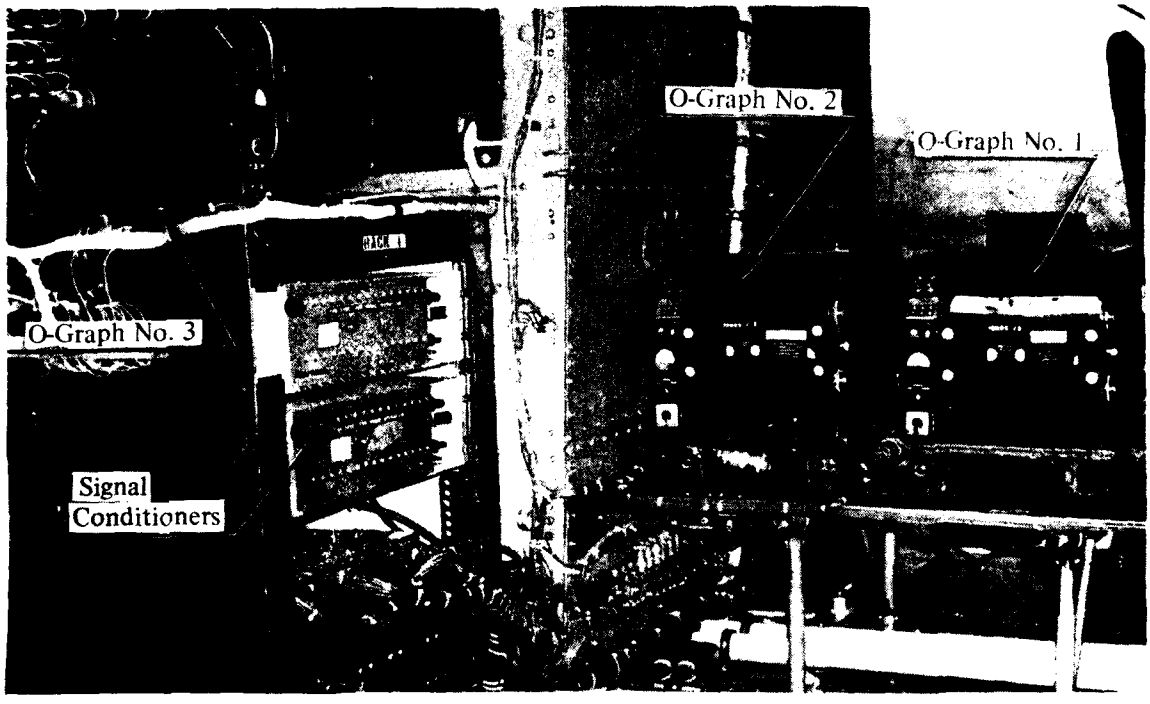

Photo 1. Oscillograph and Signal Conditioners Location

Station 84.5 (zone 5, steel)
Station 84.5 (zone 5, aluminum)
Station 55 (zone 6)

Tail rotor temperatures at the following stations:
Station 35, lower
Station 22, lower

Outside air temperature:
Rosemount (Kit A)
Lewis flush mounted cabin-roof
Tail fin

Main rotor heating signal voltage
Main rotor heating signal event
Main rotor AC phase voltage
Tail rotor AC phase voltage
Leigh liquid water content
Leigh icing signal
Leigh IRU last sum of ice accumulator
Rosemount icing severity
Rosemount analog icing signal
Rosemount probe heat event
Copilot windshield overtemp sensor temperature

SPECIAL EQUIPMENT

Hub-Mounted Camera

4. A 16mm movie camera was installed on top of the main rotor slip ring housing canister. The hub-mounted camera was designed to provide in-flight color photographic coverage of main rotor blade ice accumulation and shedding. The camera lens was electrically heated to prevent in-flight ice accumulation. Photo 2 shows the rotor hub camera assembly and its installation.

Ice Accretion Indicator Probe

5. An ice accretion indicator probe (photo 3) was mounted on the test aircraft to give the copilot a visual cue to ice buildup on the helicopter. It was composed of a small symmetrical air foil (OH-6A tail rotor blade section) with a 3/16-inch diameter steel rod protruding 1-1/2 inches out from the leading edge at the center. The protruding rod was painted with multi-colored 0.2-inch stripes to provide a reference for ice thickness estimation. The unit was mounted on the copilot's door facing forward.

Leigh MK 12 Ice Detector

6. For natural icing tests in Syracuse, an additional ice detector and cockpit LWC indicator were installed on the test aircraft. The ice detector unit, a Leigh Instruments, Ltd. MK XII (IDU-3) (photo 4) is an infrared occlusion type detector identical in principle of operation to the MK 10-3D described in appendix B. The display meter used to indicate LWC is a Western Model 1822 with a two-inch diameter face. A more detailed description of the ice detector unit and LWC indicator is included in reference 12, appendix A.

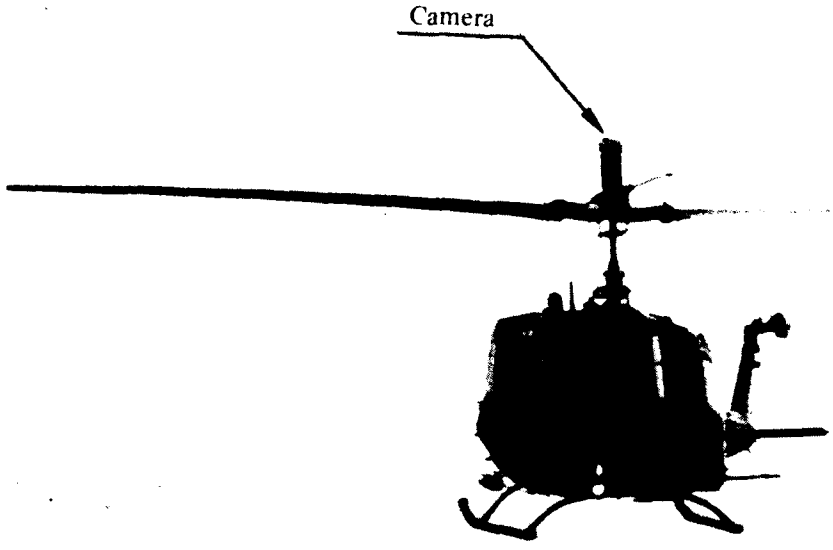

Photo 2. Hub Mounted Camera

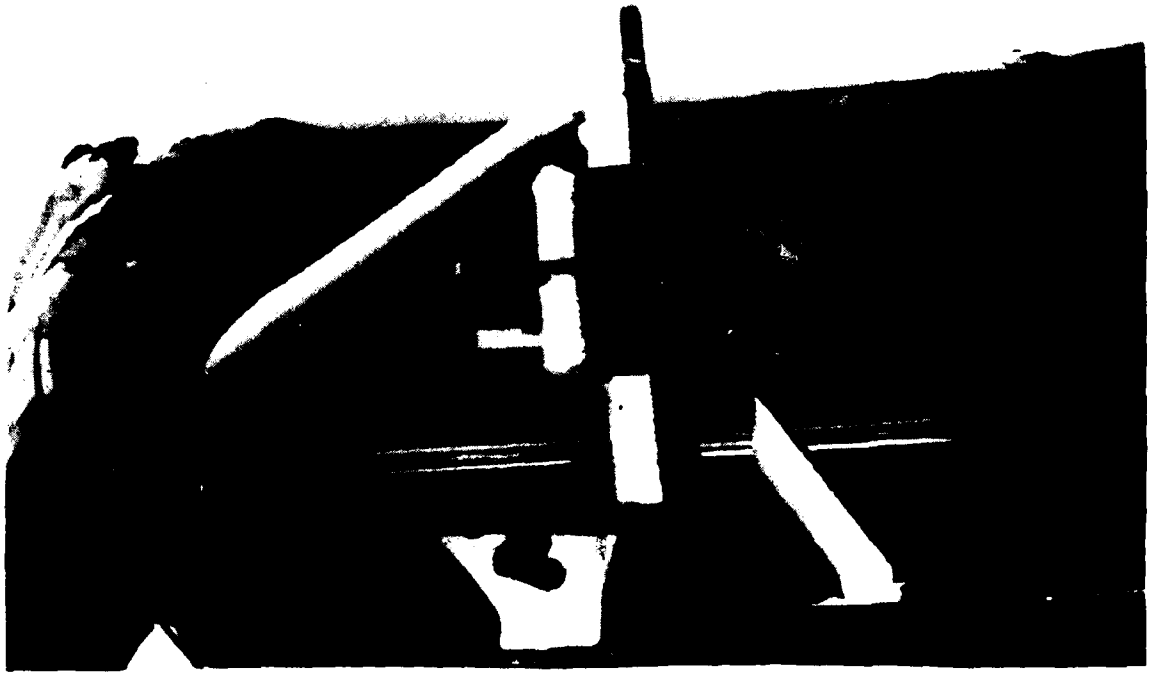

Photo 3. Ice Accretion Probe

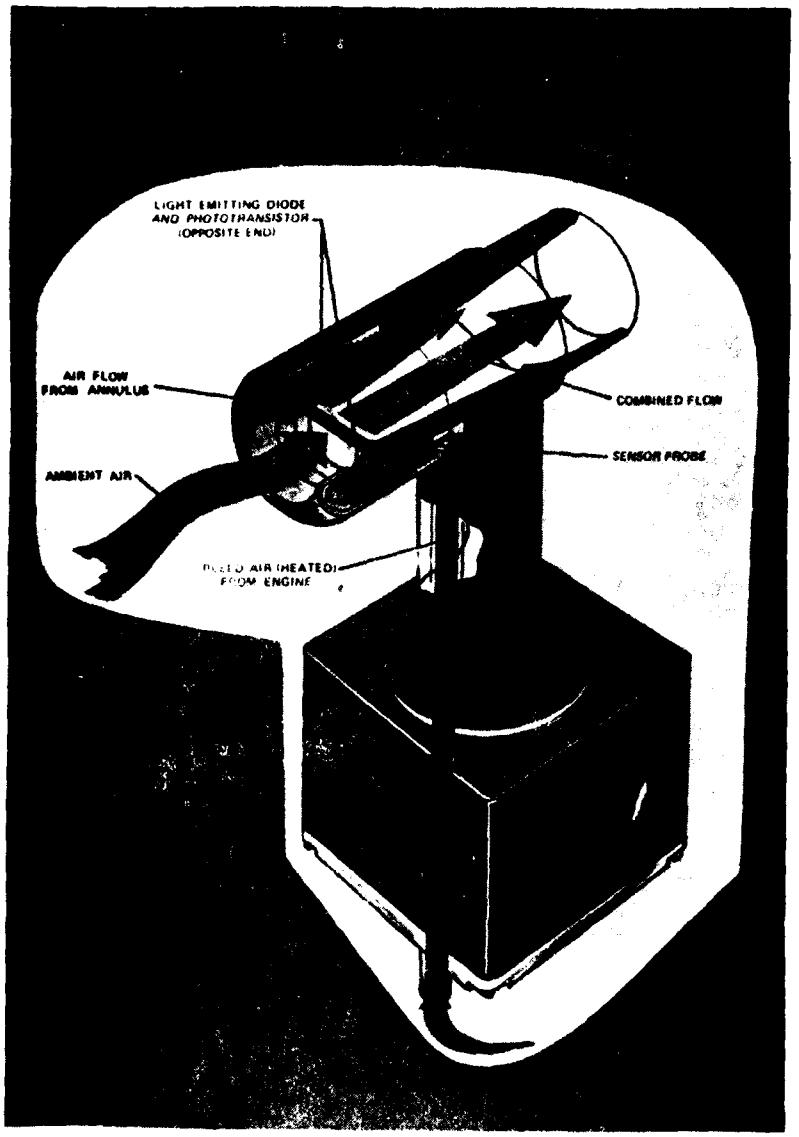

Photo 4. Leigh MK12 Ice Detector

Meteorological Research Incorporated (MRI) Equipment

7. The test objectives involving artificial and natural icing cloud parameter data (liquid water content and droplet size distribution) were obtained through MRI instrumentation. The following equipment was installed on the test aircraft: an axially scattering probe (ASP) (photo 5), a cloud particle spectrometer (CPS) (photo 6), and associated recording equipment (photo 7).

8. The ASP sizes particles by measuring the amount of light scattered into the collecting optics aperture during particle interaction through a focused laser beam. The signal pulses are AC coupled to a pulse height detector which compares their maximum amplitude with a reference voltage derived from a separate measurement of the DC light signal illuminating the particles. The system is capable of sizing particles from 2 to 30 microns diameter having velocities from 10 to 125 m/sec (20 to 240 kts).

9. In the CPS, particles are sized using a linear array of photodiodes to sense the shadowing of array elements by particles passing through its field of view. Particles are illuminated by a helium-neon laser. As shadowing of each photodiode element is dark enough, a flip-flop memory element is set. The particle size is determined by the number of elements set by a particle's passage, the size of each array element, and the magnification of the optical system.

10. Two different CPS probes were used during this evaluation. One probe contained 24 active photodiode elements capable of sizing into 15 size channels with a magnification set for a size range of 20 to 300 microns. The other probe contained 20 photodiode elements capable of sizing into 15 size channels with a magnification set for a size range of 140 to 2100 microns.

11. More detailed descriptions of the ASP and CPS are contained in reference 13, appendix A.

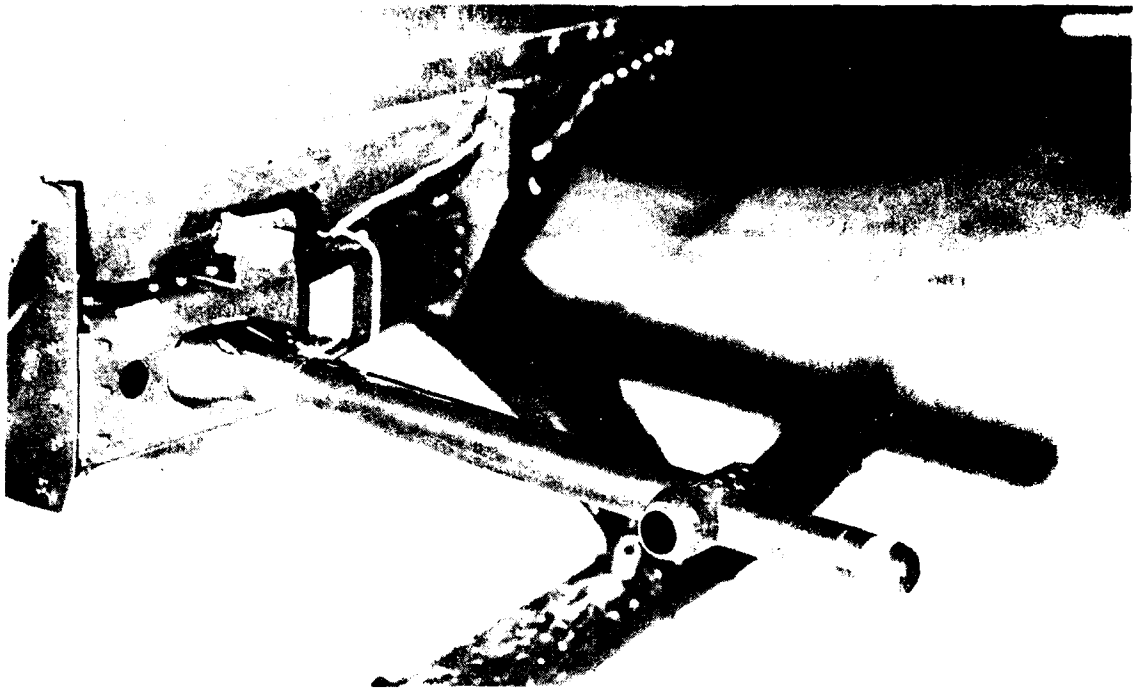

Photo 5. Axially Scattering Probe (ASP) Installation

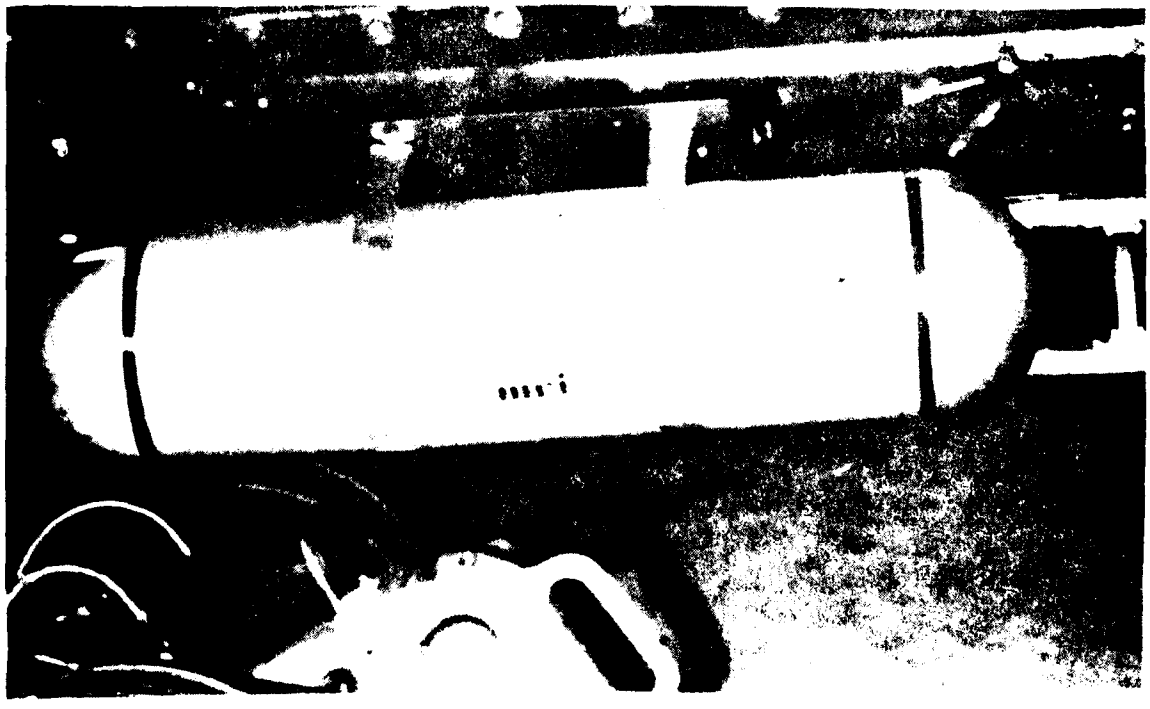

Photo 6. Cloud Particle Spectrometer (CPS) Installation

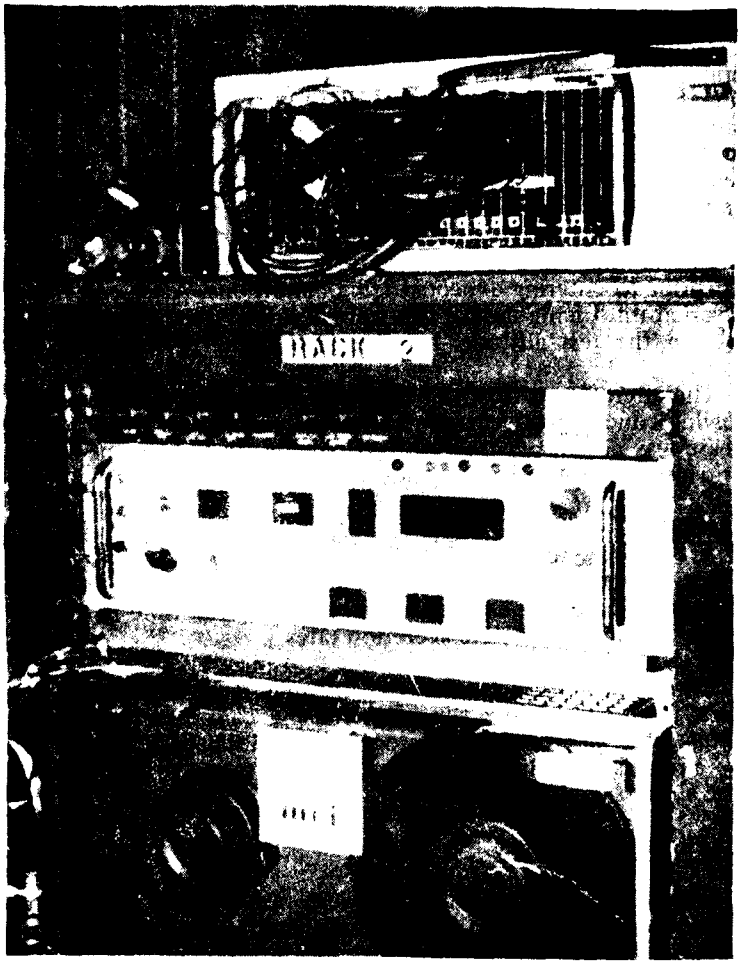

Photo 7. MRI Recorder and Signal Conditioners

APPENDIX D. TEST TECHNIQUES AND DATA ANALYSIS METHODS

GENERAL

1. Testing was conducted in two phases: artificial icing behind a spray aircraft (HISS) and natural icing. For artificial icing tests, all anti-ice systems were activated while enroute to the test area. After reaching the altitude required for the specified test temperature, baseline level flight performance data were obtained. The test aircraft then entered the spray cloud from a position below and approximately 200 feet behind the spray aircraft. Test and spray aircraft separation distance was maintained during the icing flight by information relayed from a radar altimeter mounted on the spray aircraft. Test airspeed and outside air temperature were established with the calibrated systems of the spray aircraft. All artificial icing flights were flown with a predetermined LWC and outside air temperature.

2. For natural icing tests, all anti-ice systems except the windshields were activated prior to entering expected icing conditions. After entering the cloud, altitude was varied until icing indications were obtained on the instrumentation. Once established on the test altitude, baseline level flight performance data were obtained.

3. The aircraft was flown in the icing cloud (artificial or natural) until one of the following conditions occurred: both windshields iced over, a predetermined torque increase was noted, or vibration levels increased because of main or tail rotor asymmetric ice sheds.

Ice Accretion

4. Ice accretion was monitored in flight by the copilot using the visual ice accretion indicator probe. The engineer monitored time in cloud, LWC indications, and IRU counts to correlate accretion rates.

5. Rotor blade ice accretion was documented using a high-speed motion picture camera mounted on the slip ring housing cannister. High-speed motion picture cameras were also used to photograph the test aircraft from both the chase and spray aircrafts. Postflight photographs were made to document the ice remaining on the aircraft components.

Level Flight Performance

6. Level flight performance data were obtained by establishing trim level flight at the test airspeed (90 KTAS), altitude, and outside air temperature using the test aircraft calibrated instruments. Data were recorded before and after the cloud immersion.

7. Level flight performance degradation due to ice accretion was assessed by comparing the engine power required to maintain constant airspeed and altitude before and after icing. Power required was corrected for fuel burn-off by using the nondimensional level flight performance carpet plot (ref 14, app A) for a standard UH-1H.

8. Engine inlet screen differential pressure was monitored during the icing flights to determine the effects of ice accretion on the inlets.

Autorotational Descent Performance

9. Autorotational descent performance was quantitatively and qualitatively evaluated throughout the tests at the recommended airspeed for minimum rate of descent. The data were obtained after icing the aircraft and changes in stabilized autorotational rotor speed were noted.

Weight and Balance

10. Prior to testing, the aircraft gross weight and longitudinal cg were determined by using calibrated scales. The longitudinal cg was calculated by a summation of moments about a reference datum line (FS 0.0). Additional equipment/instrumentation installed in the aircraft was weighed and the fuselage station determined to calculate a moment. The moment and weight were then used to correct the aircraft gross weight and cg.

Vibration Rating Scale

11. The Vibration Rating Scale (VRS), presented in figure 1, was used to augment crew comments on aircraft vibration levels during main or tail rotor asymmetric ice sheds.

HISS FLOW RATE CALCULATION METHOD

12. HISS water flow rates required to establish desired LWC for each flight were determined using the following procedure. Calibrated instruments were used to establish airspeed, altitude, and static air temperature for the required test conditions. The frost point was then obtained using a Cambridge Thermoelectric Dew Point Hygrometer using table 1. Saturation vapor pressure in millibars for the dew point and static air temperature was then determined using table 2. Relative humidity was then computed using the values obtained from table 2 and equation 1.

$$R_H = \frac{P_{VS}}{P_W} \times 100 \qquad (1)$$

Where:

R_H = Relative humidity (percent)

P_{VS} = Saturation vapor pressure for dew point (millibars)

P_W = Saturation vapor pressure for static air temperature (millibars)

13. The decay LWC, which is the spray cloud evaporation rate, was then computed using equation 2.

$$LWC_D = \frac{G(100-R_H)}{4.5\,G_O} \qquad (2)$$

Figure 1. Vibration Rating Scale

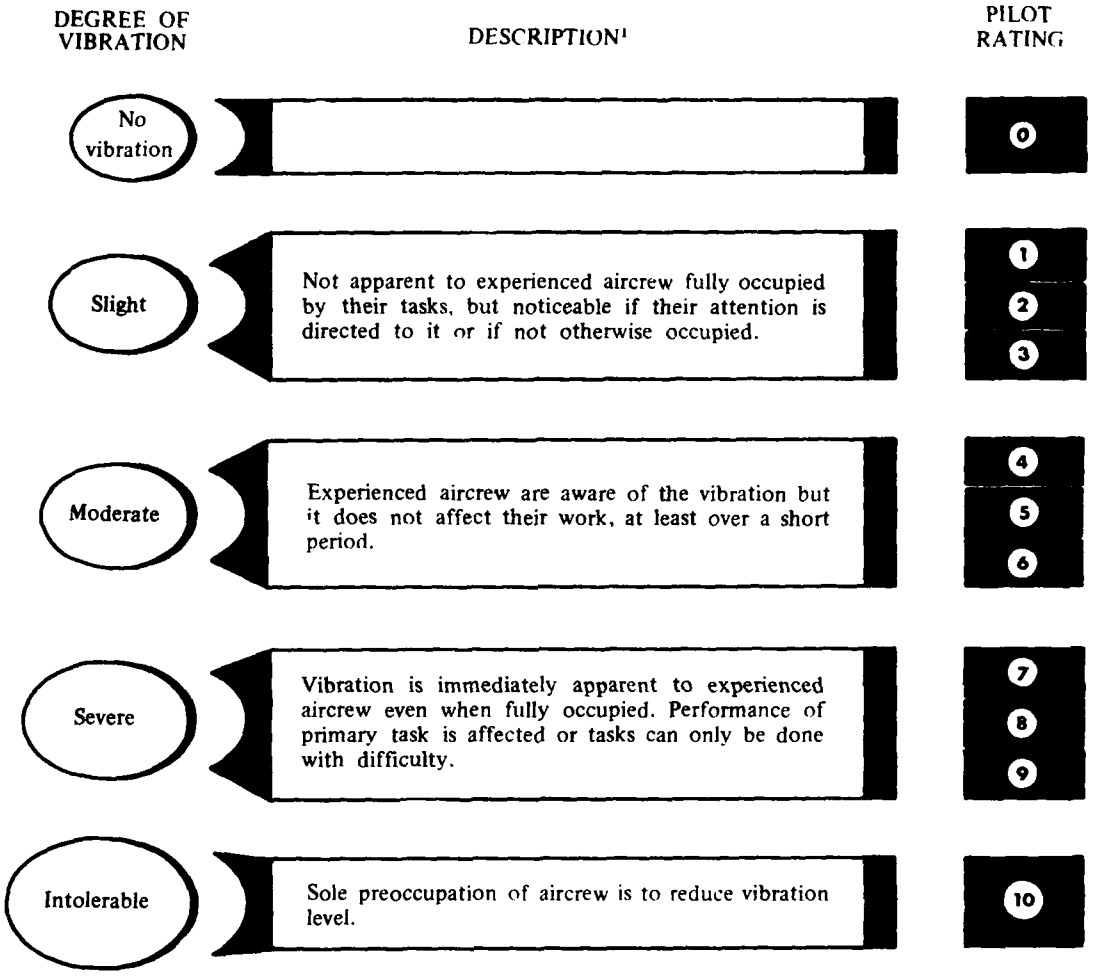

[1] Based upon the Subjective Vibration Assessment Scale developed by the Aeroplane and Armament Experimental Establishment, Boscombe Down, England.

Table 1. Cambridge Thermoelectric Dew Point Hygrometer Conversion Values (Degrees Centrigrade).

Frost Point	Dew Point	Frost Point	Dew Point
-0.0	-0.1	-13.0	-14.5
-0.5	-0.7	-13.5	-15.0
-1.0	-1.2	-14.0	-15.6
-1.5	-1.8	-14.5	-16.2
-2.0	-2.3	-15.0	-16.7
-2.5	-2.9	-15.5	-17.3
-3.0	-3.4	-16.0	-17.8
-3.5	-4.0	-16.5	-18.4
-4.0	-4.5	-17.0	-18.9
-4.5	-5.1	-17.5	-19.5
-5.0	-5.6	-18.0	-20.0
-5.5	-6.2	-18.5	-20.6
-6.0	-6.7	-19.0	-21.1
-6.5	-7.3	-19.5	-21.1
-7.0	-7.9	-20.0	-22.2
-7.5	-8.4	-20.5	-22.8
-8.0	-9.0	-21.0	-23.3
-8.5	-9.5	-21.5	-23.9
-9.0	-10.1	-22.0	-24.5
-9.5	-10.6	-22.5	-25.0
-10.0	-11.2	-23.0	-25.6
-10.5	-11.7	-23.5	-26.1
-11.0	-12.3	-24.0	-26.7
-11.5	-12.8	-24.5	-27.2
-12.0	-13.4	-25.0	-27.8
-12.5	-13.9	-25.5	-28.3

Table 2. Saturation Vapor Pressure Over Water (Millibars).

Temperature °C	.0	.1	.2	.3	.4	.5	.6	.7	.8	.9
-25	0.8070	0.7997	0.7926	0.7854	0.7783	0.7713	0.7643	0.7574	0.7506	0.7438
-24	0.8827	0.8748	0.8671	0.8593	0.8517	0.8441	0.8366	0.8291	0.8217	0.8143
-23	0.9649	0.9564	0.9479	0.9396	0.9313	0.9230	0.9148	0.9067	0.8986	0.8906
-22	1.0538	1.0446	1.0354	1.0264	1.0173	1.0084	0.9995	0.9908	0.9821	0.9734
-21	1.1500	1.1400	1.1301	1.1203	1.1106	1.1009	1.0913	1.0818	1.0724	1.0631
-20	1.2540	1.2432	1.2325	1.2219	1.2114	1.2010	1.1906	1.1804	1.1702	1.1600
-19	1.3664	1.3548	1.3548	1.3318	1.3204	1.3091	1.2979	1.2868	1.2758	1.2648
-18	1.4877	1.4751	1.4627	1.4503	1.4381	1.4259	1.4138	1.4018	1.3899	1.3781
-17	1.6186	1.6051	1.5916	1.5783	1.5650	1.5519	1.5389	1.5259	1.5131	1.5003
-16	1.7597	1.7451	1.7306	1.7163	1.7020	1.6879	1.6738	1.6599	1.6460	1.6323
-15	1.9118	1.8961	1.8805	1.8650	1.8496	1.8343	1.8191	1.8041	1.7892	1.7744
-14	2.0755	2.0586	2.0418	2.0251	2.0085	1.9921	1.9758	1.9596	1.9435	1.9276
-13	2.2515	2.2333	2.2153	2.1973	2.1795	2.1619	2.1444	2.1270	2.1097	2.0925
-12	2.4409	2.4213	2.4019	2.3826	2.3635	2.3445	2.3256	2.3069	2.2883	2.2698
-11	2.6443	2.6233	2.6024	2.5817	2.5612	2.5408	2.5205	2.5004	2.4804	2.4606
-10	2.8627	2.8402	2.8178	2.7956	2.7735	2.7516	2.7298	2.7082	2.6868	2.6655
- 9	3.0971	3.0729	3.0489	3.0250	3.0013	2.9778	2.9544	2.9313	2.9082	2.8854
- 8	3.3484	3.3225	3.2967	3.2711	3.2457	3.2205	3.1955	3.1706	3.1459	3.1214
- 7	3.6177	3.5899	3.5623	3.5349	3.5077	3.4807	3.4539	3.4272	3.4008	3.3745
- 6	3.9061	3.8764	3.8468	3.8175	3.7883	3.7594	3.7307	3.7021	3.6738	3.6456
- 5	4.2148	4.1830	4.1514	4.1200	4.0888	4.0579	4.0271	3.9966	3.9662	3.9361
- 4	4.5451	4.5111	4.4773	4.4437	4.4103	4.3772	4.3443	4.3116	4.2791	4.2468
- 3	4.8981	4.8617	4.8256	4.7897	4.7541	4.7187	4.6835	4.6486	4.6138	4.5794
- 2	5.2753	5.2364	5.1979	5.1595	5.1214	5.0836	5.0460	5.0087	4.9716	4.9347
- 1	5.6780	5.6365	5.5953	5.5544	5.5138	5.4734	5.4333	5.3934	5.3538	5.3144
- 0	6.1078	6.0636	6.0196	5.9759	5.9325	5.8894	5.8466	5.8040	5.7617	5.7197

Where:

LWC_D = Decay liquid water content (percent/second)

G = Thermodynamic function (centimeter^2/second)

R_H = Relative humidity (percent) obtained from equation 1

G_O = 60 x 10^{-8} centimeter^2/second (constant)

The value for the thermodynamic function G used in equation 2 was obtained from figure 2 using the total air temperature indicated by the HISS aircraft. Pressure dependence of G is small, so that values for 1000 millibars given in figure 2 were satisfactory for the test altitudes. The programmed LWC based on the desired test condition was then corrected for evaporation using the decay LWC calculated above and equation 3.

$$LWC_C = \frac{LWC_D}{100} \frac{D}{1.6889\ V_T} (LWC_P) + LWC_P \qquad (3)$$

Where:

LWC_C = Corrected liquid water content (gm/m^3)

LWC_D = Decay liquid water content (percent/second)

D = 200 feet (constant distance between test and spray aircraft maintained during this test)

1.6889 = Conversion factor (ft/sec/kt)

V_T = 90 knots (constant test true airspeed)

LWC_P = Programmed liquid water content (gm/m^3)

14. The corrected LWC and figure 3 were then used to determine the required water flow rate. The flow rate obtained from figure 3 and a constant bleed air pressure of 15 pounds per square inch at the nozzles (gauge) were used to establish the spray cloud.

DATA PRESENTATION

15. Two distributions are in common use when considering droplet size-distributions. When droplet numbers are being considered, a plot of n (r) against r, where n (r) dr is the number of droplets in range dr about r, is used. An alternate distribution is that of $r^3 n(r)$ against r, which is useful since $4/3\ \pi\ r^3\ n(r)$ is the contribution to the liquid water content of droplets within dr of r. The mean, median or mode of either one of these distributions may be used but since the shape of the spectrum varies widely it is usually necessary to specify the complete spectrum.

FIGURE 2
VARIATION OF THERMODYNAMIC FUNCTION
WITH TEMPERATURE AT 1000 MILLIBARS

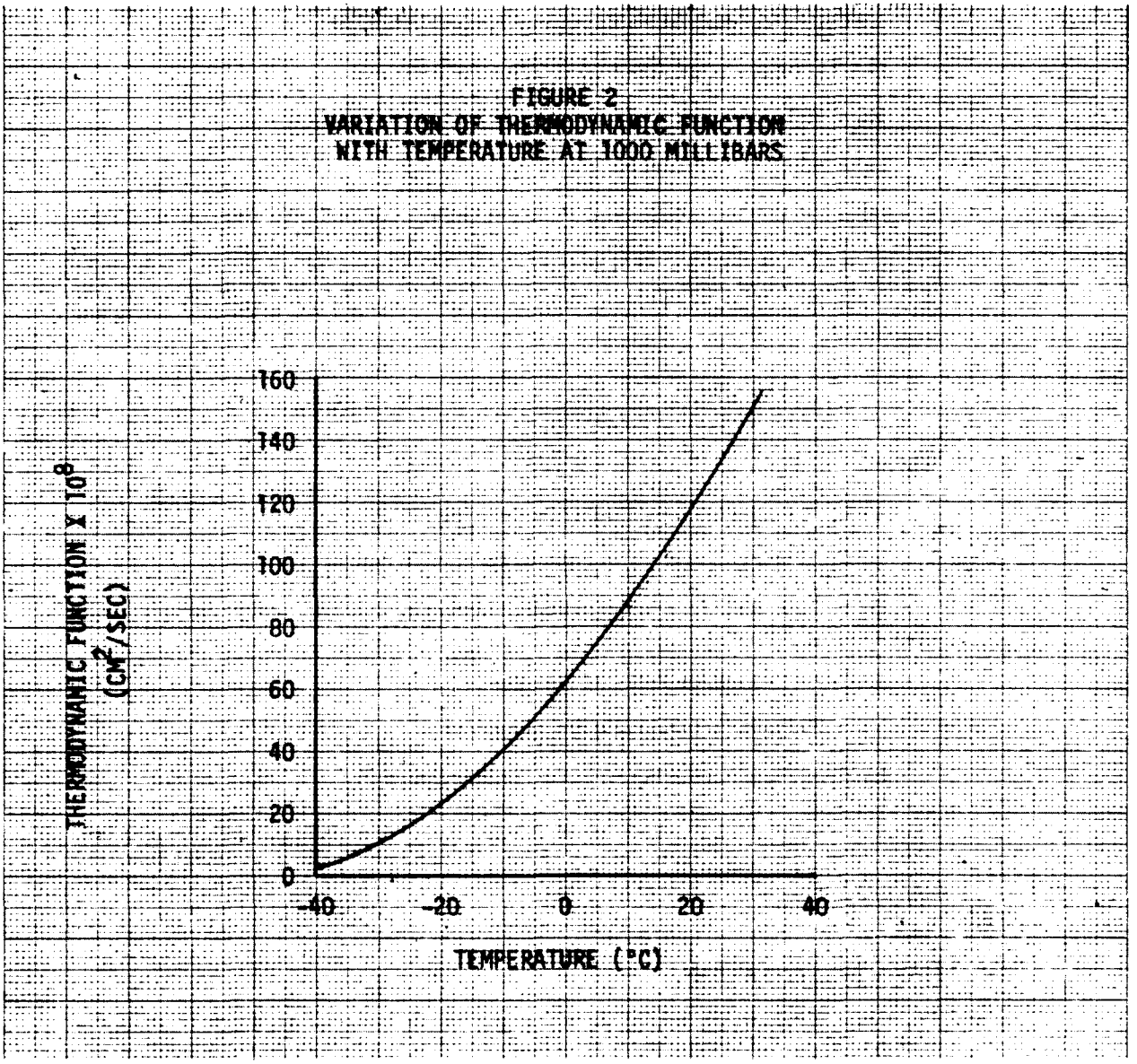

FIGURE 3
WATER FLOW RATE CHART - DUAL BOOM CONFIGURATION

NOTES: 1. DUAL BOOM CONFIGURATION
2. 200 FOOT STANDOFF DISTANCE
3. 90 KTAS

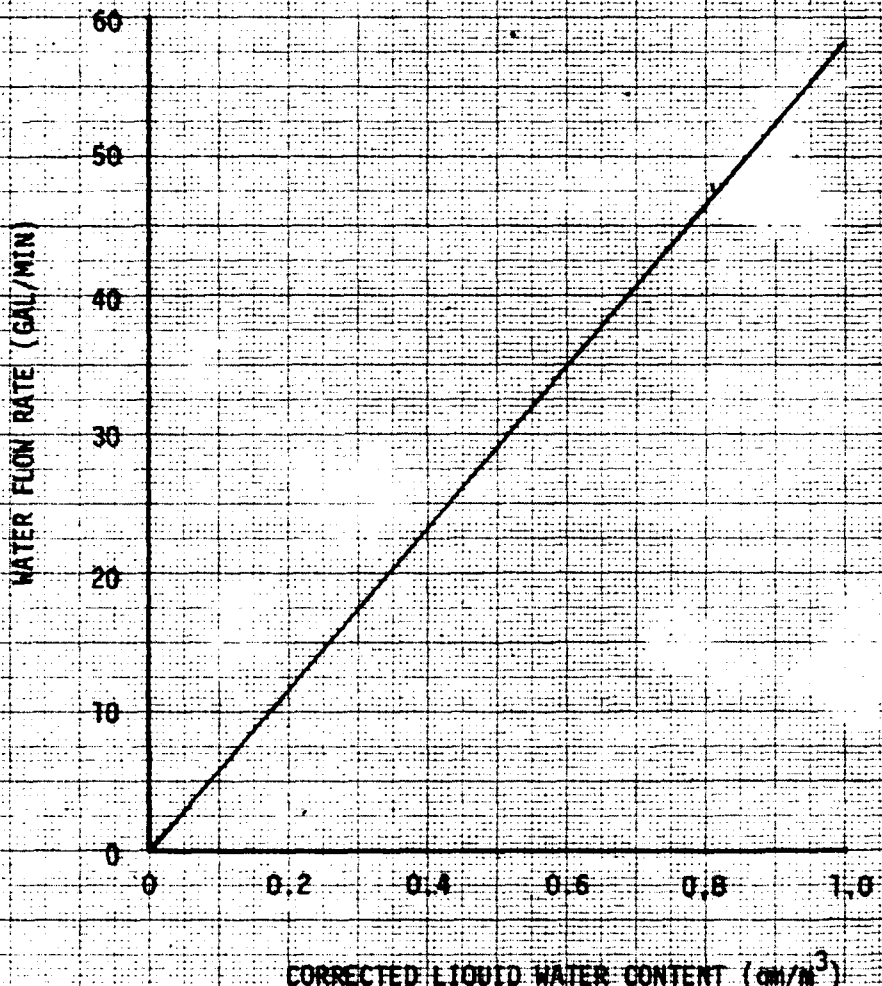

As justification for the mean volumetric diameter representations used in this report, consider the following example:

Cloud droplet radius = 0.002 cm

Rain droplet radius = 0.1 cm

Since LWC is proportional to the cube of radius

$$\frac{\text{LWC Rain} = 4/3\,\pi\,(0.1)^3}{\text{LWC cloud} = 4/3\,\pi\,(0.001)^3} = 10^6$$

The rain droplet is equivalent to 1 million cloud droplets. If presented as a numerical concentration, both droplets carry the same weight in the concentration data.

MRI CALCULATION OF LWC

16. The output from the laser nephelometers was in terms of the number of particles in each size channel. These data were then used to calculate the LWC of each sample point by the following equation.

$$LWC = w\left(\frac{4\pi}{3}\right)\sum_{i=1}^{n}\left(D_i/2\right)^3\ N_i \qquad (4)$$

Where:

w = density of liquid water

D_i = Mean diameter for the ith channel

N_i = the number of droplets in the ith channel

n = number of channels

Mass distribution is the droplet concentration weighted by the mass of the droplet of the appropriate size,

$$m_i = \frac{\pi}{6}\ D_i^3 \times w \qquad (5)$$

then

$$M_i = P_i \times m_i \qquad (6)$$

where

M_i = quantity plotted as droplet mass

P_i = droplet concentration

m_i = mass of droplet of size observed in channel i

APPENDIX E. TEST DATA

INDEX

FIGURE 1 RELATIVE HUMIDITY EFFECT

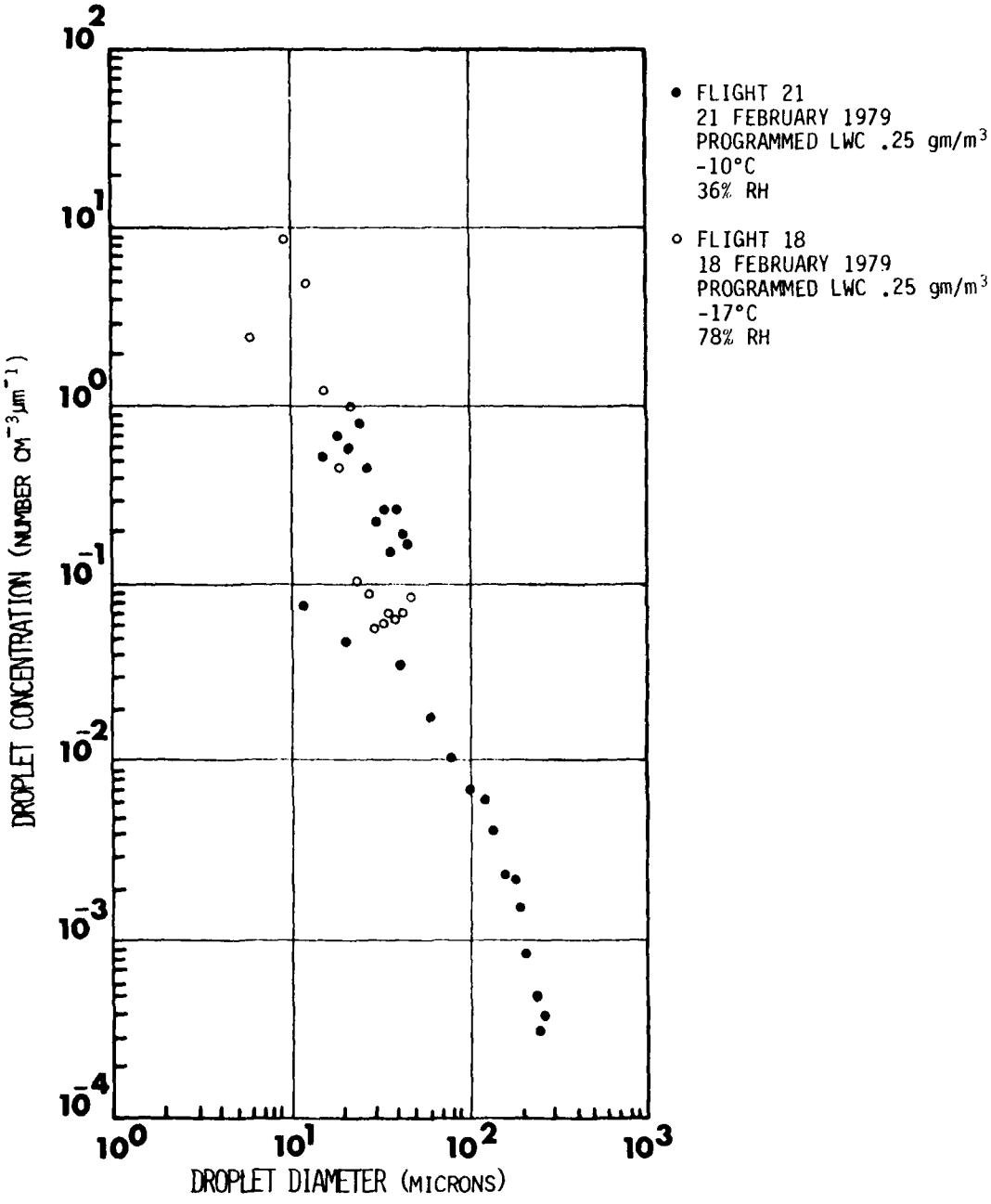

FIGURE 2 RANGE EFFECT

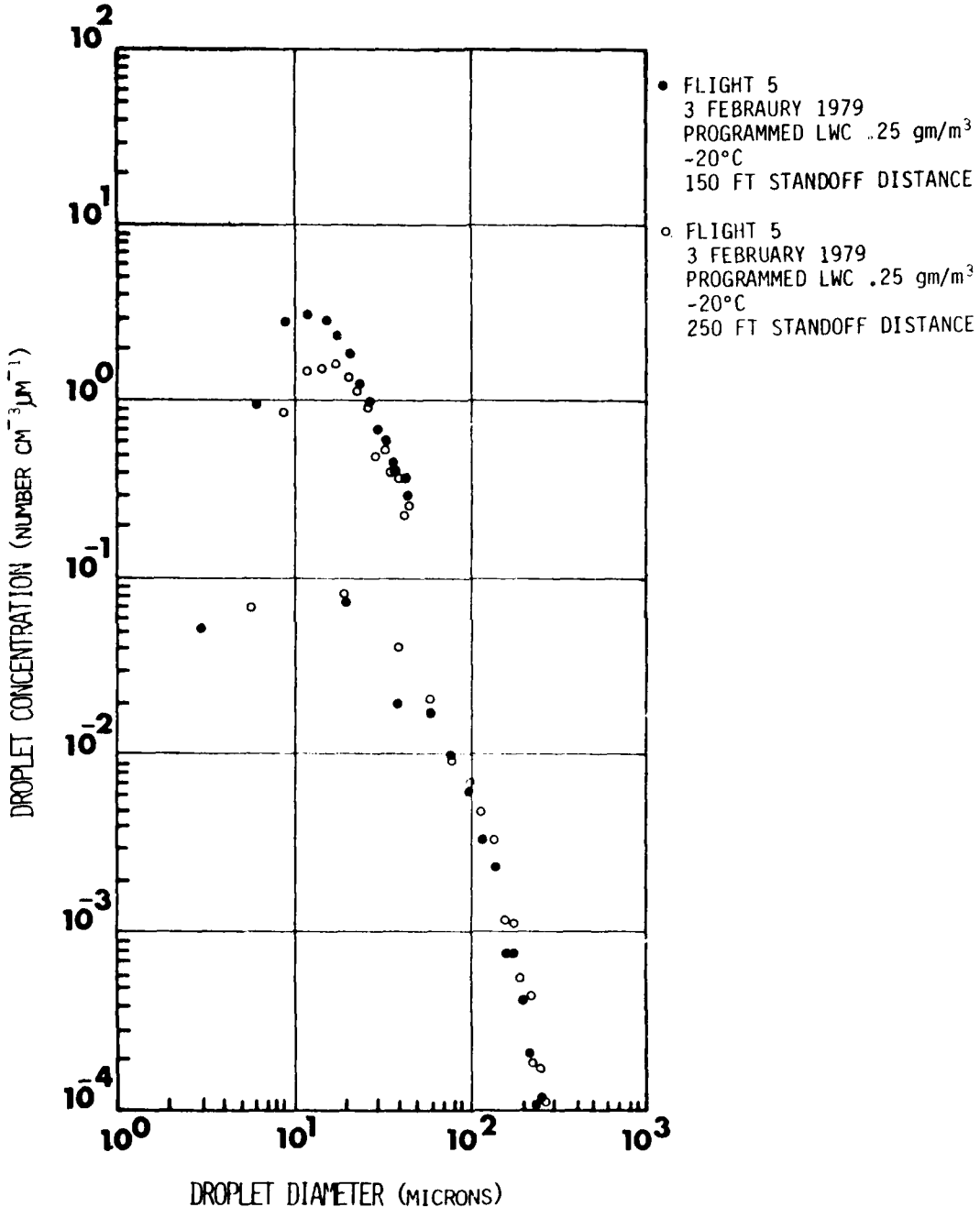

FIGURE 3 FLOW RATE EFFECT

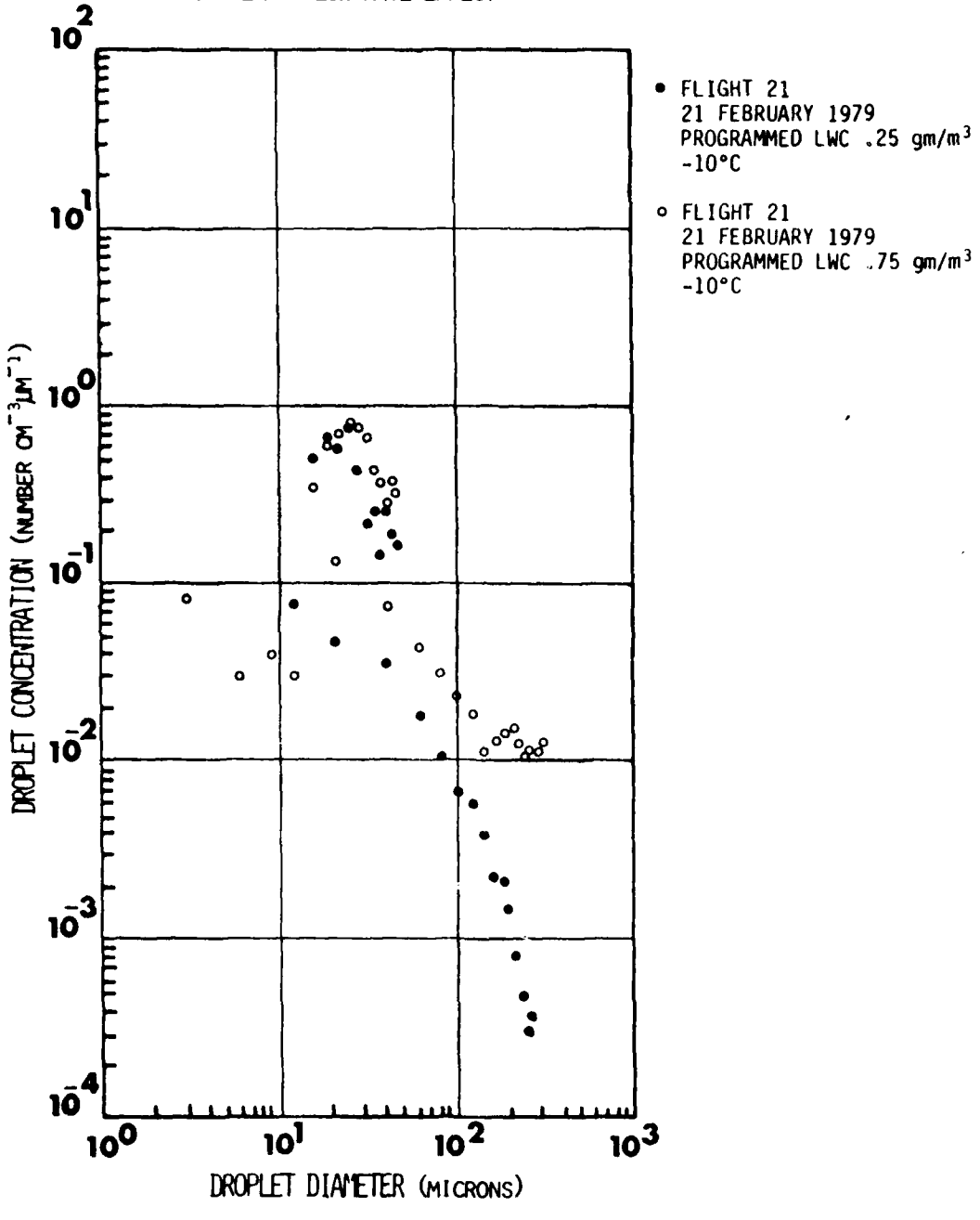

FIGURE 4
VERTICAL CROSS SECTION
of HISS PLUME
(MEDIAN DROPLET SIZE)

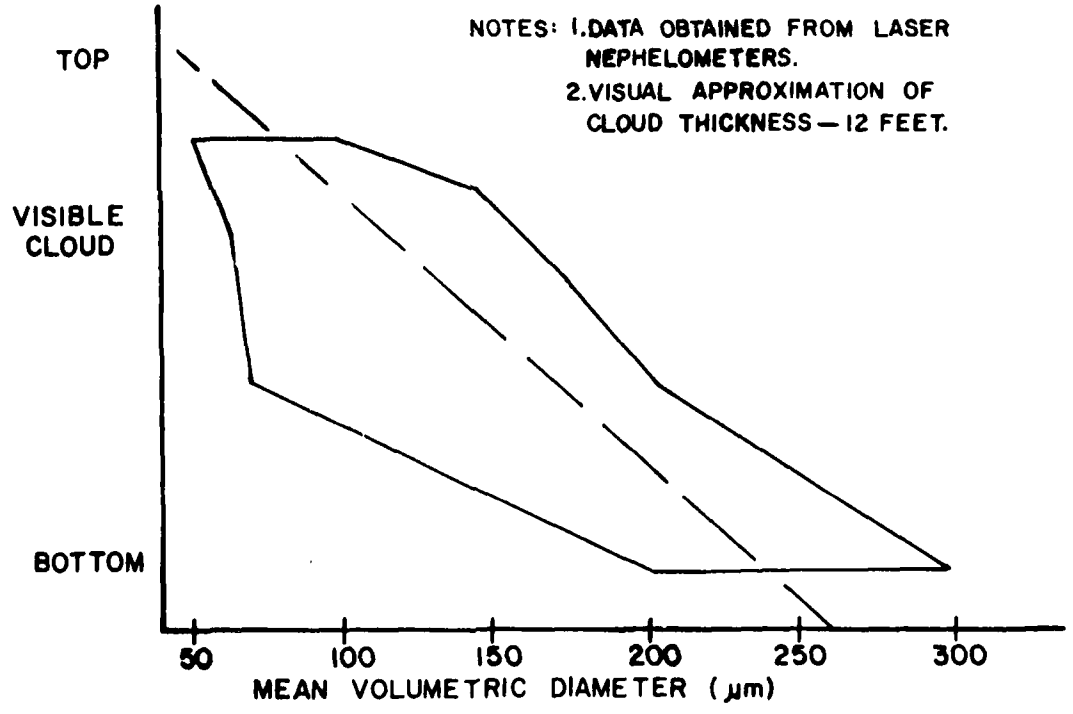

FIGURE 5
Vertical Cross Section
of HISS Plume
(LIQUID WATER CONTENT)

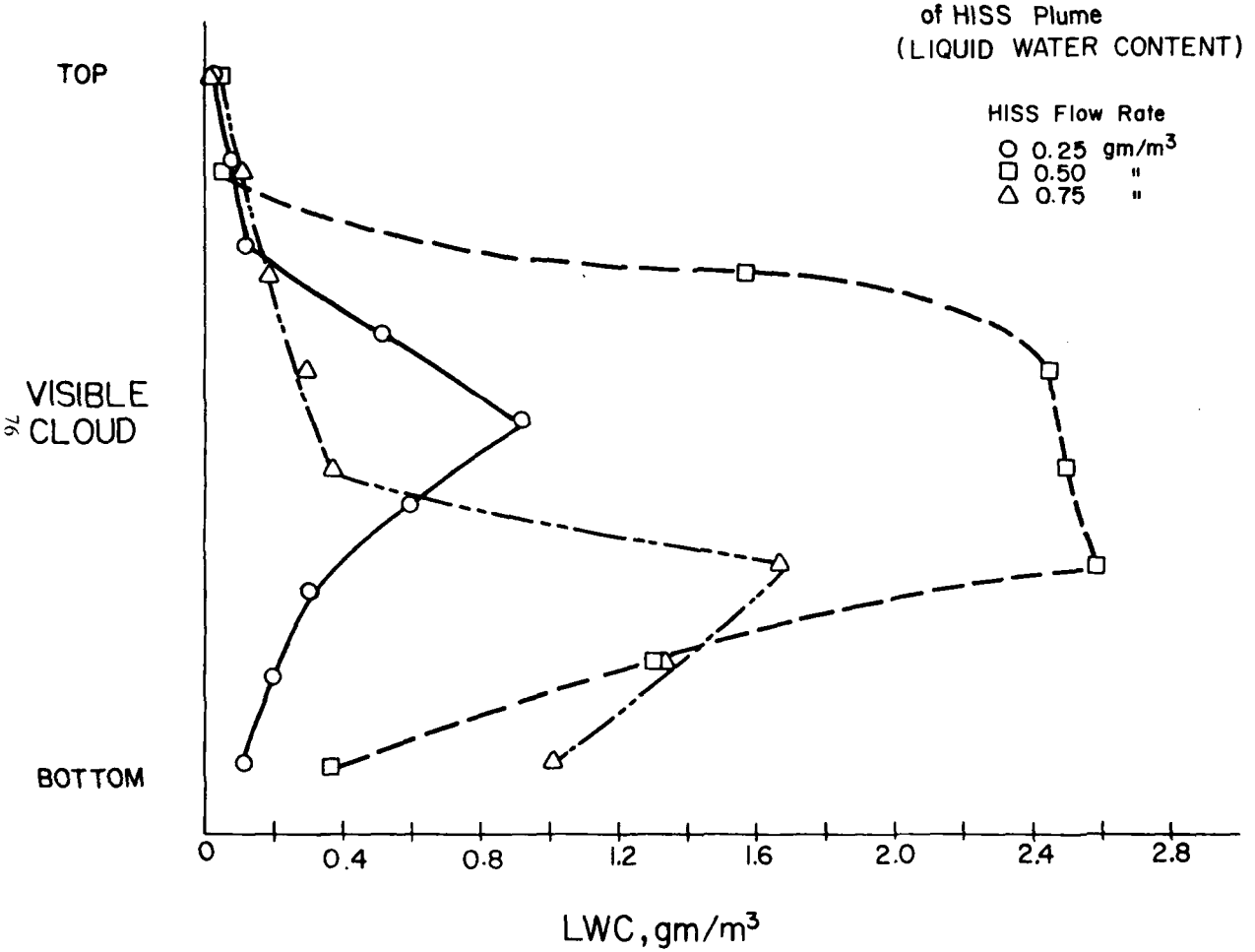

FIGURE 6 COMPARISON OF HISS PLUME TO NATURAL CLOUD

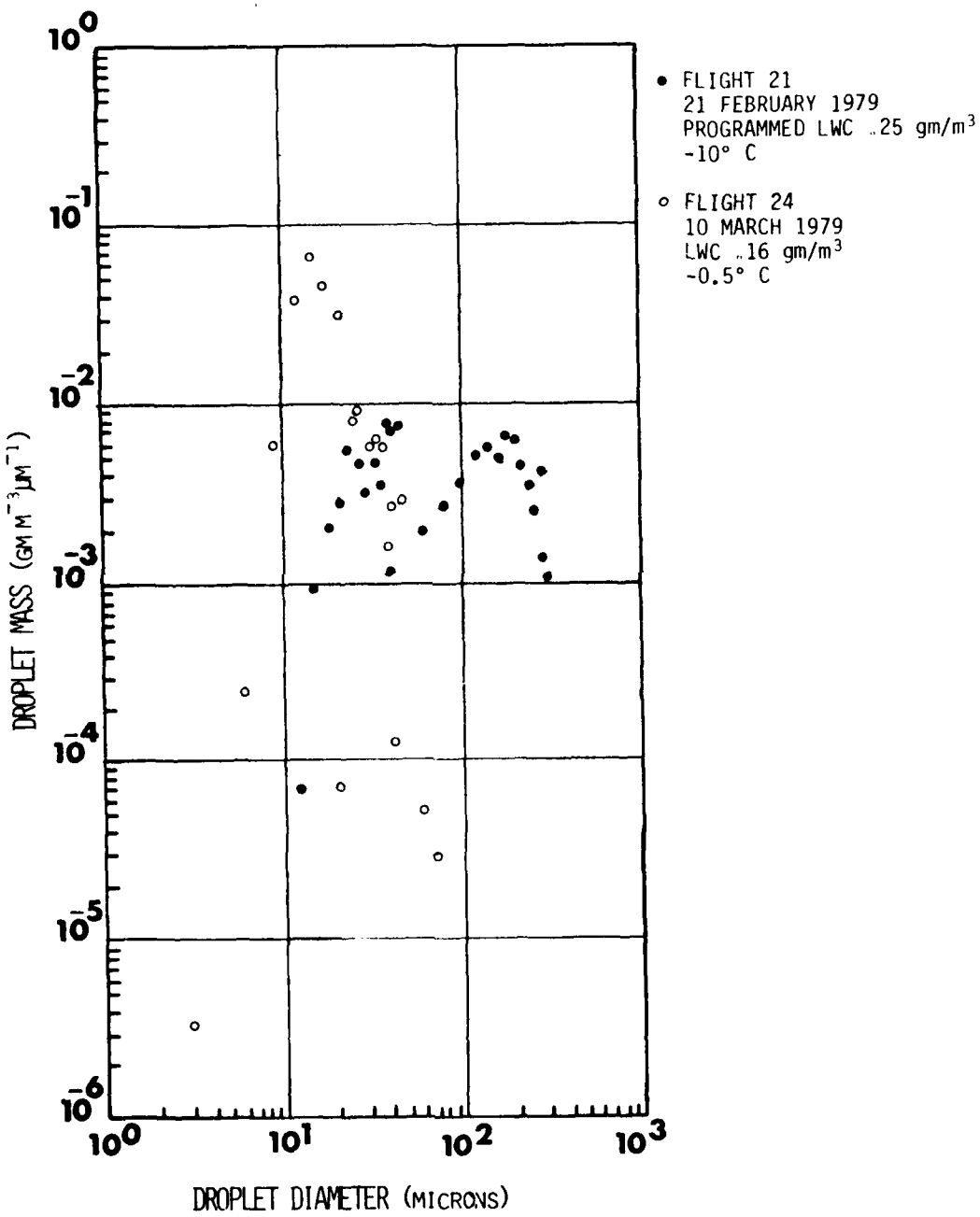

FIGURE 7 NATURAL CLOUD

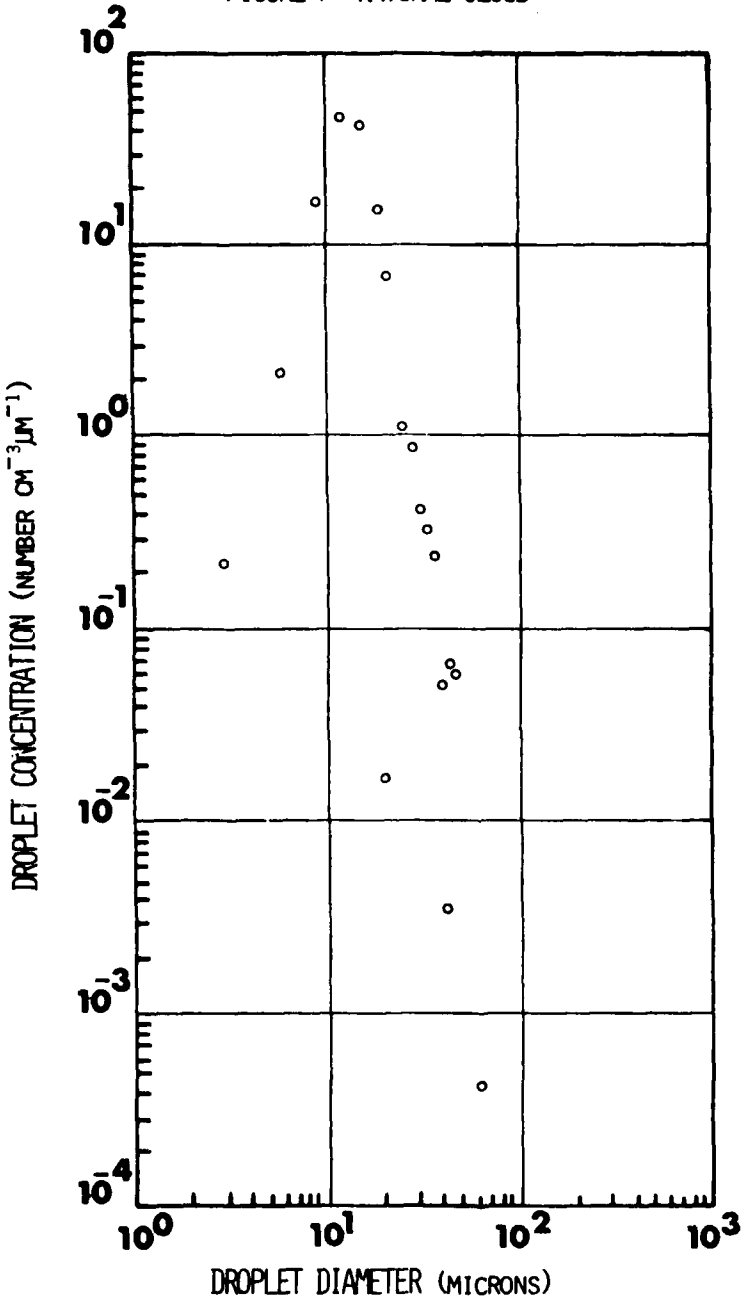

FLIGHT 24
10 MARCH 1979
LWC .16 gm/m^3
-0.5°C

FIGURE 8 NATURAL CLOUD

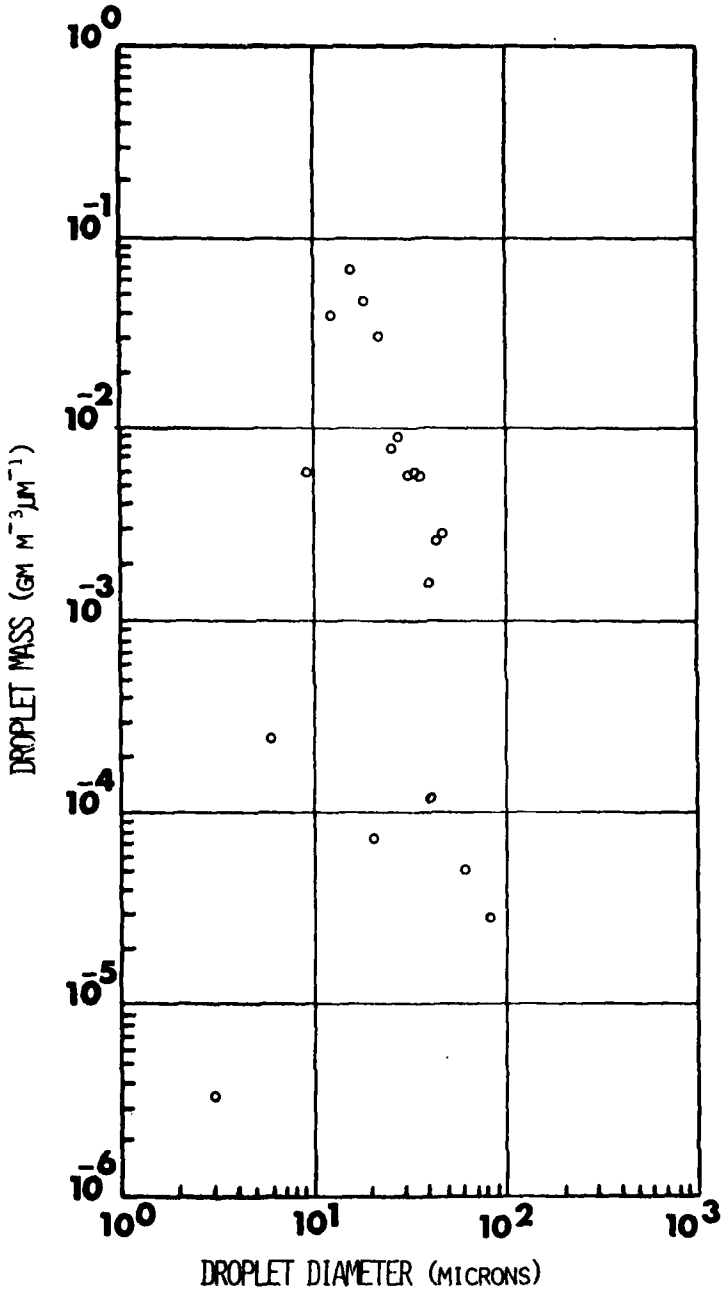

FLIGHT 24
10 MARCH 1979
LWC .16 gm/m^3
-0.5°C

FIGURE 9 NATURAL CLOUD MEAN VOLUMETRIC DROPLET SIZE

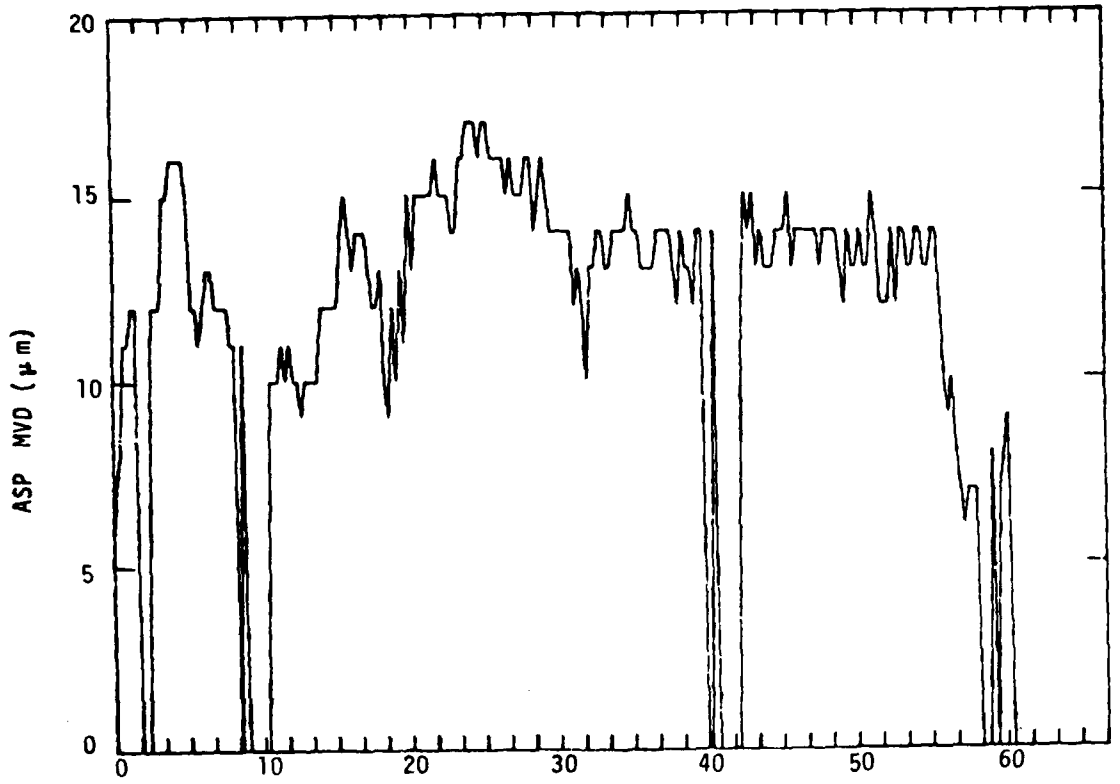

START TIME = 0943:20
10 MARCH 1979, Flt. A-23/29A

-6° C
7600 H_p

FIGURE 10 NATURAL ICING LIQUID WATER CONTENT

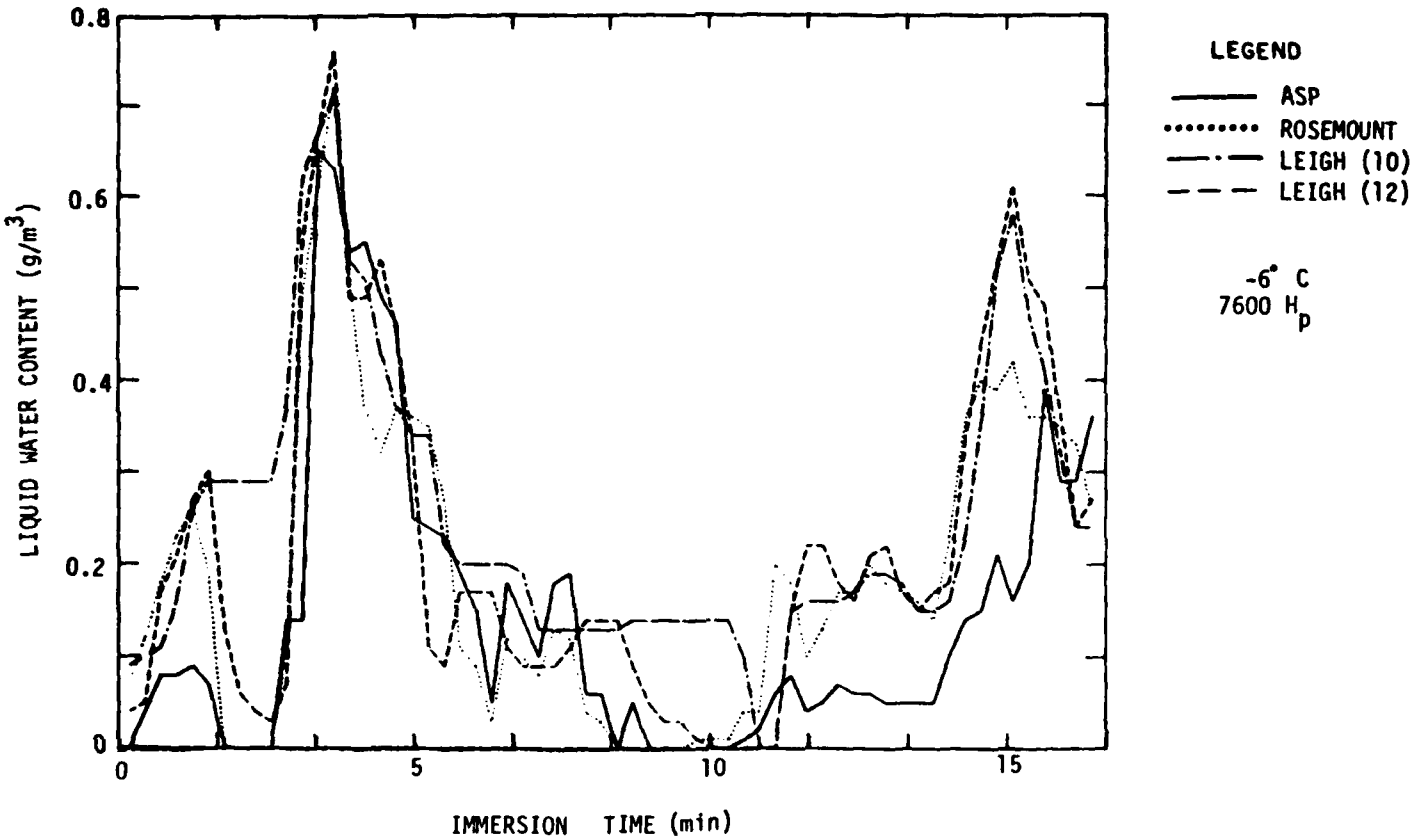

START TIME = 09:43:20 EST

10 March 1979, Flt. A-23/29A

FIGURE 11 LUDLAM LIMIT EFFECT

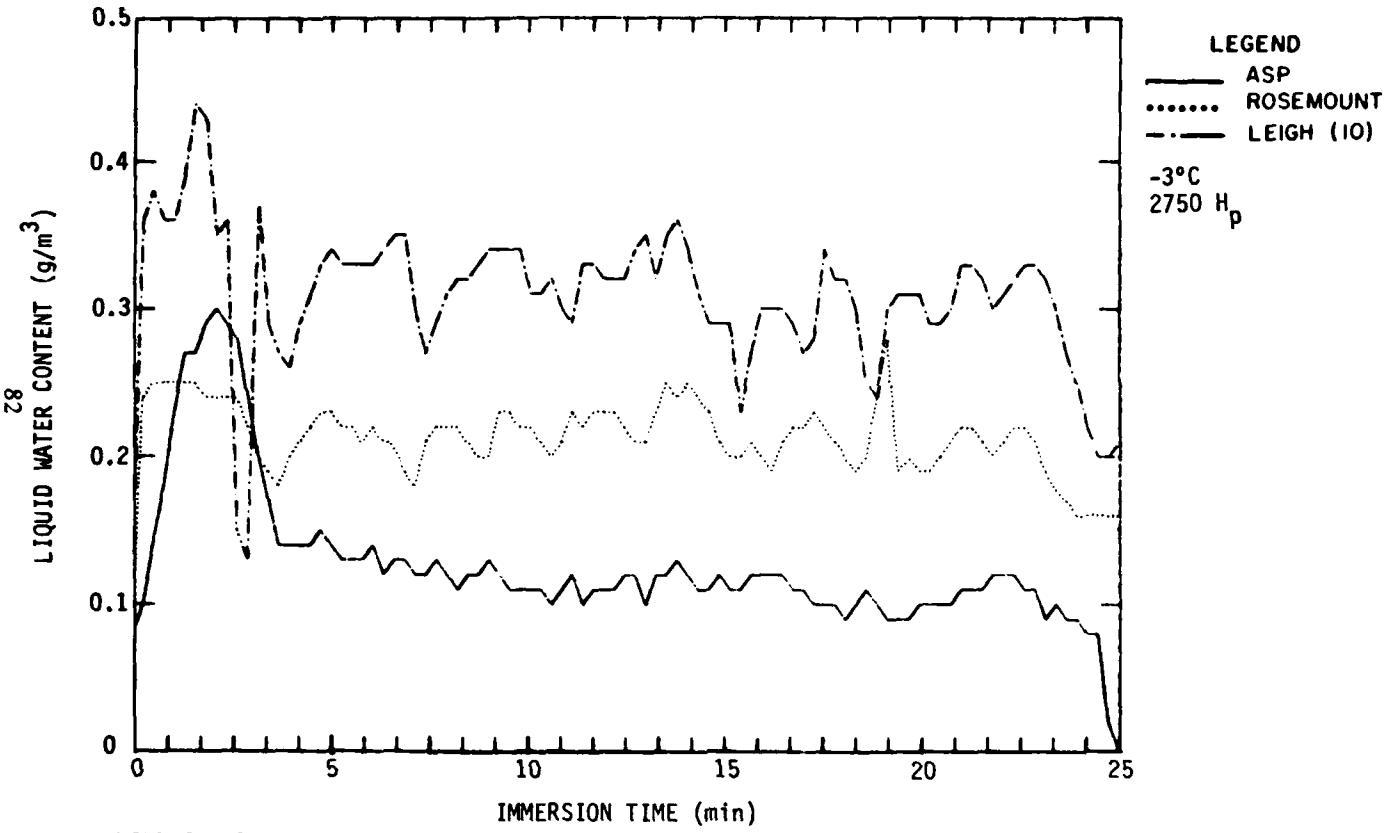

CLOUD 2 START TIME = 0918:20 CST
20 February 1979, Flt. A19/22A

FIGURE 12 COMPARISON OF NATURAL CLOUDS

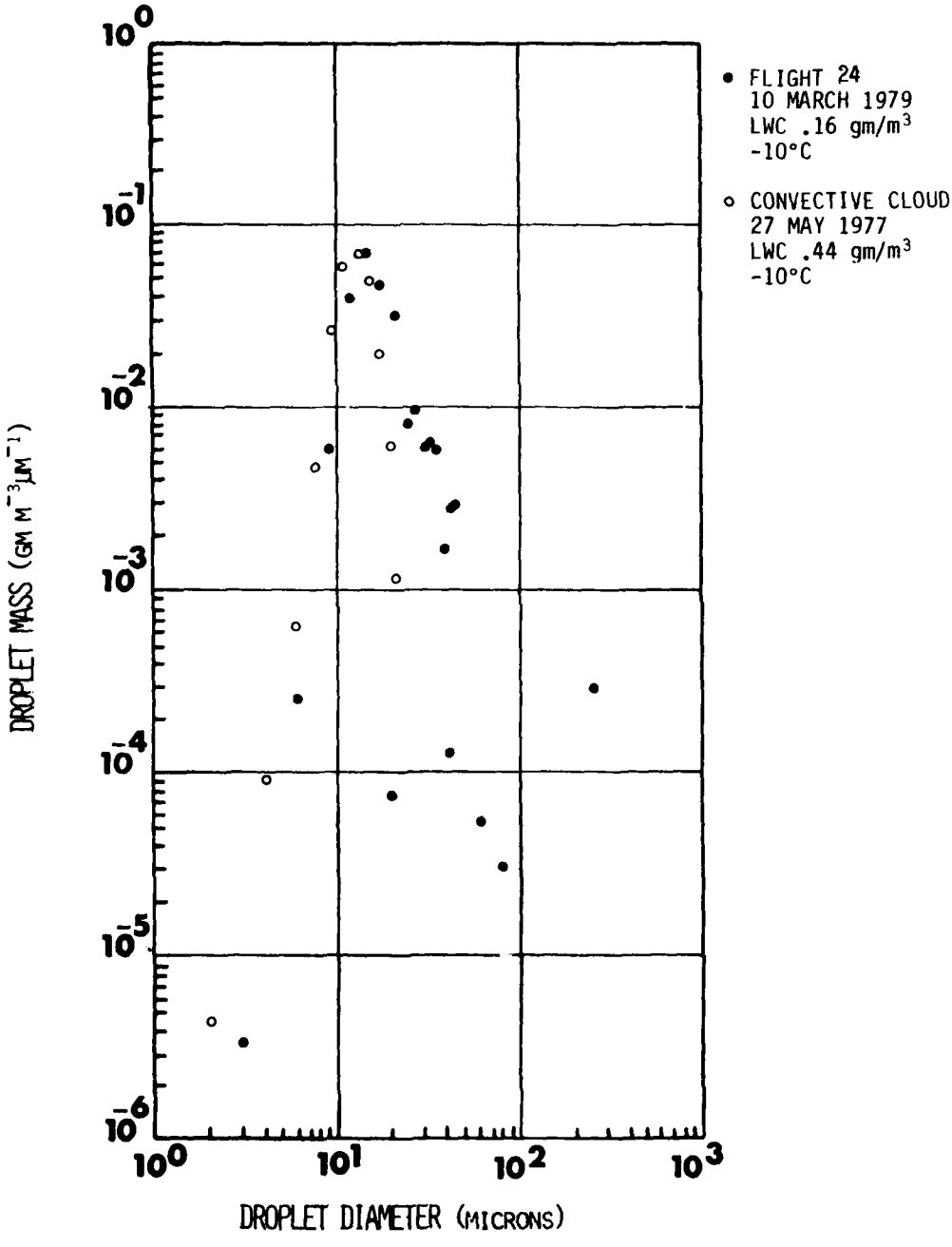

FIGURE 13 FREEZING RAIN

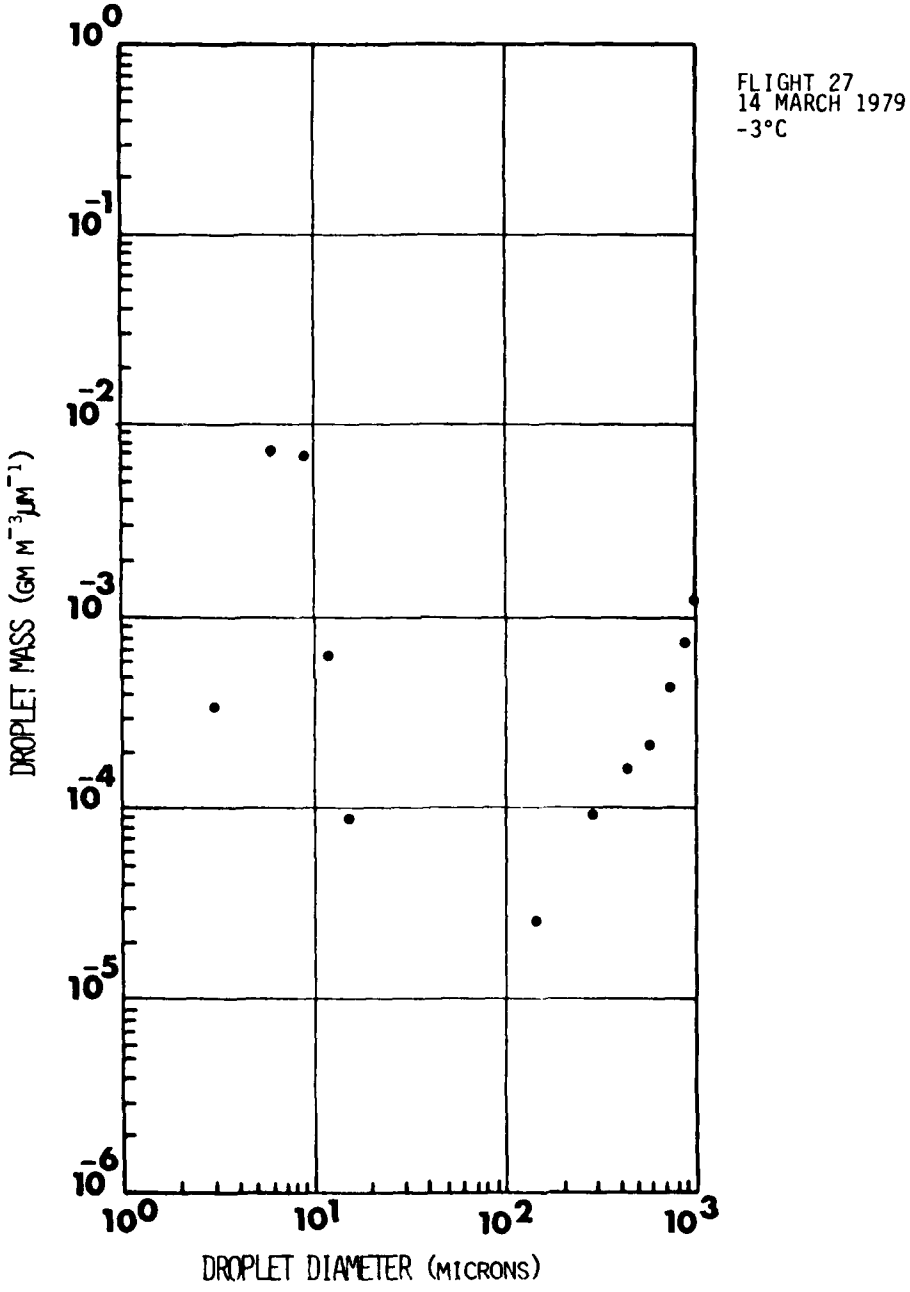

FIGURE 14 FREEZING RAIN MEAN VOLUMETRIC DROPLET SIZE

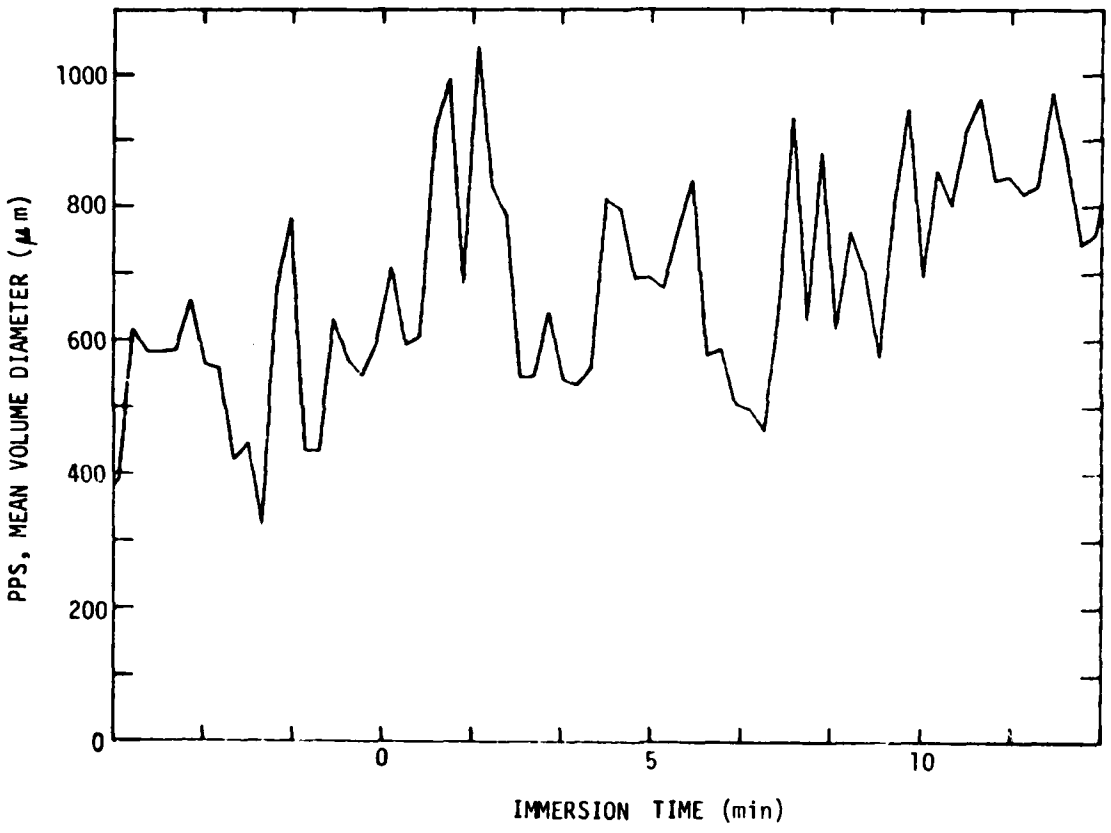

START TIME = 14:06:40 (EST)

14 March 1979, Flt. A-27/31B

FIGURE 15 FREEZING RAIN LIQUID WATER CONTENT

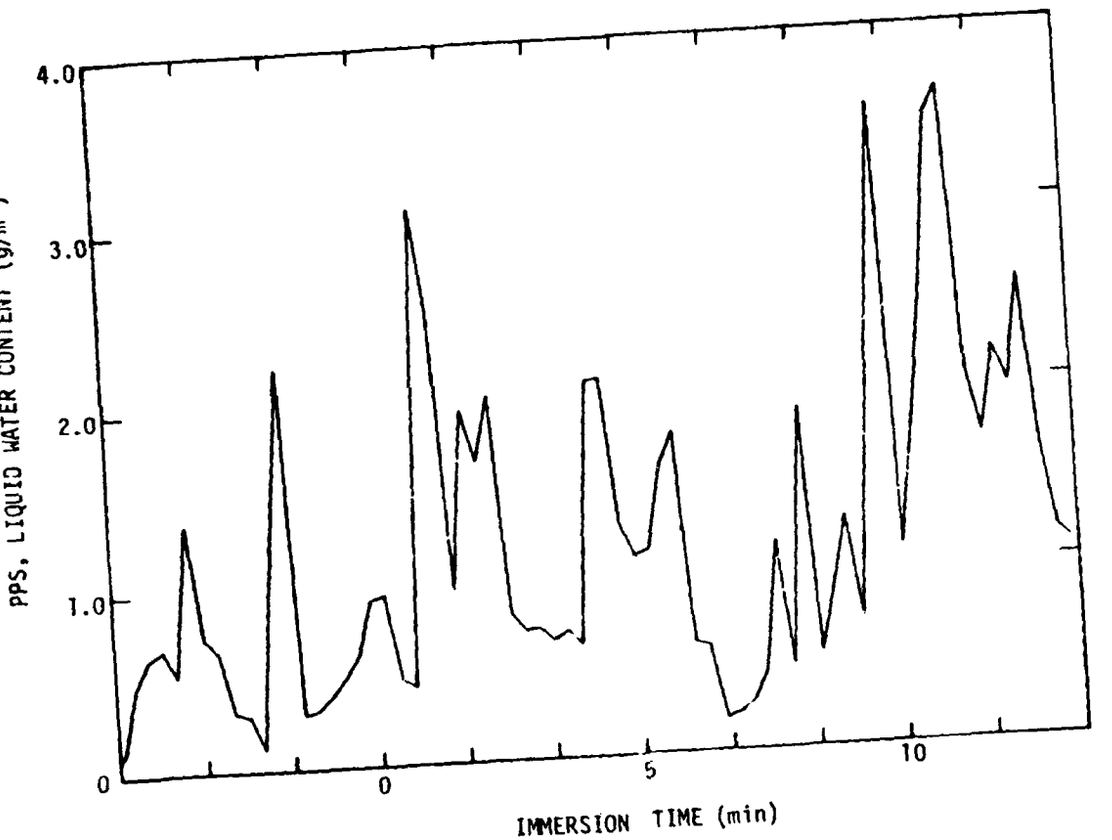

-3.2° C
3050 H_p

START TIME = 14:06:40 (EST)

14 March 1979. Flt. A-27/318

FIGURE 16
OCCURRENCE OF SPANWISE FREEZING POINT
JUH-1H USA SN 70-16318

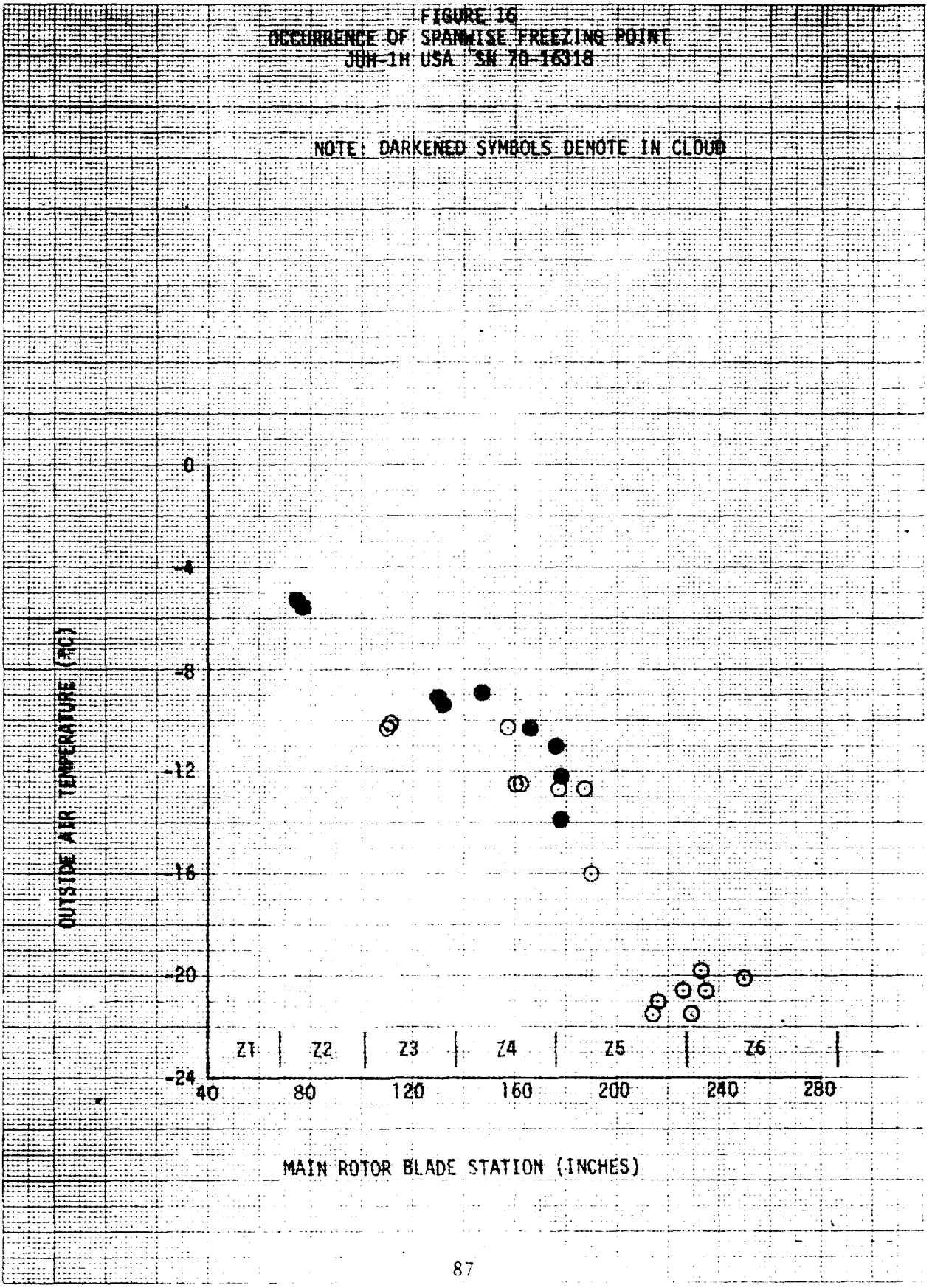

FIGURE 17
ASYMMETRIC SHED OCCURRENCE DURING NATURAL ICING
JUK-1H USA S/N 76-16318

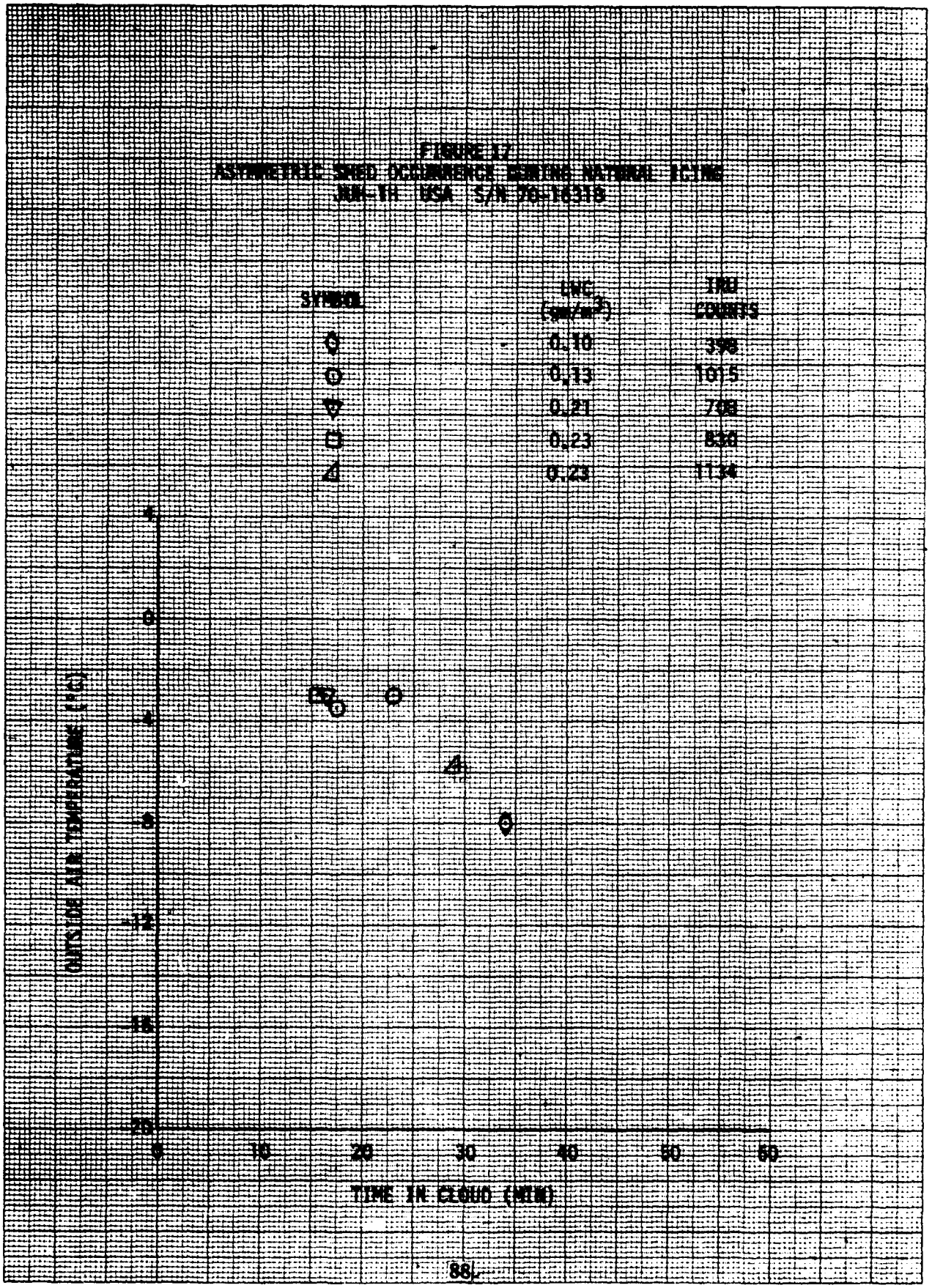

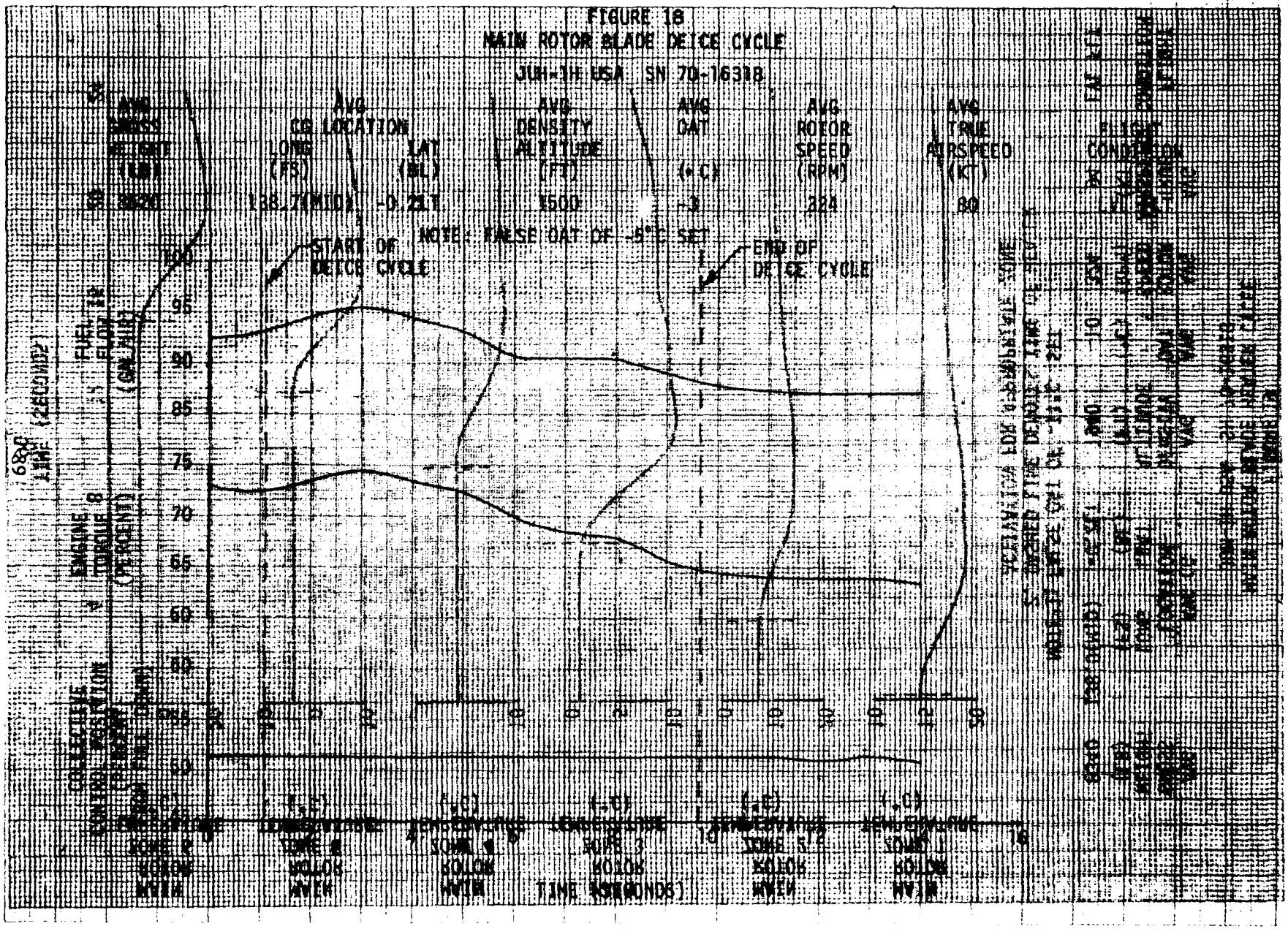

FIGURE 18
MAIN ROTOR BLADE DEICE CYCLE
JUH-1H USA SN 70-16318

AVG GROSS WEIGHT (LB)	AVG CG LOCATION LONG (FS)	AVG CG LOCATION LAT (BL)	AVG DENSITY ALTITUDE (FT)	AVG OAT (°C)	AVG ROTOR SPEED (RPM)	AVG TRUE AIRSPEED (KT)	FLIGHT CONDITION
8820	138.7(MID)	-0.2LT	1500	-3	324	80	LVL FLT

NOTE: FALSE OAT OF -5°C SET

FIGURE 19
MAIN ROTOR BLADE HEATER CYCLE
OGE-2H USN SN 79-23028

GROSS WEIGHT (LB)	PRESSURE ALTITUDE (FT)	OAT (°C)	AMB TEMP (°C)	AVG ROTOR SPEED (RPM)	TRUE AIRSPEED (KT)	FLIGHT CONDITION
8540	136.0(MSD) / +6.2CT	1940	-10	324	94	LVL FLT

NOTES: 1. FALSE OAT OF -11°C SET
2. DASHED LINE DENOTES TIME OF HEATER ACTIVATION FOR APPROPRIATE ZONE

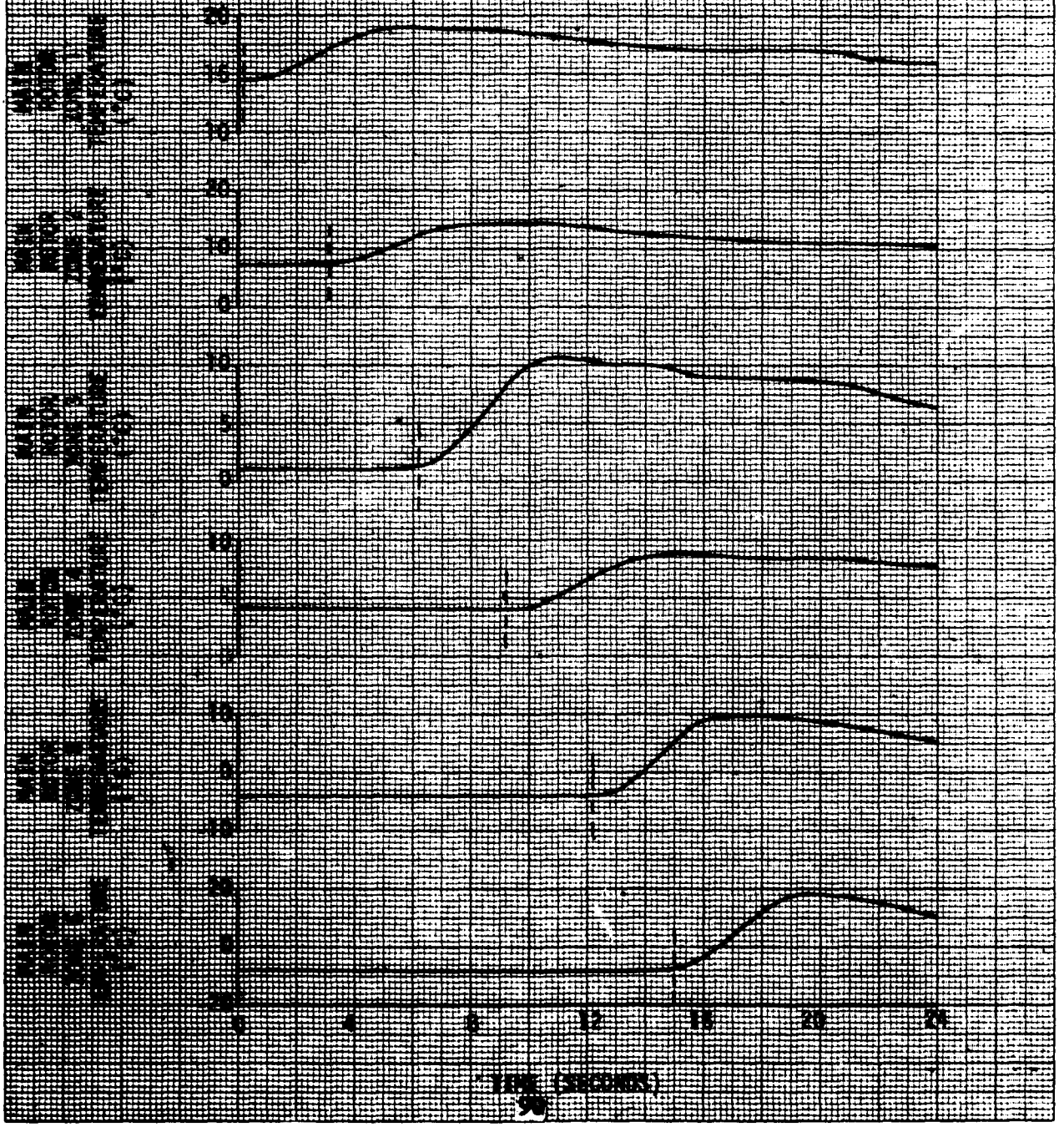

FIGURE 20
TOTAL ICE COVERAGE OF WINDSHIELDS DURING ARTIFICIAL ICING
JUH-1H USA S/N 70-16518

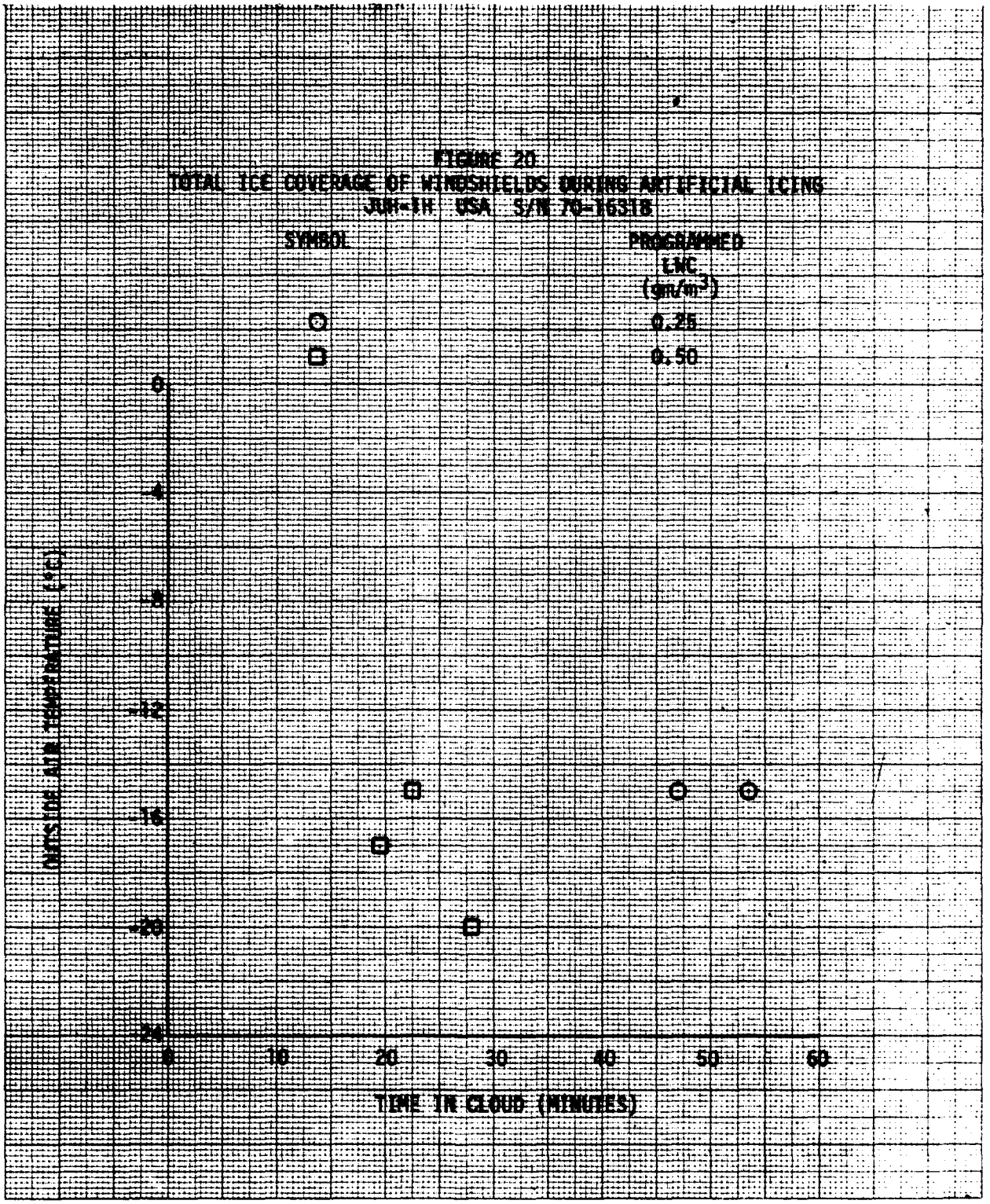

DISTRIBUTION

Deputy Chief of Staff for Research, Development, and Acquisition (DAMA-WSA, DAMA-RA, DAMA-PPM-T)	4
US Army Materiel Development and Readiness Command (DRCPM-CO, DRDCDE-DW-A, DRCSF-A, DRCQA)	20
US Army Aviation Research and Development Command (DRDAV-DI)	12
US Army Training and Doctrine Command (ATCD-CM-C)	1
US Army Materiel Systems Analysis Activity (DRXSY-CM, DRXSY-MP)	3
US Army Test and Evaluation Command (DRSTE-TO, DRSTE-CT, USMC LnO)	3
Director, Research & Technology Laboratories/Ames	2
Research & Technology Laboratory/Aeromechanics (DAVDL-AL-D)	2
Research & Technology Laboratory/Propulsion (DAVDL-PL-D)	2
Research & Technology Laboratory/Structures	2
Research & Technology Laboratory/Applied Technology Lab (DAVDL-ATL-D, Tech Library)	1
US Army Human Engineering Laboratory (DRXHE-HE)	1
US Army Aeromedical Research Laboratory (SGRD-UAC)	1
US Army Infantry School (ATSH-TSM-BH)	1
US Army Aviation Center (ATZQ-D-MT)	3
US Army Aircraft Development Test Activity (PROV) (STEBG-CO-T, STEBG-PM, STEBG-CT)	5
US Army Safety Center (IGAR-TA, IGAR-Library)	2
US Army Maintenance Management Center (DRXMD-ED)	1
US Army Transportation School (ATSP-CD-MS)	1
US Army Logistics Center (ATCL-M)	1
US Army Foreign Science and Technology Center (AMXST-WS4)	1
US Military Academy	3
US Marine Corps Development and Education Command	2

US Naval Air Test Center	1
US Air Force Aeronautical Systems Division (ASD-ENFTA)	1
US Air Force Flight Dynamics Laboratory (TST/Library)	1
US Air Force Flight Test Center (SSD/Technical Library, TEEE)	3
Department of Transportation Library	1
US Army Bell Plant Activity (DAVBE-ES)	5
AVCO Lycoming Division	5
Defense Documentation Center (DDC-TCA)	12
Federal Aviation Adminstration, [Dev Sec C, ALG-313 (BAG)]	50